5-31-2012

An Energy Based Nanomechanical Properties Evaluation Method for Cementitious Materials

Kaushal K. Jha
Florida International University, kjha001@fiu.edu

DOI: 10.25148/etd.FI12080804

FLORIDA INTERNATIONAL UNIVERSITY

Miami, Florida

AN ENERGY BASED NANOMECHANICAL PROPERTIES EVALUATION METHOD FOR CEMENTITIOUS MATERIALS

A dissertation submitted in partial fulfillment of

the requirements for the degree of

DOCTOR OF PHILOSOPHY

in

CIVIL ENGINEERING

by

Kaushal Kumar Jha

2012

To: Dean Amir Mirmiran
College of Engineering and Computing

This dissertation, written by Kaushal Kumar Jha, and entitled An Energy Based Nanomechanical Properties Evaluation Method for Cementitious Materials, having been approved in respect to style and intellectual content, is referred to you for judgment.

We have read this dissertation and recommend that it be approved.

_____
Amir Mirmiran

_____
Ton-Lo Wang

_____
Arvind Agarwal

_____
Nakin Suksawang, Major Professor

Date of Defense: May 31, 2012

The dissertation of Kaushal Kumar Jha is approved.

_____
Dean Amir Mirmiran
College of Engineering and Computing

_____
Dean Lakshmi N. Reddi
University Graduate School

Florida International University, 2012

DEDICATION

I dedicate this dissertation to my parents. Their support, encouragement and constant love motivated me a lot to pursue this endeavor that had been difficult and challenging.

ACKNOWLEDGMENTS

I would like to take this opportunity to acknowledge those individual who contributed immensely in my research. Writing this dissertation has been a great endeavor for me, and therefore I am grateful for all the help and support that I received.

First and foremost, I wish to extend my deepest gratitude to Prof. Nakin Suksawang, my academic advisor, for providing me continuous encouragement, support and outstanding guidance during this study. I thank him for introducing me to this interdisciplinary research, which eventually became a great learning experience. He constantly inspired and motivated me to achieve my academic goals, for which I will remain indebted throughout my life.

I am equally indebted to Prof. Arvind Agarwal who, as committee member, provided me invaluable help and made this dissertation possible. I greatly appreciate his valuable thoughts and constructive suggestions on numerous occasions, which was crucial in my understanding of several aspects of nanomechanics. His generous support in carrying out nanoindentation test is thankfully acknowledged.

I would like to extend my special thanks to Prof. Ton-Lo Wang and Prof. Amir Mirmiran for serving on my dissertation committee and supporting me throughout this study.

I would also like to appreciate Dr. Debrupa Lahiri for the help she extended to me in carrying out nanoindentation experiment on several metal and cement paste samples.

I would like to thank my wife Pushpa for the unconditional love and support she extended to me throughout the course of this study. I owe to my daughters Kritika and Kashika who took their father's preoccupation in their stride.

Last, but not the least, the financial support by the University Graduate School in the form of Dissertation Year Fellowship (DYF), which is instrumental for timely completion of this study, is gratefully acknowledged.

ABSTRACT OF THE DISSERTATION

AN ENERGY BASED NANOMECHANICAL PROPERTIES EVALUATION METHOD FOR CEMENTITIOUS MATERIALS

by

Kaushal Kumar Jha

Florida International University, 2012

Miami, Florida

Professor Nakin Suksawang, Major Professor

Advances in multiscale material modeling of structural concrete have created an upsurge of interest in the accurate evaluation of mechanical properties and volume fractions of its nano constituents. The task is accomplished by analyzing the response of a material to indentation, obtained as an outcome of a nanoindentation experiment, using a procedure called the Oliver and Pharr (OP) method. Despite its widespread use, the accuracy of this method is often questioned when it is applied to the data from heterogeneous materials or from the materials that show pile-up and sink-in during indentation, which necessitates the development of an alternative method.

In this study, a model is developed within the framework defined by contact mechanics to compute the nanomechanical properties of a material from its indentation response. Unlike the OP method, indentation energies are employed in the form of dimensionless constants to evaluate model parameters. Analysis of the load-displacement data pertaining to a wide range of materials revealed that the energy constants may be used to determine the indenter tip bluntness, hardness and initial unloading stiffness of the material. The proposed model has two main advantages: (1) it does not require the computation of the

contact area, a source of error in the existing method; and (2) it incorporates the effect of peak indentation load, dwelling period and indenter tip bluntness on the measured mechanical properties explicitly.

Indentation tests are also carried out on samples from cement paste to validate the energy based model developed herein by determining the elastic modulus and hardness of different phases of the paste. As a consequence, it has been found that the model computes the mechanical properties in close agreement with that obtained by the OP method; a discrepancy, though insignificant, is observed more in the case of C-S-H than in the anhydrous phase. Nevertheless, the proposed method is computationally efficient, and thus it is highly suitable when the grid indentation technique is required to be performed. In addition, several empirical relations are developed that are found to be crucial in understanding the nanomechanical behavior of cementitious materials.

TABLE OF CONTENTS

LIST OF TABLES

LIST OF FIGURES

CHAPTER 1

INTRODUCTION

1.1 Background and Motivation

Concrete, the most widely used construction material in the world, is composed of constituents of different sizes that vary over a wide range of scales, from the nanoscale of the elementary chemical components to the macroscale of fine and coarse aggregates [1]. It is now widely accepted that the fundamental properties of concrete such as strength, durability, early age rheology, creep and shrinkage, fracture behavior, etc. are affected by the performance of its constituents to a great extent [2-3]. Many of these properties, by convention, are determined from experiments conducted at the macroscopic scale, where the contributions from the chemical components of concrete to its specific properties are difficult to quantify. This necessitated the development of multiscale material model in which the properties of individual phase are considered [1, 4-7].

The complex microstructure of concrete is divided into four elementary levels, as depicted schematically in figure 1.1. These four levels respect the condition of the scale separability, i.e., the difference in the length scale between two adjacent levels differs at least by an order of magnitude [1]. The first level corresponds to a length scale where the mechanical properties of cementitious materials are linked to the physical chemistry involved in their formation. The characteristic length scale of this level is supposed to be 10^{-8} and 10^{-6} m, the smallest material length scale accessible by mechanical testing so far. This level is chiefly comprised of low and high density Calcium-Silicate-Hydrate (C-S-H) formed by the hydration of cement clinkers (C_3S and C_2S) after mixing them with water. Their morphology

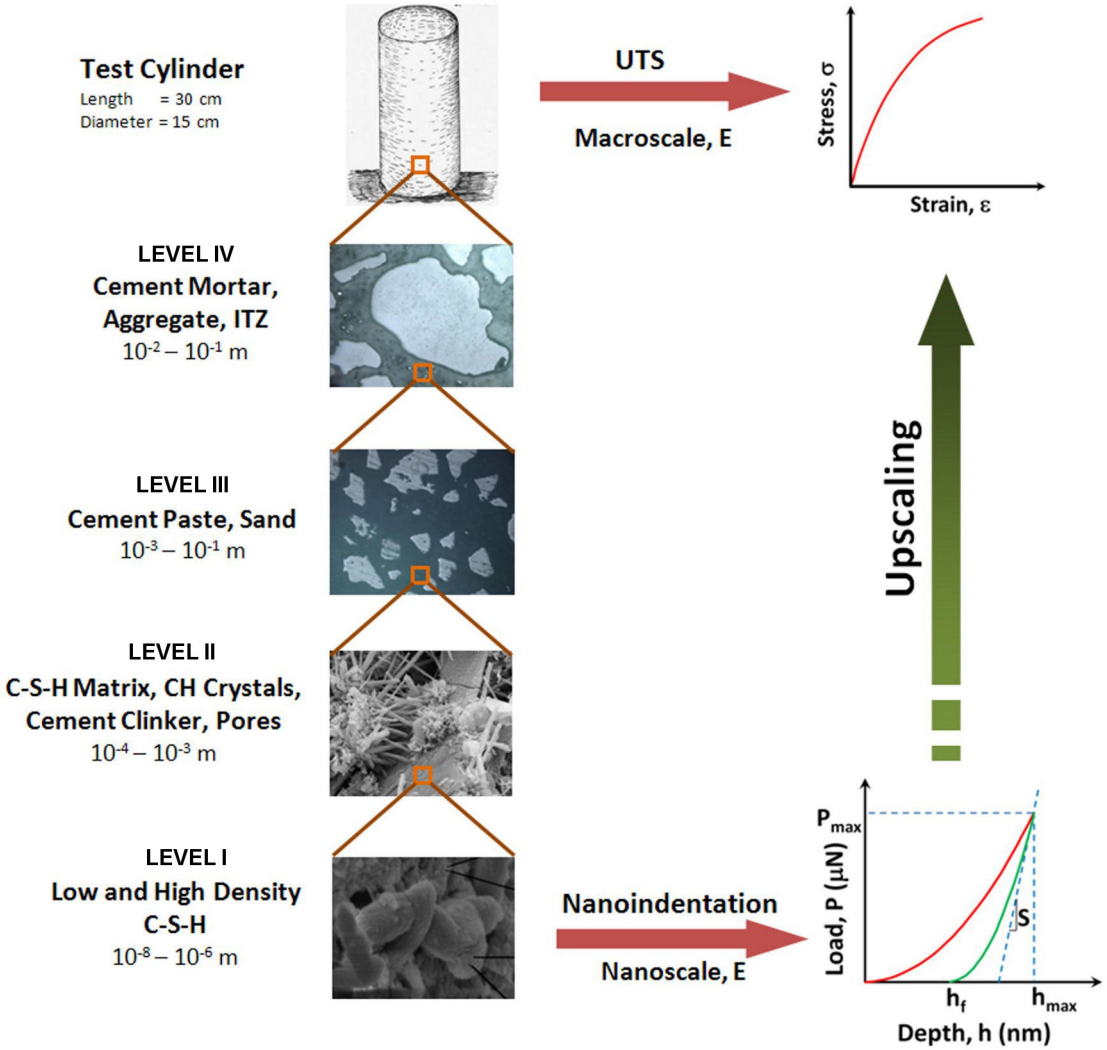

Figure 1.1: The concept of multiscale material modeling.

and volume fractions may be affected by the water-to-cement ratio. The model by Jennings [8-9] suggests that C-S-H are organized in 'globules' comprising of solid (basic building blocks) of size 2.2 nm and 18 % nanoporosity with a characteristic size of 5.6 nm, as shown in figure 1.2. Many such globules form C-S-H solids with gel porosity whose percentage depends on its type. In level II, homogeneous C-S-H with large CH crystals, aluminates, cement clinker inclusions, water, etc. are included. Likewise, sand particles and the

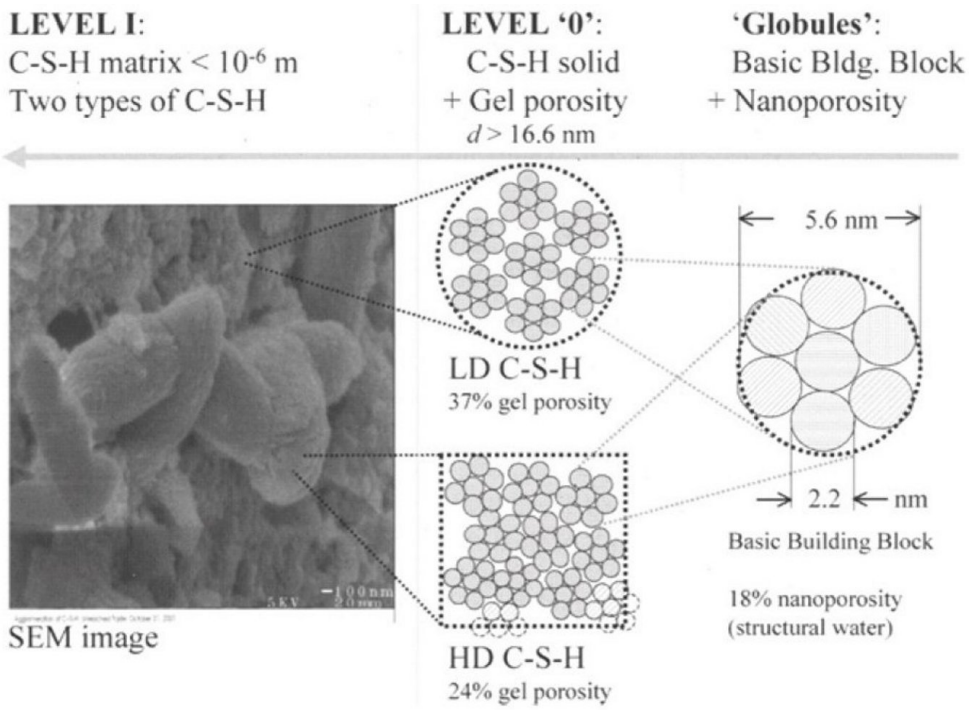

Figure 1.2: Colloidal model of C-S-H by Jennings: Gel porosity vs. Nanoporosity [6].

homogenous cement paste matrix are considered as the constituents of level III. Finally, in level IV, concrete is described as composite material with aggregates, the interfacial transition zone (ITZ) and homogeneous mortar matrix as its components. Multiscale modeling allows us to upscale the information from level I to level IV successively. For instance, the elastic moduli of C-S-H can be upscaled to evaluate the elastic modulus of cementitious materials at level II. The task is accomplished by employing methods such as self-consistent and/or Mori-Tanaka schemes [10-12] used in the analysis of a composite material. While applying these schemes, each level is treated as a composite material in which one or more phases are considered embedded in another. The representative value of one level acts as the input parameter for the next higher level. To begin such analysis, the mechanical properties and volume fractions of the phases present in level I are required to be

known. The volume fractions of the phases may be determined using hydration kinetic models [9].

Nanoscaled materials are often added to concrete to improve its strength and durability. For instance, addition of nanosilica (with an average size of 10 nm) in concrete results in the reduction of porosity by filling the voids created by the arrangement of larger particles and in quicker gain in strength [13-25]. It also reduces the cement requirement for the concrete, which not only addresses the environmental concern, but also helps alleviate the problem of heat generation and shrinkage associated with high cement content. Fly ash and microsilica

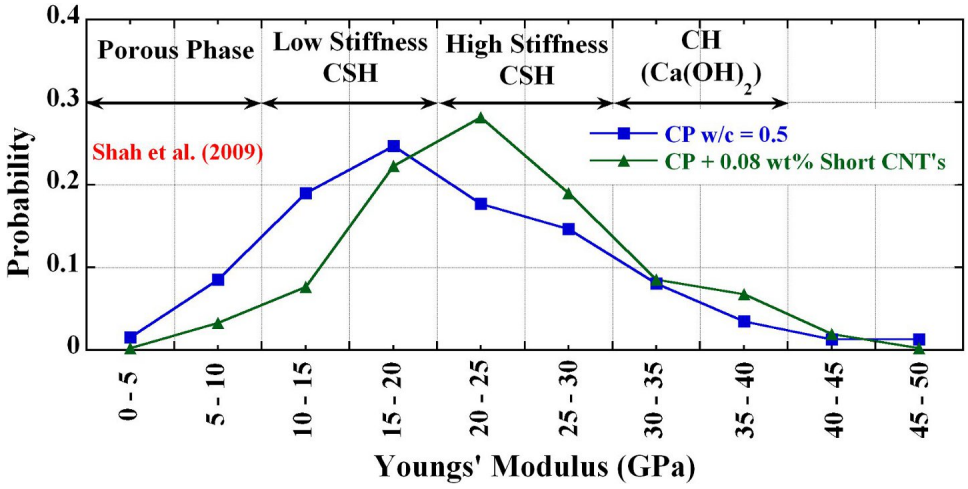

Figure 1.3: Probability plots of Young's modulus of pure cement paste and cement paste reinforced with 0.08 wt% short MWCNTs [22].

(silica fume), byproducts from power plants, steel mills, and other manufacturing facilities, are added in concrete to improve its properties. Because of their pozzolanic properties, these materials react with calcium hydroxide to yield additional C-S-H which is important from the viewpoint of the strength and durability of concrete. Similarly, carbon nanotubes are being added to cementitious materials to increase its strength and fracture toughness [22-25].

Figure 1.3 depicts how the elasticity of the cementitious materials is affected by the small addition of carbon nanotube.

As explained above, concrete exhibits heterogeneity at all level of length scales and its macroscopic material properties (strength and stiffness) are governed by the corresponding properties and volume fractions of its basic building blocks (C-S-H). A question, at this stage, arises as to how the material properties as well as the volume fractions of its nano constituents can be measured or computed with a great level of certainty. Advances in instrumentation have provided us convenient and promising tools that can be used for this purpose [26]. During the last one decade, atomic force microscope and nanoindentation equipment have been applied extensively in the determination of mechanical properties such as indentation modulus and hardness of cementitious materials [27-37]. Besides the measurement of mechanical properties, considerable knowledge on small scale behavior of cementitious materials has been gained through the outcome of the indentation. For instance, Constantinides and Ulm found, by nanoindentation, that the C-S-H exists in two different forms [28] and exhibits unique nanogranular behavior, which is driven by particle-to-particle contact forces [38]. Using a similar analysis, Vandamme and Ulm later revealed that a third form of C-S-H with significantly high packing density also exists [36]. Furthermore, the fact that C-S-H creeps logarithmically has been established with the help of nanoindentation [37]. However, there are certain important issues that remain unresolved. Mondal et al. [2, 39] found that the elastic modulus of the interfacial transition zone does not increase with the distance from the interface, which is diametrical to the conventional belief. Again, the validity statistical indentation technique applied in the determination of mechanical properties and volume fractions of different phases of cementitious materials has

been questioned [40-43]. One important area, which has not received the attention of experts, is the assessment of the method used in the analysis of nanoindentation data from the cementitious materials. Note that the method used for such assessment is believed to be applicable to a material that is linear, isotropic and homogeneous. It is normally speculated that erroneous mechanical properties may be obtained if the existing method is applied to the heterogeneous materials. The extent to which the accuracy of the method is affected by material's heterogeneity is, however, not known. Therefore, the development of an alternative method is envisioned in this research.

1.2 Problem statement

Nanoindentation load-displacement data are analyzed on the basis of Sneddon's solution for indentation of elastic half-space with rigid axisymmetric indenters. This solution provides a theoretical framework to compute mechanical properties such as indentation (or reduced) modulus and hardness of a material, which requires prior knowledge of two nanomechanical quantities: initial unloading stiffness and area of contact between the indenter and the specimen. In the standard Oliver and Pharr (OP) method, these quantities are evaluated from the unloading curve represented by a power law.

Although the method is widely used in the evaluation of mechanical properties for many materials, there are certain issues that demand further study. First, large variability in the power law parameters, even for a given material, indicates that neither indenter geometry nor materials response to indentation could be characterized on the basis of their magnitude, and thus lack in physical meaning. Second, the area of contact between the indenter and specimen is computed from the area function, which is established with respect to a test material with

known elastic modulus. In the calibration process, corrections, due to the lack of axial symmetry of the indenter and due to the improper boundary condition in the Sneddon's solution, are often omitted. This might have severe consequences on the measured mechanical properties. The accuracy of the methods used to predict the correction factors is still debated in the material science community. Moreover, the OP method yields an erroneous contact area if a material has a tendency to pile-up around the indenter while testing. Third, a large numbers of indentations are needed if the mechanical properties and volume fractions of the different phases present in a heterogeneous material are to be accurately calculated. In this situation, the OP method may prove to be computationally expensive. Therefore, the development of a computationally efficient model capable of predicting the mechanical properties of a material accurately, which does not require the measurement or evaluation of the area of contact at all, is warranted.

1.3 Research goals and objectives

This dissertation deals with the evaluation of nanomechanical properties such as indentation modulus and hardness of a material using the nanoindentation load-displacement record. Overall, the research goal is to develop a sound mathematical model to extract the indentation modulus and the hardness using parameters that can be determined very accurately even for highly heterogeneous samples such as from cementitious materials. The approach is based on experimental observations and numerical simulations of the responses to indentation pertaining to a wide range of materials. Specific objectives that will be met to achieve this research goal are to:

- Identify parameters that can adequately describe the indenter geometry and material response to indentation.
- Modify and extend the existing work-of-indentation approach to determine conventional hardness of a wide range of materials.
- Develop a semi-analytical approach to evaluate the initial unloading stiffness using the elastic work-of-indentation.
- Gain further insight on the nanomechanical response of cementitious materials through empirical observations.
- Develop a nanomechanical properties evaluation method for cementitious materials using the Sneddon's solution incorporating the conventional hardness determined by the modified work-of-indentation approach and initial unloading stiffness evaluated from elastic work.

1.4 Structure of this dissertation

This thesis is structured and organized as follows. Chapter 2 aims at presenting reviews on the different nanomechanical properties' evaluation procedures that are currently adopted in the material science community. Starting with the fundamentals of contact mechanics and followed by the nanoindentation technique, the strengths and weaknesses of each of these methods are examined and areas of potential improvements are identified. Additional requirements for nanoindentation and subsequent data analysis in view of the microstructure of the heterogeneous cementitious materials are also briefly discussed.

Chapter 3 deals with the characterization of nanoindentation load-displacement curves using dimensionless energy based parameters. Elastic and elasto-plastic finite element

simulations are carried out to show that total and elastic energy constants may be used to characterize indenter geometry and material response to indentation, respectively. The effect of tip rounding on the performance of a pyramidal indenter of Berkovich type is explained on the basis of simulation results. Finally, their effectiveness in the determination of nanomechanical quantities such as indenter tip radius, nominal hardness and contact depth are described.

A novel procedure to determine the initial unloading stiffness or contact stiffness from the elastic energy constant is outlined in chapter 4. Analytical differentiation of the power function, capable of representing the unloading response of a material (at least in the initial stage), usually overestimates the contact stiffness. Analysis of the nanoindentation data from materials that have a wide range of recovering capabilities upon the withdrawal of load is presented to find the factors responsible for the overestimation of the contact stiffness.

Chapter 5 focuses on the determination of conventional hardness of a material from the nanoindentation loading curve. A theoretical basis is presented to show that the hardness values determined from the work-of-indentation approach and by the standard Oliver and Pharr method are fundamentally different. A procedure to evaluate conventional hardness from the nominal hardness determined using the work-of-indentation approach incorporating the effect of indenter tip rounding explicitly is outlined in this chapter.

Chapter 6 is devoted to the analysis of the nanoindentation load-displacement data from the cementitious materials. In view of the creeping behavior of the cementitious materials, a dwelling portion is always desirable in the load-displacement curves. With the modification of the total and elastic energy constants, a procedure to evaluate the indentation modulus and hardness for different phases of cementitious materials is developed that essentially

incorporates the modified work-of-indentation approach and contact stiffness determined from the elastic energy constant into the fundamental relation. In addition, this chapter provides further insight on the nanomechanical behavior of the cementitious material through empirical observations.

The last chapter summarizes the conclusions drawn from this study and highlights the key areas where further improvements could be made to expand the capabilities of the model presented herein.

1.5 References

[1] Constantinides, G., and Ulm, F.J. (2004). "The effect of two types of C-S-H on the elasticity of cement-based materials: Results from nanoindentation and micromechanical modeling." *Cement and Concrete Research*, 34, 67-80.

[2] Mondal, P., Shah, S.P., and Marks, L.D. (2008). "Nanoscale characterization of cementitious materials." *ACI Materials Journal*, 105, 174-179.

[3] Corr, D., and Shah, S.P. (2005). "Concrete materials science at the nanoscale." In: Dhir, R.K., Newlands, M.D., and Csetenyi, L.J., editors. Application of Nanotechnology in Concrete Design. Proceedings of the International Conference held at the University of Dundee, Scotland, UK, Thomas Telford, 1-10.

[4] Ulm, F.J. (2003). "Chemomechanics of concrete at finer scales." *Materials and Structures*, 36, 426-438.

[5] Bernard, O., Ulm, F.J., and Lemarchand, E. (2003). "A multiscale micromechanics-hydration model for the early-age elastic properties of cement-based materials." *Cement and Concrete Research*, 33, 1293-1309.

[6] Ulm, F.J., Constantinides, G., and Heukamp, F.H. (2004). "Is concrete a poromechanics materials? – A multiscale investigation of poroelastic properties." *Materials and Structures*, 37, 43-58.

[7] Pichler, C., Lackner, R., and Mang, H.A. (2007). "A multiscale micromechanics model for the autogeneous-shrinkage deformation of early-age Cement based Materials." *Engineering Fracture Mechanics*, 74, 35-58.

[8] Jennings, H.M. (2000). "A model for the microstructure of calcium silicate hydrate in

cement pastes." *Cement and Concrete Research*, 30, 101-116.

[9] Tennis, P.D., and Jennings, H.M. (2000). "A model for two types of calcium silicate hydrates in the microstructure of the cement pastes." *Cement and Concrete Research*, 30, 855-863.

[10] Hershey, A.V. (1954). "The elasticity of an isotropic aggregate of anisotropic cubic crystals." *Journal of Applied Mechanics*, 21, 236-.

[11] Kroner, E. (1977). "Bounds for effective elastic moduli of disordered materials." *Journal of Mechanics and Physics of Solids*, 25, 137-155.

[12] Mori, T. and Tanaka, K. (1973). "Average stress in matrix and average elastic energy of materials with misfitting inclusions." *Acta Metallurgica*, 21, 571-574.

[13] Li, G. (2004). "Properties of high-volume fly ash concrete incorporating nano-SiO_2", *Cement and Concrete Research*, 34, 1043-1049.

[14] Mondal, P., Shah, S.P., Marks, L.D. and Gaitero, Juan J. (2010). "Comparative study of the effects of microsilica and nanosilica in concrete." *Transportation Research Record: Journal of the Transportation Research Board*, 2141, 6-9.

[15] Lin, D.F., Lin, K.L., Chang, W.C., Luo, H.L., and Cai, M.Q. (2008). "Improvements of nano-SiO_2 on sludge/fly ash mortar. *Waste Management*, 28, 1081-1087.

[16] Bjornstrom, J., Martinelli, A., Matic, A., Borjesson, L., and Panas, I. (2004). "Accelerating effects of colloidal nano-silica for beneficial calcium–silicate–hydrate formation in cement." *Chemical Physics Letters*, 392, 242–248.

[17] Ji, T. (2005), "Preliminary study on the water permeability and microstructure of concrete incorporating nano-SiO_2." *Cement and Concrete Research*, 35, 1943–1947.

[18] Jo, B-W., Kim, C-H., Tae, G-h., and Park, J-B. (2007). "Characteristics of cement mortar with nano-SiO2 particles." *Construction and Building Materials*, 21, 1351–1355.

[19] Li, H., Xiao, H-g., and Ou, J-p. (2004). "A study on mechanical and pressure-sensitive properties of cement mortar with nanophase materials." *Cement and Concrete Research*, 34, 435–438.

[20] Qing Y, Zenan Z, Deyu K, and Rongshen, C. (2007). "Influence of nano-SiO2 addition on properties of hardened cement paste as compared with silica fume." *Construction and Building Materials*, 21, 539–545.

[21] Li, H., Zhang, M.-H., and Ou, J.-P. (2006). "Abrasion resistance of concrete containing

nanoparticles for pavement." *Wear*, 260, 1262–1266.

[22] Shah, S.P., Konsta-Gdoutos, M.S., Metaxa Z.S., and Mondal, P. (2009). "Nanoscale modification of cementitious materials." In: Bittnar, Z., Bartos, P.J.M., Nemecek, J., Smilauer, V., Zeman, J., editors. Nanotechnology in construction 3. Proceedings of the third international symposium on nanotechnology in construction. Springer, 125–30.

[23] Konsta-Gdoutos, M.S., Metaxa, Z.S., and Shah, S.P. (2010). "Multi-scale mechanical and fracture characteristics and early-age strain capacity of high performance carbon nanotube/cement nanocomposites." *Cement and Concrete Composites*, 32, 110-115.

[24] Metaxa, Z.S., Seo, J.-W. T., Konsta-Gdoutos, M.S., Hersam, M.C., and Shah, S.P. (2012). "Highly concentrated carbon nanotube admixture for nano-fiber reinforced cementitious materials", *Cement and Concrete Composites*, 34, 612-617.

[25] Yazdanbakhsh, A. and Grasley, Z. (2012). "The theoretical maximum achievable dispersion of nanoinclusions in cement paste." *Cement and Concrete Research*, 42, 798-804.

[26] Sanchez, F., and Sobolev, K. (2010). "Nanotechnology in concrete – A review." *Construction and Building Materials*, 24, 2060-2071.

[27] Velez, K., Maximilien, S., Demidot, D., Fantozzi, G., and Sorrentino, F. (2001). "Determination by nanoindentation of elastic modulus and hardness of pure constituents of Portland cement clinker." *Cement and Concrete Research*, 31, 555-561.

[28] Constantinides, G., Ulm, F.J., and Van Vliet, K.J. (2003). "On the use of nanoindentation for cementitious materials." *Materials and Structures*, 36, 191-196.

[29] Hughes, J. J., and Trtik, P. (2004). "Micro-mechanical properties of cement paste measured by depth-sensing nanoindentation: A preliminary correlation of physical properties with phase type." *Materials Characterization*, 53, 223-231.

[30] Mondal, P., Shah, S.P., and Marks, L.D. (2007). "A reliable technique to determine the local mechanical properties at the nanoscale for cementitious materials." *Cement and Concrete Research*, 37, 1440-1444.

[31] Zhu, W., Hughes, J. J., Bicanic, N., and Pearce, C. J. (2007). "Nanoindentation mapping of the mechanical properties of cement paste and natural rocks." *Materials Characterization*, 58, 1189-1198.

[32] Nemecek, J. (2009). "Creep effects in nanoindentation of hydrated phases of cement pastes." *Material Characterization*, 60, 1028-1034.

[33] Pichler, C., and Lackner, R. (2009). "Identification of logarithmic-type creep of

calcium-silicate-hydrates by means of nanoindentation." *Strain*, 45, 17-25.

[34] Jones, C.A., and Grasley Z.C. (2011). "Short-term creep of cement paste during nanoindentation." *Cement and Concrete Composites*, 32, 12-18.

[35] Jones, C.A., Grasley Z.C., and Ohlhausen, J. A. (2012). "Measurement of elastic properties of calcium silicate hydrate with atomic force microscopy." *Cement and Concrete Composites*, 34, 468-477.

[36] Vandamme, M., Ulm, F.J., and Fonollosa, P. (2010). "Nanogranular packing of C-S-H at substochiometric conditions." *Cement and Concrete Research*, 40, 14-26.

[37] Vandamme, M., and Ulm, F.J. (2009). "Nanogranular origin of concrete creep." *Proceedings of the National Academy of Sciences*, 106, 10552-10557.

[38] Constantinides, G., and Ulm, F.J. (2007). "The nanogranular nature of C-S-H." *Journal of the Mechanics and Physics of Solids*, 55, 64-90.

[39] Mondal, P. Shah, S.P., and Marks, L.D. (2009). "Nanomechanical properties of interfacial transition zone in concrete." In: Bittnar, Z., Bartos, P.J.M., Nemecek, J., Smilauer, V., Zeman, J., editors. Nanotechnology in construction 3. Proceedings of the third international symposium on nanotechnology in construction. Springer, 315-320.

[40] Trtik P., Munch, B., and Lura, P., (2009). "A critical examination of statistical nanoindentation on model materials and hardened cement pastes based on virtual experiments." *Cement and Concrete Composites*, 31, 705-714.

[41] Ulm, F.J., Vandamme, M., Jennings, H. M., Vanzo, J., Bentivegna, M., Krakowiak, K.J., Constantinides, G., Bobko, C.P., and Van Vliet, K.J. (2010). "Does microstructure matter for statistical nanoindentation techniques?" *Cement and Concrete Composites*, 32, 92-99.

[42] Lura, P., Trtik P., and Munch, B. (2011). "Validity of recent approaches for statistical nanoindentation of cement pastes." *Cement and Concrete Composites*, 33, 457-465.

[43] Davydov, D., Jirasek, M., and Kopecky, L. (2011). "Critical aspects of nano-indentation technique in application to hardened cement paste." *Cement and Concrete Research*, 41, 20-29.

CHAPTER 2

PRINCIPLE AND METHODS OF NANOINDENTATION

2.1 Introduction

Nanoindentation is an important and reliable experimental technique that can be used in the mechanical characterization of a small volume of materials. In this method, a smooth surface of a material is indented with a probe to acquire the load vs. penetration depth history (a cycle of loading and unloading curves). The load-penetration curves so obtained contain useful information that need to be transformed into meaningful mechanical properties such as elastic modulus, hardness, yield strength, strain hardening exponent, fracture toughness, contact creep modulus, etc. However, to carry out such analysis, a proper understanding and interpretation of the indentation data is essential. Several methods with varying domain of application are available in the literature. These methods may be broadly classified either as a reverse or as a forward analysis tools. In the reverse analysis, the material properties of interest are extracted from the nanoindentation data. The material response to indentation is modeled by assuming the suitable values of material properties in a typical forward analysis. While the reverse analysis is largely empirical, the forward analysis is usually performed using the finite element method. These methods can also be grouped depending on the portion of the load-displacement curves used in the analysis. For instance, the method proposed by Oliver and Pharr may be categorized as an unloading curve method as it uses the information contained in the unloading response only. Majority of the nanoindentation data analysis procedures employ the Sneddon's solution for indentation of elastic half-space by a rigid indenter to evaluate the elastic modulus and hardness of a material.

Until recently, this experimental technique has been considered highly suitable for a material that is linear, isotropic and homogeneous. Now, it is extensively being used in the characterization of natural composites such as biological and cementitious materials. The analysis of indentation data from such materials involves the use of some elementary statistics relations. In this chapter, several nanoindentation data analysis procedures, along with their underlying principles, are reviewed to identify the potential areas of improvement in view of the response of heterogeneous materials to indentation.

2.2 Sneddon's solution

Suppose that a punch can be described as a solid of revolution by rotating an arbitrary function given by $z = f(\rho)$ about the z-axis, as shown in figure 2.1. When a load, P, is applied to the punch, it is displaced into the elastic half-space through a distance, h forming a circle of contact with radius a at the surface. Sneddon [1] derived, using Hankel transforms, the following expressions for h and P, respectively.

$$h = \int_{x=0}^{x=1} \frac{f'(x)\,dx}{\sqrt{1-x^2}} \tag{2.1}$$

$$P = \frac{4\mu a}{(1-\nu)} \int_{x=0}^{x=1} \frac{x^2 f'(x)\,dx}{\sqrt{1-x^2}} \tag{2.2}$$

where $f(x)$ is the indenter shape function expressed in terms of a non-dimensional variable x defined by $x = \rho / a$ such that $0 < x < 1$ in the region of contact. Oliver and Pharr [2] showed that the initial unloading stiffness or contact stiffness is independent of the indenter geometry. To prove this, Eq. (2.2) may be written in the following form:

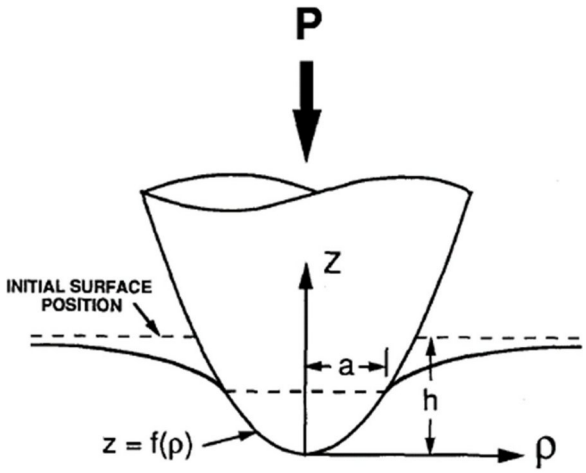

Figure 2.1: The geometry used by Sneddon's in the derivation of the load-displacement relations for a rigid punch of arbitrary profiles [2].

$$P = \frac{4\mu a}{(1-\nu)}\left[\int_{x=0}^{x=1} \frac{f'(x)\,dx}{\sqrt{1-x^2}} - \int_{x=0}^{x=1} \sqrt{1-x^2}\, f'(x)\,dx\right] \tag{2.4}$$

If differentiated with respect to x, Eq. (2.4) will boils down to

$$\frac{dP}{da} = \frac{4\mu a}{(1-\nu)}\frac{dh}{da} + \frac{P}{a} - \frac{4\mu a}{(1-\nu)}\frac{d}{da}\int_{x=0}^{x=1} \sqrt{1-x^2}\, f'(x)\,dx \tag{2.4}$$

Note that second and third terms in the above expression are equal and cancel out (detailed proof is given in Oliver and Pharr [2]) giving a simplified expression for the contact stiffness, which may be expressed as:

$$\frac{dP}{dh} = \frac{dP/da}{dh/da} = \frac{4\mu a}{(1-\nu)} \tag{2.5}$$

By using relations $A = \pi a^2$ and $\mu = E/[2(1+\nu)]$, a fundamental relation among the contact stiffness, the elastic modulus and the area of contact may be obtained as:

$$S = \frac{dP}{dh} = \frac{2}{\sqrt{\pi}} \sqrt{A} \frac{E}{\left(1-\nu^2\right)} \tag{2.5}$$

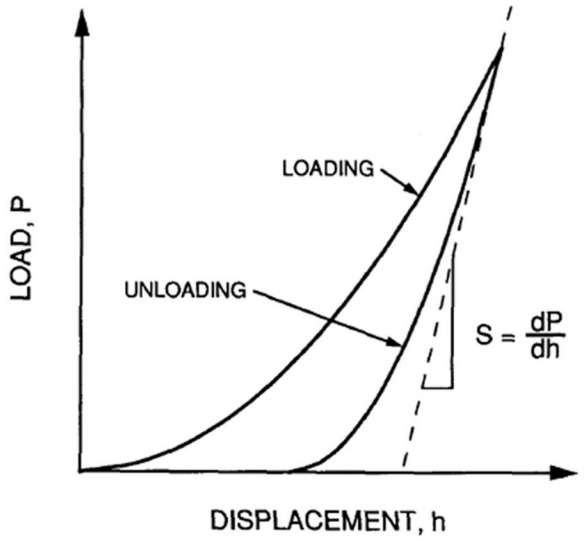

Figure 2.2: Typical indentation load-displacement data.

where S is the initial unloading stiffness or contact stiffness, E is the elastic modulus and ν is the Poisson's ratio of the elastic half-space. Note that the above equation is independent of the indenter geometry and is applicable to any profile describable as a solid of revolution. The contact stiffness may be determined as a slope of the unloading curve at the point of the maximum depth of penetration. Application of Eq. (2.5) in the determination of elastic modulus requires an independent measurement of the area of contact and reasonable estimates of the Poisson's ratio of a material.

2.3 Nanoindentation

As explained above, one needs experimental load-displacement curves in order to determine the contact stiffness, which can be reliably and conveniently obtained from a depth-sensing instrumented indentation. Nanoindentation is a type of depth sensing

instrument, which measures the load and corresponding displacement with a resolution better than 1nN and 0.02nm, respectively. In this technique, a material with smooth surface indented to record the load-displacement response during both penetration as well as withdrawal of the punch. The equipment can be operated either in the load or in the displacement-controlled mode. It is preferable to introduce peak load hold period in the loading sequence to minimize the effect of non-elastic deformation on the unloading response. Sometimes several cycles of loading/unloading are carried out to minimize the effect of reverse plasticity. Recent nanoindentation equipment is fitted with Scanning Probe Microscope (SPM) which can capture images with a nanoscale resolution. Nanoindentation usually leaves only a small imprint, and thus it is regarded as a nondestructive test method.

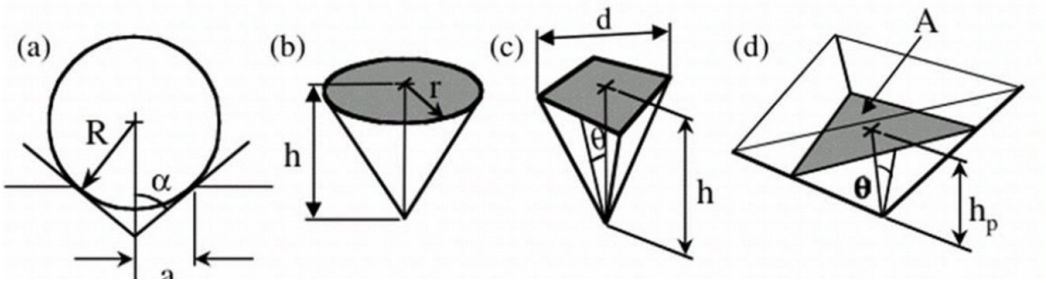

Figure 2.3: Indentation parameters for (a)spherical, (b) conical, (c) Vickers, and (d) Berkovich indenters [3].

Indenters of different geometry such as conical, pyramidal and spherical of various sizes are employed in the nanoindentation experiments. Some of these are depicted in figure 2.3. Pyramidal or conical indenters are geometrically self-similar implying that the ratio of the length of the diagonal or radius of circle of contact to the depth of indentation remains always constant for increasing indenter load [3]. Spherical indenter, unlike conical or pyramidal indenters, is not self-similar. With the increase in load on the indenter, the radius

of circle of contact increases faster than the penetration depth. The self-similarity is a desirable indenter property that has important implications in the indentation measurements and analyses [4].

A three-sided Berkovich pyramid is the most commonly used indenter in small scale indentation. This type of indenter is relatively easier to construct as compared to the four-sided Vickers indenter. A Berkovich indenter with a face angle of 65.27^0 has the same projected area-to-depth ratio as the Vickers indenters. The tip radius of a new Berkovich indenter varies in the range 50-100nm. A cube-corner is another type of pyramidal indenter that is also frequently used in the indentation measurement. Berkovich and cube-corner indenters are equivalent to a conical indenter with a half-included angle equal to 42.28^0 and 70.32^0, respectively.

The choice of an indenter with a particular geometry also depends on the type of material properties intended to be measured from the indentation test. For instance, a cube-corner is a preferred choice in the determination of the fracture toughness of a brittle material [3]. Owing to the sharpness of the cube corners, much higher stresses and strains are produced in the region of contact. As a result, well-defined cracks are formed around the hardness impression, which facilitates the measurement of this kind of property of a material. The stress-strain curve of a material can be obtained from the indentation measurement as well, but only with a spherical indenter. Cheng and Cheng [5] concluded that the load-displacement curves obtained using conical or pyramidal indenters can produce a multiple stress-strain curves. Therefore, a unique stress-strain relationship is not possible using these indenters. A spherical indenter provides smooth transition from elastic to elastic-plastic contact. This makes a spherical indenter highly suitable for measuring the mechanical

properties of soft material. Contact damage in service conditions could be replicated with the help of a spherical indenter.

2.4 Indenter geometry and Sneddon's solution

Pyramidal indenters are the most common indenters used in the nanoindentation experiment which does not confirm to the axisymmetric conditions. Since Eq. (2.5) is strictly applicable when the indenter geometry is described as a solid of revolution, a modification to this equation is required if the load-displacement curves are to be acquired with a pyramidal indenter. King [4], based on numerical studies, found that the shape corrected fundamental relation may be written as:

$$S = \beta \frac{2}{\sqrt{\pi}} \sqrt{A_c} \frac{E}{\left(1-\nu^2\right)} \tag{2.6}$$

Constant β accounts for the lack of axial symmetry for pyramidal indenters and is equal to 1.034 and 1.012 for indenters with triangular and square cross-sections, respectively. Researchers, however, have diverging views regarding the determination of this shape correction factor β [7-15]. A review by Oliver and Pharr [7] suggests that for the Berkovich indenter it should fall in the range 1.023 to 1.085, the value 1.05 being a good choice. Strader et al. [9] showed that it depends on the half included angle of the indenter and found a mean value of 1.055 and 1.097 for Berkovich and cube-corner indenter, respectively. They found that β decreases at small indenter angle, but increases when the indenter angle is in the excess of 55^0. This trend in its variation is remained unexplained. Most recently, Meza et al. [12] showed that this factor depends on the maximum penetration depth and the indenter tip

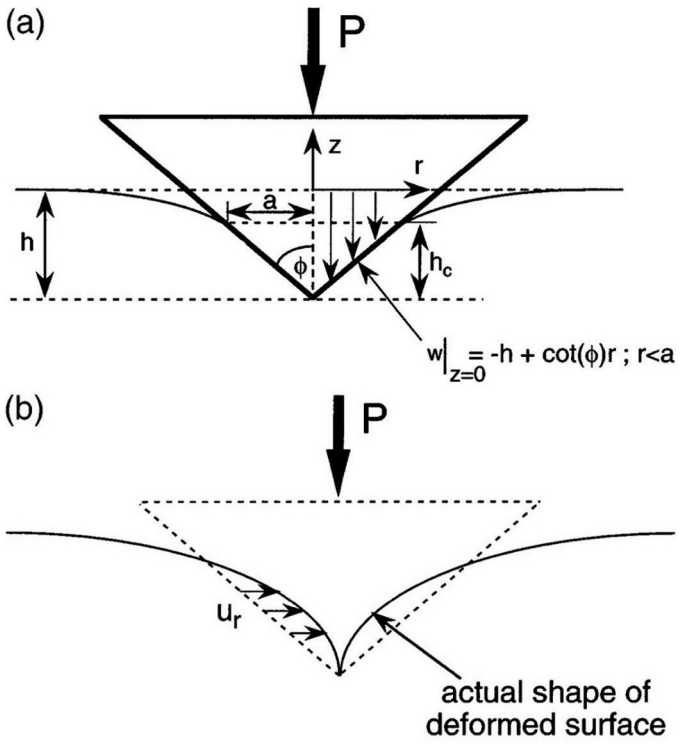

Figure 2.4: (a) Geometry used by Sneddon to describe indentation of an elastic half-space by a right circular cone. (b) Shematic representation of of the actual shape of the deformed surface predicted by Sneddon's analysis whne the radial displacements are taken into account [13].

radius. Using finite element method and dimensional analysis, they derived an expression for β as:

$$\beta = \frac{2}{\pi}\frac{\left(h_{\max}+\xi\right)}{\left[h_{\max}-\frac{\varepsilon}{2}\left(h_{\max}+\xi\right)\right]} \tag{2.7}$$

where, $h_{\max}$ is the maximum depth of penetration, ξ is the apex height, which is a measure of the tip bluntness, and ε is the geometry factor. It has been shown that Eq. (2.5) underestimates the contact stiffness due to the improper boundary condition imposed by Sneddon while describing the indentation of an elastic half-space by a right circular cone. He,

by neglecting the radial displacements, assumed that the shape of the deformed surface in the region of contact is also conical, as shown in figure 2.4a. Hay et al. [13] suggested that such assumption is valid only in the case of an incompressible material. When the radial displacements are finite, the actual deformed surface is subtly curved, as shown in figure 2.4b. They introduced a correction factor γ in the fundamental relation to account for the actual boundary condition. Therefore, Eq. (2.6) may be rewritten as:

$$S = \gamma\beta \frac{2}{\sqrt{\pi}} \sqrt{A_c} \frac{E}{\left(1-\nu^2\right)} \tag{2.7}$$

According to Hay et al. [13], this correction factor is a function of Poisson's ratio of a material and the half-included angle θ of an indenter. For a Berkovich and Cube-corner indenters, γ is given by Eqs. (2.8) and (2.9), respectively.

$$\gamma = \pi \frac{\pi/4 + 0.15483073 \cot\theta \dfrac{\left(1-2\nu\right)}{4\left(1-\nu\right)}}{\left(\pi/2 - 0.83119312 \cot\theta \dfrac{\left(1-2\nu\right)}{4\left(1-\nu\right)}\right)^2} \tag{2.8}$$

$$\gamma = 1 + \frac{\left(1-2\nu\right)}{4\left(1-\nu\right)\tan\theta} \tag{2.9}$$

θ is, respectively, equal to 42.28^0 and 70.32^0 for cube-corner and Berkovich indenters.

Xu and Li [14] found that the first-order correction factor given by Eq. (2.8) is applicable to conical indentation of elastic deformation-dominated materials and not to Berkovich indentation. They developed, on the basis of finite element simulations of indentation on elastic as well as elasto-plastic materials. A revised relationship for the estimation of correction factor, which has the form given by Eq. (2.10).

$$\gamma = 1.14\pi \frac{\pi/4 + 0.05544 \cot\theta \dfrac{(1-2\nu)}{4(1-\nu)}}{\left(\pi/2 - 0.2976 \cot\theta \dfrac{(1-2\nu)}{4(1-\nu)}\right)^2} \tag{2.10}$$

It is argued that the above relationship gives a better estimation of correction factor for Berkovich indentations on both elastic and elasto-plastic materials. One important point, which is worth mentioning here, is that there exists ambiguity not only in the values of these correction factors, but also in their understanding. Researchers often consider the correction factors β and γ to be the same [9]. It should be noted that β is related to the shape of the indenter and is always equal to 1.0 as far as an indenter is describable as a solid of revolution. On the other hand, γ is related to the shape of the deformed surface and should be applied to the Sneddon's solution irrespective of the type of indenter. This was well recognized by Troyon and Lafaye [15] and applied in their studies. Xi and Lu also suggested that both of these correction factors must be considered while analyzing the load-displacement data acquired with the help of a pyramidal indenter to obtain accurate values of mechanical properties. They suggested that a combined correction factor α obtained by the multiplication of β and γ may be used to account for both of these shapes. Eq. (2.10), in fact, determines α. This new factor can also be determined by indenter tip modeling and two-slope method [15]. However, their effectiveness in the determination of mechanical properties of a material is yet to be fully realized. Finally, it is important to note that the omission of these correction factors has more severe consequences on the measured hardness than on the elastic modulus.

2.5 Determination of mechanical properties

As mentioned earlier, mechanical properties of a material may be determined from the information contained in the load-displacement curves obtained from a nanoindentation experiment. Several methods are available in the literatures which differ mainly in the interpretation of nanoindentation data [16-25]. Some of these methods are discussed here.

2.5.1 Oliver and Pharr method

One of the most commonly used methods for analyzing nanoindentation load–displacement data is that proposed by Oliver and Pharr [17]. The method is based on the premise that the behavior of the material during unloading is largely elastic, in which the elastic punch theory can be applied to extract its hardness and elastic modulus. The use of elastic punch theory as given by Eq. (2.5) requires evaluation of the initial unloading stiffness and measurement of the area of contact between the indenter and the specimen. Once the measurement of contact area is complete, the hardness $\left(H\right)$ of a material may be determined from its fundamental definition as:

$$H = \frac{P_{\max}}{A_c} \tag{2.11}$$

where $P_{\max}$ is the peak indentation load, and A_c is the projected contact area at peak load. The initial unloading stiffness may be determined analytically by evaluating the derivative of the expression used to represent the unloading curve. Oliver and Pharr [4] suggested that the experimental unloading curve may be best described using a power-law relation, which has the following form.

$$P = A\left(h - h_f\right)^m \tag{2.12}$$

where h_f is a residual depth of penetration, A and m are the coefficient and exponent of the power-law, respectively. These parameters are determined by non-linear least square fitting of the experimental unloading data. Derivative of Eq. (2.12) evaluated at the maximum depth of penetration gives the initial unloading stiffness as:

$$S = \left(\frac{dP}{dh}\right)_{h=h_{\max}} = mA\left(h_{\max} - h_f\right)^{m-1} \tag{2.13}$$

In this way, the first parameter of the Sneddon's solution is determined in the standard Oliver and Pharr method. The projected contact area may be measured from the hardness impression left after the withdrawal of the punch. To avoid the difficulty involved in imaging the hardness impression, Oliver and Pharr developed a computational method to determine the projected contact area, which may be described as follows. Referring to figure 2.5, the penetration depth h, at any instant, may be considered as a sum of the contact depth $\left(h_c\right)$ and the material surface deflection $\left(h_s\right)$, and, the following relation holds at the maximum

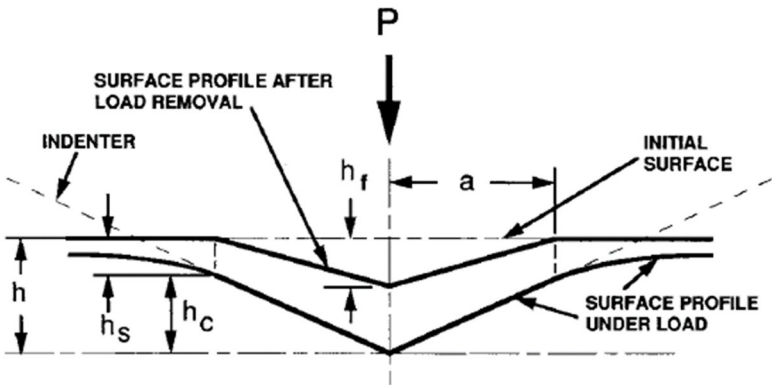

Figure 2.5: A scematic representation of a section through an indentation showing various quantities used in the analysis [17].

penetration depth.

$$h_{\max} = h_c + h_s \tag{2.14}$$

The surface deflection is proportional to the peak indentation load to initial unloading stiffness ratio, and using Eq. (2.14), the depth along which the contact is made may be expressed as:

$$h_c = h_{\max} - \varepsilon \frac{P_{\max}}{S} \tag{2.15}$$

where ε is a constant which depends on the geometry of the indenter: for a Berkovich indenter $\varepsilon = 0.75$. However, its dependence on the power-law exponent has been described in some studies [26-29]. Pharr and Bolshakov [27] showed that it varies according to the

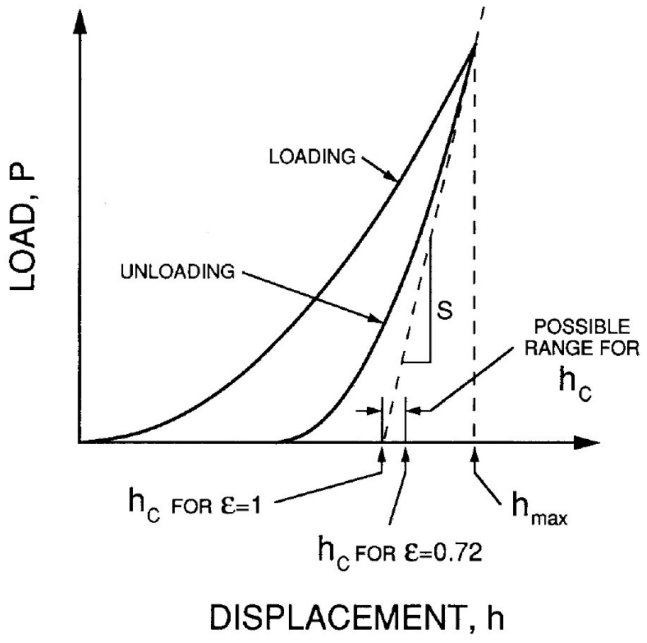

Figure 2.6: A schematic representation of load versus indenter displacement showing quantities used in the analysis as well as a graphical interpretation of the contact depth [17].

relation given by Eq. (2.16).

$$\varepsilon(m) = \left[1 - \frac{2(m-1)\Gamma\left(\frac{m}{2(m-1)}\right)}{\sqrt{\pi}\Gamma\left(\frac{1}{2(m-1)}\right)} \right] \tag{2.16}$$

Depending upon ε value, h_c varies in a range as indicated in figure 2.6. When geometric factor is 0.72, the contact depth corresponds to the plastic depth as defined by Doerner and Nix [16]. With known value of contact depth, the contact area may be determined. For an ideally sharp conical indenter, it is given by: $A_c = 24.56h_c^2$. As some bluntness at the tip of the indenter is inevitable, the determination of contact area is not straight forward. The tip bluntness can be properly accounted for by constructing an area function. This is an iterative procedure and is determined using a test material whose elastic modulus is precisely known. Steps involved in the area function technique are well described in Ref. [17]. The area function is expressed as an eight-parameter harmonic average of polynomials as expressed by:

$$A_c = C_0 h_c^2 + \sum_{i=1}^{7} C_i h_c^{1/2^i} \tag{2.17}$$

Constants appearing inside the summation in Eq. (2.17) take blunting at the tip into account and are determined by fitting the area vs. contact depth data obtained from a test material. Knowing the values of contact stiffness and the area of contact, the hardness and the reduced elastic modulus of a material may be determined with the help of Eqs. (2.5) and (2.11). If an indenter has finite deformations, the elastic modulus may be determined using the following relations.

$$\frac{1}{E_r} = \frac{1-\nu_i^2}{E_i} + \frac{1-\nu_s^2}{E_s} \tag{2.18}$$

where E_s, ν_s are the elastic modulus and Poisson's ratio of materials; and E_i and ν_i are that of the indenter. For diamond, the elastic constants $E_i = 1140GPa$ and $\nu_i = 0.07$ are often used. In general, the procedure described above yields elastic modulus and hardness values with accuracy better than 5% for a wide range of materials [30].

Although the Oliver and Pharr method is very precise and refined, it has some limitations as well. The contact depth determined in this manner becomes erroneous if a material shows significant pile-up around the hardness impression. Whether a material has actually piled-up may be decided based on the value of $h_f / h_{\max}$ ratio; no pile-up if it is less than 0.70. Thus, the method fails to estimate the contact depth if this ratio is greater than 0.70. It has also been reported that the method yields erroneous value when it is applied to the data from heterogeneous materials [24] or from viscoelastic material [31]. However, the extent to which the accuracy of this method is affected by the heterogeneity of a material is not known.

Sawa and Tanaka [32] reported that it may not be possible to obtain a unique area function according to the Oliver and Pharr method. Its dependence on the initial guess precludes it from being unique. Furthermore, area function is generally established to take the bluntness of the tip of the indenter. In fact, an indenter tip deteriorates with every indent and to maintain the repeatability of the test results one need to establish area function at regular intervals, which is very cumbersome. It also depends on the material and the type of nanoindentation equipment. The omission of the correction factors, as discussed previously, in the calibration process might severely affect the accuracy of the contact area.

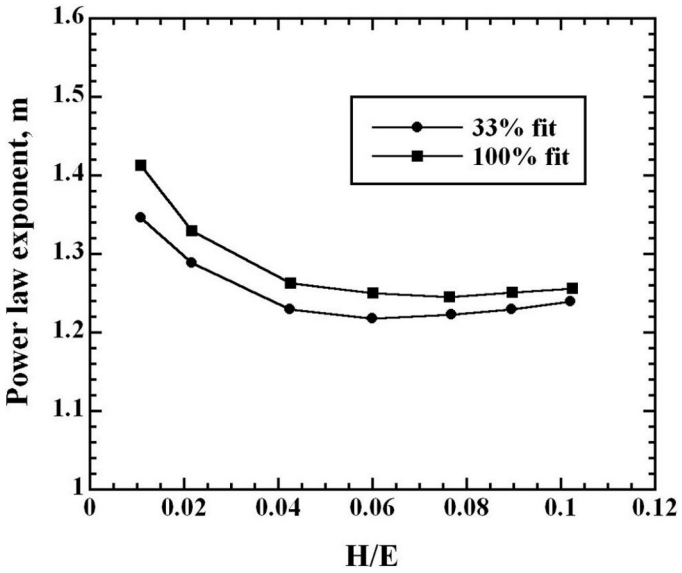

Figure 2.7: Influence of the amount of data included in the fitting procedure on the power-law exponent [39].

The interpretation of the unloading response on the basis of the power-law exponent has been questioned by several researchers [33-39]. The exponent is supposed to be the indicator of the punch geometry. It is equal to 1, 1.5 and 2, respectively, for flat, solid of revolution and conical punch. When an experimental unloading curve acquired with a Berkovich indenter is fitted by a power-law, the resulting exponent, according to Oliver and Pharr, may fall in the range 1.2-1.6, which was later justified on the basis of the "effective indenter shape" theory [27]. Gone et al. [33] suggested that the unloading response obtained by a Berkovich indenter can be described by a conical punch approximation provided the residual stress that arises during indentation is properly accounted for in the fitting function. However, the exponent greater than 2 can be observed, even in the case of a material for which the mechanical properties are accurately determined using power-law [34-37]. These parameters are found to depend on the peak indentation load varies considerably even for a

material. Result from a critical examination by Marx and Balke [39] suggests that the exponent also depends on the fraction of the unloading data used in the fitting process. Figure 2.7 shows the effect of amount of data on m for a wide range of materials. VanLandingham et al. [39] reported that the power-law is not suitable to describe the unloading response from polymers they tested. Instead, they used spline function to get accurate fit. Therefore, an alternative way to represent an unloading curve is desirable.

2.5.2 Hainsworth et al. Method

Unlike the Oliver and Pharr method, this method utilizes the information contained in a loading curve in the determination of elastic modulus or hardness of a material. It has been shown that a loading curve obtained with an ideally sharp indenter may be well described by a relation in which the load varies linearly with the displacement squared. In notation,

$$P = K_{\exp} h^2 \tag{2.19}$$

The proportionality constant $K_{\exp}$, which depends on the material properties and on the indenter type, is obtained through curve fitting of the experimental data. By considering the elasto-plastic deformations that occur during indentation, Hainsworth et al. [18] derived an alternative expression for the loading curve as:

$$P = E\left(\Phi_m \sqrt{\frac{E}{H}} + \psi_m \sqrt{\frac{H}{E}}\right)^{-2} h^2 \tag{2.20}$$

where E and H, respectively, describe the modulus of elasticity and hardness of a material under consideration. Indenter constants Φ_m and Ψ_m relate the characteristic contact radius of

a rigid plastic indenter to plastic and elastic components of the total deformations, respectively. According to Hainsworth et al. [18], these constants depend only on the indenter type; for a sharp Berkovich indenter, they are found to be 0.194 and 0.930. Elastic modulus of a material may be determined by equating the coefficients of h^2 in Eqs. (2.19) and (2.20) provided the hardness of that material is known. Thus, we may write

$$E\left(\Phi_m\sqrt{\frac{E}{H}}+\psi_m\sqrt{\frac{H}{E}}\right)^{-2}=K_{\exp} \tag{2.21}$$

Jha et al. [19] developed a mathematical basis for the determination of indenter constants, which is briefly discussed here. The subscript 'm' is dropped from Φ_m and Ψ_m in order to treat them as variables so that a relationship between the two can be established. Rearranging Eq. (2.21) in terms of Φ and Ψ, one may write:

$$\frac{\Phi}{H^*}+\frac{\Psi}{E^*}=1 \tag{2.22}$$

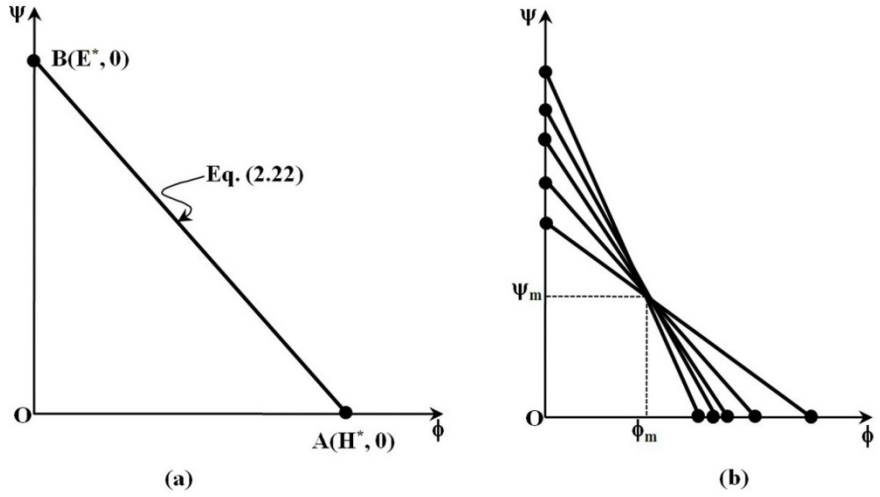

Figure 2.8: (a) Relationship between ϕ and ψ; and (b) family of lines in the ϕ and ψ space [19].

where,

$$H^* = \sqrt{\frac{H}{K_{exp}}} \qquad E^* = \frac{E}{\sqrt{HK_{exp}}} \tag{2.23}$$

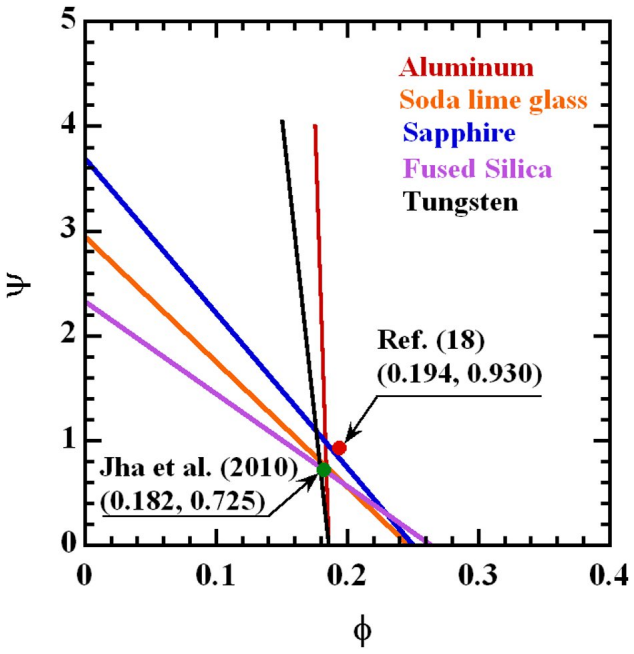

Figure 2.9: Determination of indenter constants using the experimental data from Ref. [17].

Eq. (2.22) represents a straight line with intercepts H^* and E^* in ϕ and ψ space, respectively, as shown in figure 2.8a and provides the basis for the determination of indenter constants. Terms H^* and E^* are referred to as normalized hardness and elastic modulus, respectively. It can be inferred that ϕ and ψ are linearly dependent, and any pair of values lying on the locus defined by Eq. (2.22) will give a best fit to the experimental curve. While H and E are material specific, K_{exp} depends on both material type and the geometry of the indenter. Thus, the line represented by Eq. (2.22) is unique for a material indented with a

punch of specified geometry. If the indenter constants depend only on the indenter geometry, lines from different materials should intersect at one point as shown in figure 2.8b. The coordinates of the point of intersection gives the values of the indenter constants. To verify this, Jha et al. [19] made use of the experimental data mentioned in the paper by Oliver and Pharr [17]. As shown in figure 2.9, lines from all the materials, except sapphire, intersect at one point giving rise to values of ϕ and ψ as 0.182 and 0.725, respectively. The deviation of a sapphire line from the intersecting point may be attributed to the bluntness at the tip of the indenter. Note that the parameter $K_{\exp}$ is strongly affected by the indenter tip radius. Again, a blunt indenter may behave like an ideally sharp indenter if the maximum depth of penetration is sufficiently large as compared to the tip radius. Further study is required to show the dependence of the indenter constants on the factors such as tip radius and half-included angle of the indenter. If the indenter constants and hardness values are precisely known, the elastic modulus may be calculated from:

$$E = \frac{H\psi_m \sqrt{K_{\exp}}}{\sqrt{H} - \phi_m \sqrt{K_{\exp}}} \tag{2.24}$$

2.5.3 Malzbender et al. Method

A P-h^2 relation similar to Eq. (2.20) is also derived by Malzbender et al. [20]. Their derivation, however, is based on the Sneddon's solution given by Eq. (2.5) and the normal definition of the hardness. Using the condition given by Eq. (2.14), they obtained a relationship between the load and penetration depth, which may be expressed as:

$$P = E_r \left(\frac{1}{\sqrt{24.50}} \sqrt{\frac{E_r}{H}} + \varepsilon \sqrt{\frac{\pi}{4}} \sqrt{\frac{H}{E_r}} \right)^{-2} h^2 \tag{2.25}$$

Notice that Eqs. (2.20) and (2.25) differ in at least two aspects; it does not require the determination of indenter constants and uses reduced modulus in place of Young's modulus. By comparing these two equations, one would obtain $\Phi = 0.202$ and $\Psi = 0.638$ for $\varepsilon = 0.72$; these values are very close to the value determined by Hainsworth et al. and Jha et al. The difference, according to Malzbender et al., arises probably due to the assumption of non-perfect indenter used in Eq. (2.20). No indenter is perfectly sharp in reality; some rounding at the tip is inevitably present. Thus, Eq. (2.25) cannot be employed to describe the load-displacement curve acquired with a blunt indenter. Using the area function suitable for blunt indenter [20, 41-42], they propose a revised equation in the following form:

$$P = E_r \left(\frac{1}{\sqrt{C}} \sqrt{\frac{E_r}{H}} + \varepsilon \sqrt{\frac{\pi}{4}} \sqrt{\frac{H}{E_r}} \right)^{-2} (h + \xi)^2 \tag{2.25}$$

where ξ is the apex height as shown in figure 2.10.

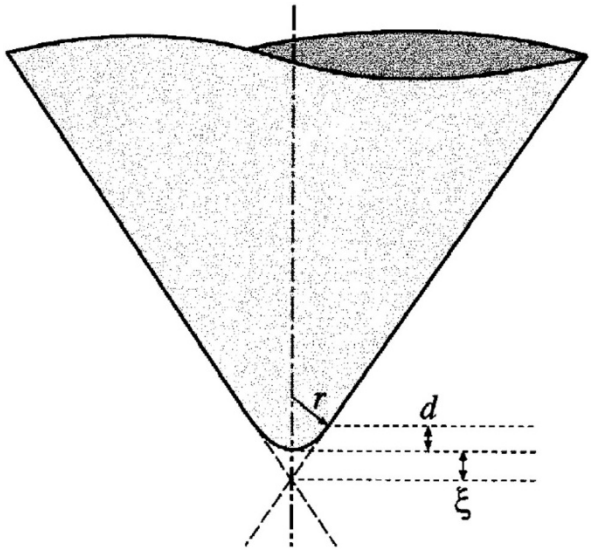

Figure 2.10: Schematic diagram showing the geometry of a rounded indenter tip [20].

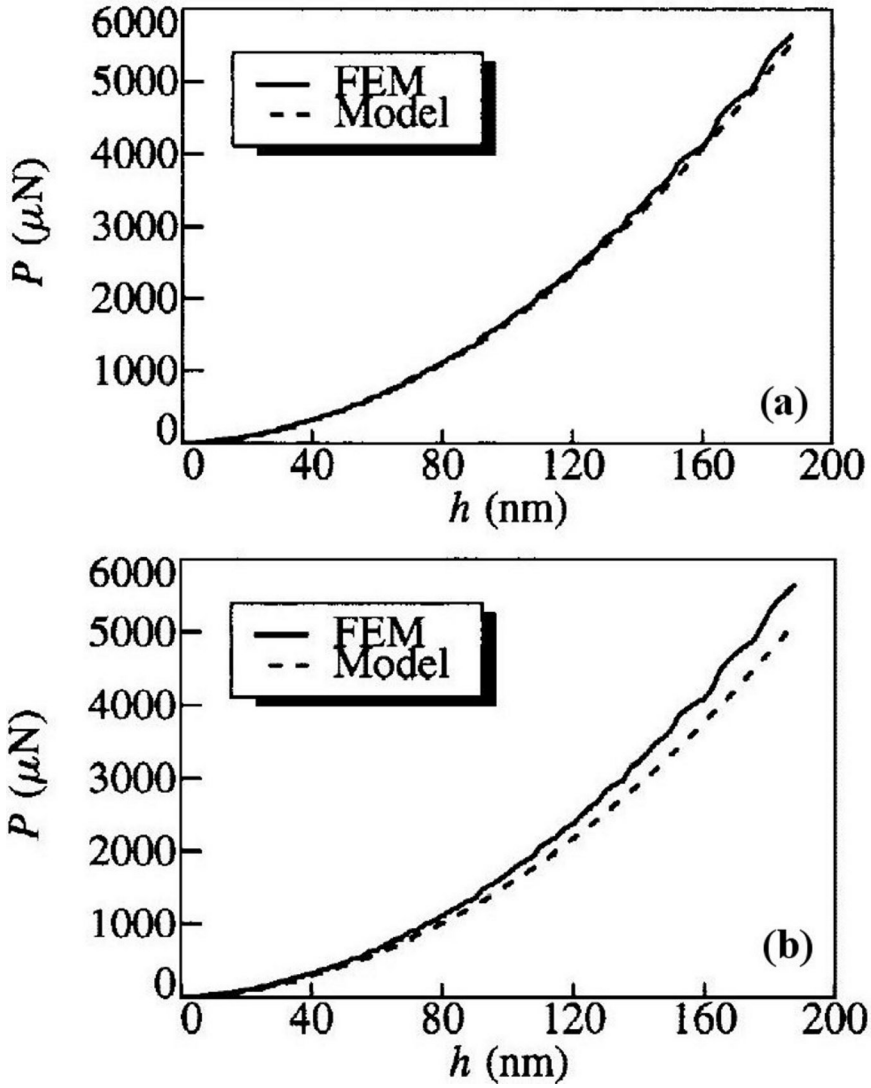

Figure 2.11: Comparison the load-displacement curves: (a) FEM vs. Eq. (2.25); and (b) FEM vs. Eq. (2.20) when $C = 24.51, \xi = 6.22nm, H = 8.0GPa$ & $E = 150GPa$ *[20].*

Malzbender et al. found that Eq. (2.25) models the loading curve obtained by the finite element simulation more closely as compared to Eq. (2.25), as shown in figure 2.11. Thus, if the elastic modulus and hardness of a material along with the apex height of the indenter are known, then the material response to indentation may be predicted with the help of Eq.

(2.25). Conversely, if $K_{\exp}$, ξ and E (or H) are known, then H (or E) may be determined. Since either the elastic modulus or the hardness of material can be determined from the analysis of the loading curve, these methods are more suitable for the forward analysis. Loading curve methods do not require calculation of the contact area at all, and thus has clear advantage over the conventional Oliver and Pharr method. One of the main disadvantages of these methods is that either E or H, not both, can be determined.

A modified expression for the loading curve is derived by Troyon and Martin [21]. They expressed the geometric factor as a function of the exponent and incorporated the Hay's correction factor γ in Eq. (2.25). The equation for a loading curve in the modified form is:

$$P = E_r \left(\frac{1}{\sqrt{C}} \sqrt{\frac{E_r}{H}} + \frac{\varepsilon(m)}{\gamma} \sqrt{\frac{\pi}{4}} \sqrt{\frac{H}{E_r}} \right)^{-2} (h + \xi)^2 \tag{2.26}$$

Using the nanoindentation data from fused silica, Troyon and Martin concluded that a close agreement between the hardness values determined from the analysis of loading curve and the Oliver and Pharr method may be obtained if above mentioned corrections are applied.

2.5.4 Work-of-indentation approach

The hardness of a material can also be determined from the information contained in the loading curve. An area under the loading curve is a measure of the energy dissipated or the total work done during indentation. The elastic component of the total work done is given by the area under the unloading curve (figure 2.12). Energy absorbed by the plastic deformation is given by the difference of the two as:

$$W_P = W_T - W_E \tag{2.27}$$

Stillwell and Tabor [43] pioneered the concept of determining the hardness of a material from the work of indentation. They expressed the conventional hardness of a material – peak load divided by the plastic area – as the ratio of plastic work to volume, i.e., the following relation holds.

$$\frac{\text{Load}}{\text{Plastic area}} = \frac{\text{Plastic Work}}{\text{Plastic Volume}} \tag{2.28}$$

While the plastic work can be computed from the loading curve, the hardness impression can be used to determine the required volume. However, the determining a volume this way is a

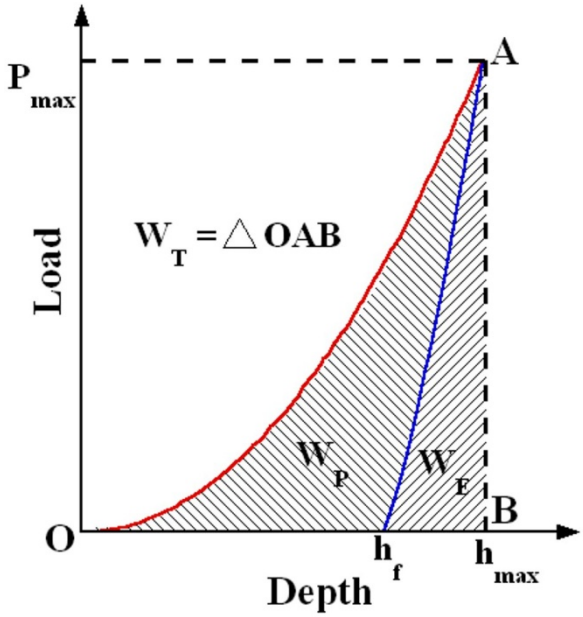

Figure 2.12: Schematic load-displacement curve showing the indentation works.

tedious, time consuming and requires great effort. Tuck et al. [44] developed a simplified method to determine the hardness of the material which is known as work-of-indentation approach in the literature. The approach is briefly described in what follows. The total work (W_T) done or the area under the loading curve may be determined by:

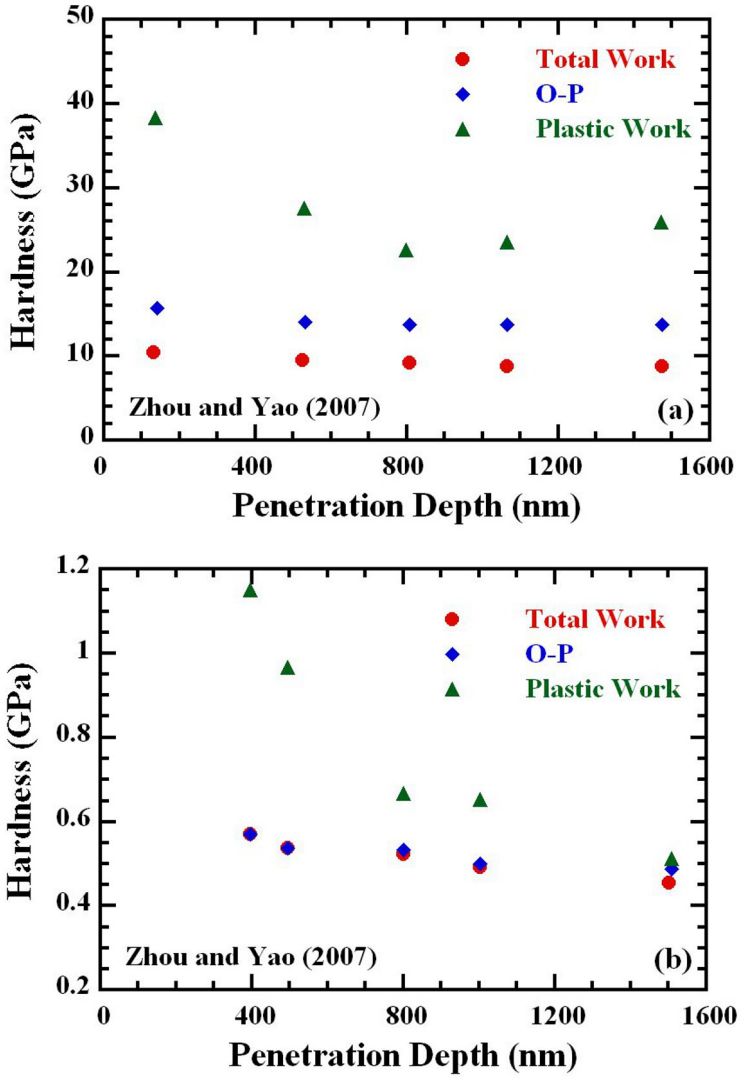

Figure 2.13: Comparison of the hardness values determined by the work-of-indentation approach and the Oliver and Phar method for signgle crystal (1)Silicon; and (b) Aluminum [47].

$$W_T = \int_0^{h_{\max}} P dh \tag{2.29}$$

As stated earlier, the loading curve obtained by a sharp indenter can be described using Kick's law: $P = Ch^2$. This law assumes that the hardness is constant with the load applied. The following mathematical definition of the hardness was used in their derivation.

$$H = \frac{kP}{h^2} \tag{2.30}$$

where k is a constant which takes into account the indenter geometry and the choice of hardness definition; its value is 0.0408 for a Berkovich indenter. On substitution of Kick's law and Eq. (2.29) into Eq. (2.30), the following equation may be obtained.

$$H = \frac{kP_{\max}^3}{9W_T^2} \tag{2.31}$$

The hardness of a material sometimes considered as a function of plastic deformation alone. Tuck et al. suggested this definition of the hardness can be easily incorporated in the work-of-indentation approach by replacing the total work in Eq. (2.31) by the plastic work as:

$$H = \frac{kP_{\max}^3}{9W_P^2} \tag{2.32}$$

Varying conclusions regarding the viability of the work-of- indentation approach exists in the

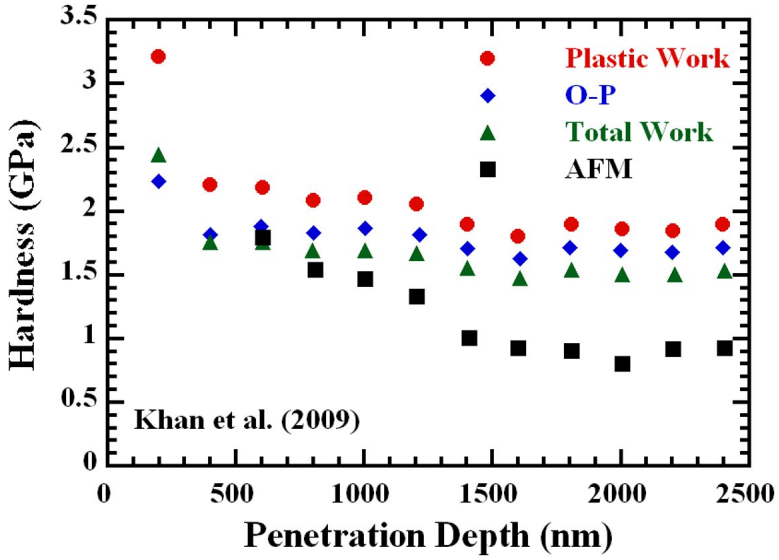

Figure 2.14: Hardness calculated using the four different methods for the Al-2024 [46].

literature. Several researchers have shown that this approach yields reasonable value of hardness for many materials [44-46]. Zhou and Yao [47] employed work-of-indentation approach to determine the hardness values for silicon and aluminum. Result shows that hardness values determined using Eq. (2.30) compare well with that obtained by the Oliver and Pharr method in the case of aluminum, but differ greatly for silicon. Khan et al. [46] reported that the hardness values determined from the total and plastic works shows good agreement with the literature values for the material considered. It generally overestimates the hardness values if the plastic work is used. These results are presented in figure 2.13 and 2.143. On the basis of these results, one may conclude that the work-of-indentation approach may provide reasonable estimate of hardness values only for soft materials when their load-displacement curves are acquired with a sharp indenter. This method fails at very low loads and small penetration depths apparently due to the tip bluntness [44].

2.5.5 Cheng and Cheng Method

Using a scaling approach to indentation, Cheng and Cheng [31] revealed an approximate relationship between the ratio of hardness to elastic modulus and the ratio of irreversible work to total work of indentation, which may be written as:

$$\frac{W_E}{W_T} = 5\frac{H}{E_r} \tag{2.33}$$

Above equation is based on the finite element simulations of indentation on Von-Mises materials with and without work hardening. By combining Eqs. (2.7) and (2.11) and taking $\gamma = \beta = 1$, one may obtain another equation involving the reduced modulus and hardness of the material:

$$\frac{4}{\pi}\frac{P_{\max}}{S^2} = \frac{H}{E_r^2} \tag{2.34}$$

Eqs. (2.33) and (2.34) represent two independent relations that can be solved for E_r and H, as all other quantities are measurable from load-displacement data. Thus, using this method, these properties are evaluated in a manner that does not require the estimation of contact area at all. Despite this advantage, the method has limited experimental verifications. Kusano and Hutchings [48] obtained consistent values of elastic modulus and hardness for carbon nitride films by Cheng and Cheng method. Pharr and Bolshakov [27] stated that the ratio of irreversible to total work may not be entirely independent of work hardening especially for soft materials. The relationship of this kind has been studied by a number of researchers [49-55]. It may be rewritten in the following generalized form:

$$\frac{W_E}{W_T} = \kappa^{-1}\frac{H}{E_r} \tag{2.35}$$

These studies, however, greatly differ in a way the proportionality constant κ^{-1} is determined. Details on this constant are well summarized in an article by Malzbender [56]. A study by Alkorta et al. [58, 59], however, found that κ^{-1} is not a constant and explicitly depends on the correction factor γ, power-law exponent m, half-included angle θ and amount of piling-up c. In terms of these parameters, proportionality factor may be written as:

$$\kappa^{-1} = \frac{\pi\tan\theta}{\gamma}\frac{3m}{2(1+m)}c \tag{2.35}$$

The validity of the Cheng and Cheng method in the determination of hardness and elastic modulus using nanoindentation data is questionable, as the relation given by Eq. (2.35) is influenced by the amount of pile-up. In other words, Cheng and Cheng method has limitation similar to the Oliver and Pharr method when they are applied to soft materials.

2.5.6 Two-slope method

The elastic modulus and hardness of a material may be determined from the slopes of the loading and unloading curves by a technique called two-slope method [24]. The slopes are evaluated at the maximum depth of penetration, as shown in figure 2.15. Main advantage of this method is that it does not require the computation of contact area to evaluate the mechanical properties. This method uses the definition of hardness, Sneddon's solution and an expression for the loading curve similar to one given by Eq. (2.25) all of which are restated here for the sake of convenience.

$$H = \frac{P_{\max}}{A_c} \tag{2.36}$$

$$S = \alpha \sqrt{\frac{4}{\pi}} E_r \sqrt{A_c} \tag{2.37}$$

$$P = E_r \left(\frac{1}{\sqrt{C}} \sqrt{\frac{E_r}{H}} + \frac{\varepsilon}{\alpha} \sqrt{\frac{\pi}{4}} \sqrt{\frac{H}{E_r}} \right)^{-2} (h + \xi)^2 \tag{2.38}$$

Using Eqs. (2.36) to (2.38), Oliver [24] derived expressions for reduced elastic modulus (E_r), contact area (A_c) and hardness (H) of a material, respectively, as:

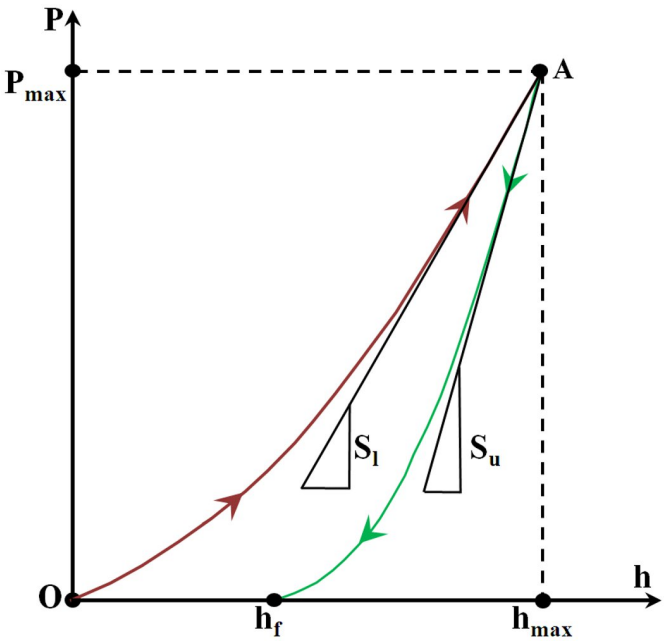

Figure 2.15: Load-displacement diagram showing terminology used in the two-slope method.

$$E_r = \sqrt{\frac{\pi}{C}} \frac{1}{2P_{\max}\alpha} \left(\frac{S_u^2 S_l}{2S_u - \varepsilon S_l} \right) \tag{2.39}$$

$$A_c = CP_{\max}^2 \left(\frac{2S_u - \varepsilon S_l}{S_u S_l} \right)^2 \tag{2.40}$$

$$H = \frac{1}{CP_{\max}} \left(\frac{2S_u - \varepsilon S_l}{S_u S_l} \right)^{-2} \tag{2.41}$$

Note that the factor β was used in the original derivation. Oliver, using the above equations, determined the elastic modulus and hardness for fused silica and tungsten, which accord well with those obtained from the area function technique at all depths considered. Although the slope model does not require the measurement of the contact area, it provides the same level of accuracy as that given by the Oliver and Pharr method. Troyon and Huang [21] derived above equations in a slightly different manner. The approaches differ only in the way the

correction factors are implemented. It is expected that the two-slope method may not be applicable when the dwelling portion is also present in the nanoindentation load-displacement curves.

2.6 Relation between nanomechanical quantities

The load-penetration curves obtained by means of nanoindentation contain wealth of information that may be used for the characterization of both indenter geometry as well as material's response to indentation and for the determination of various mechanical properties. Quantities such as the peak indentation load, maximum depth of penetration and residual depth can be readily obtained from these curves. Indentation energies, slopes, plastic and contact depths, tip bluntness, percentage elastic recovery, etc. are the quantities that are derived from the information contained therein. These nanomechanical quantities bear specific relation with each other. For instance, the hysteresis loop energy – defined as the

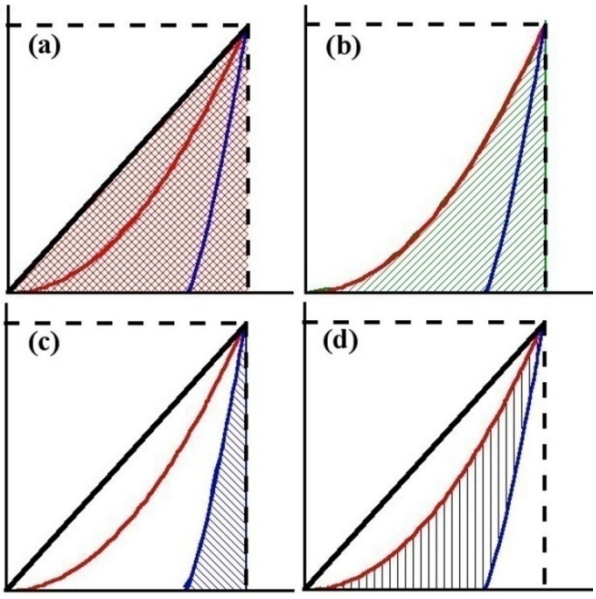

Figure 2.16: Graphical representation of indentation energies: (a) absolute; (b) total; (c) elastic; and (d) plastic.

area enclosed between the indentation loading and unloading curves – is related to the three-half power of the peak indentation load [60]. This relation may enable one to determine the true hardness of a brittle material. Empirical relations are generally developed to simplify the methods used in the analysis of nanoindentation data.

Attaf [61-63] developed various relationships between different nanomechanical quantities. It is shown that 15 different indentation energies can be determined from the experimental load-displacement curves. Among them, four are relevant in this study and are discussed in detail. The total and elastic energies are evaluated from the area under the loading and unloading curves, respectively and their difference provides the plastic work. The absolute energy is defined as the maximum energy that can be dissipated in an indentation experiment and is given by the area of the triangle with vertices $(0,0),(0,h_{\max})$ and $(P_{\max},h_{\max})$. These are graphically shown in figure 2.16. Using the indentation data on ceramic oxides (SiO_2, TiO_2, Ta_2O_5), Attaf [61] showed that these indentation energies are proportional to each other. The ratio of two indentation energies is termed as energy constant. The ratio of absolute to total, absolute to elastic and absolute to plastic are, respectively, termed as total, elastic and plastic energy constants. In mathematical notations:

$$v_T = \frac{W_S}{W_T}; \quad v_E = \frac{W_S}{W_E}; \quad v_P = \frac{W_S}{W_P} \tag{2.42}$$

s. t.:

$$\frac{1}{v_T} = \frac{1}{v_P} + \frac{1}{v_E} \tag{2.43}$$

where, v_T, v_E and v_P are, respectively, known as the total, elastic, and plastic energy constants. Four kinds of penetration depths are considered in the indentation analysis:

maximum, residual, contact and plastic depths. The last one is defined as a point on the h-axis where the tangent to the unloading curve at the initial point meets. If this depth is known the initial unloading stiffness or contact stiffness may be calculated. Like indentation energies, for a given material, each of these depths is found to be proportional to each other. In addition, Attaf [63] derived a relation between the contact depth and the maximum depth of penetration, which is given by:

$$h_c = \frac{2(v_E - 1)}{(2v_E - 1)} h_{\max} \tag{2.44}$$

The contact depth predicted by Eq. (2.44) deviates by less than 5% for SiO_2, TiO_2, and Ta_2O_5 as compared to that determined by the Oliver and Pharr method.

It has also been shown that the indentation energies and the penetration depth described above bear one-to-one correspondence with the area of contact and peak indentation load. All of these empirical relationships can be expressed in the form of a unified correlations diagram developed by Attaf [62], as shown in figure 2.17. This correlation diagram has seven loops; each loop describes the relationship either among three or four nanomechanical quantities. Coefficients in a loop confirm to particular a condition, which is obtained by eliminating the quantities of that loop. All the expressions contained in the unified correlations diagram have a common parameter in the exponent, known as the β-material, which is, according to Attaf, unique for a given material. β-material may be used to determine the reduced elastic modulus and hardness of a material.

$$E_r = K_E P_{\max}^{2\beta_{mat}} \tag{2.45}$$

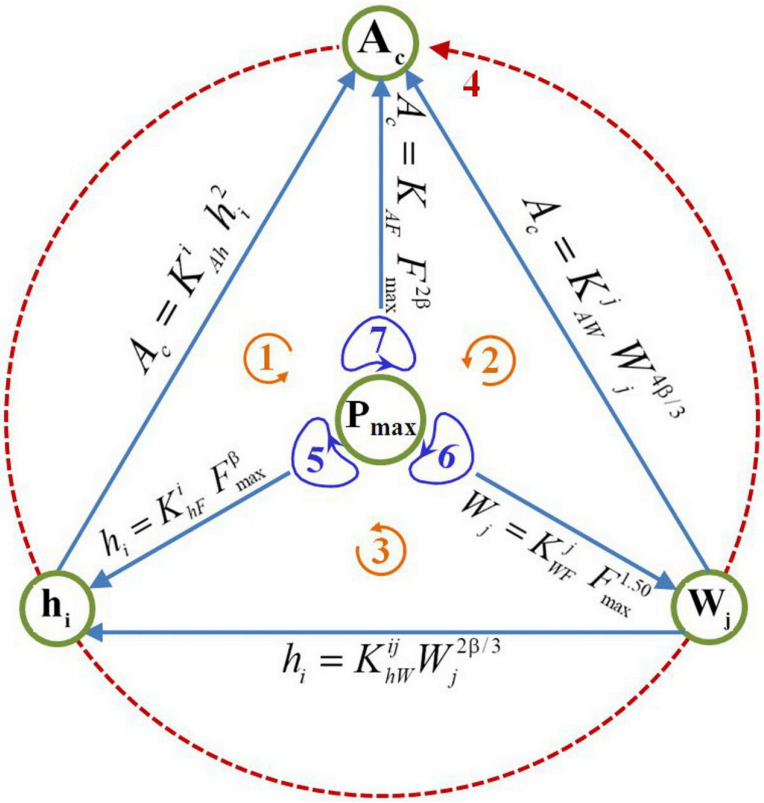

Figure 2.17: Unified correlations diagram showing relationships among several nanomechanical quantities [12]. Examples of loops: Loop 1: $P_{\max} - h_i - A_c - P_{\max}$, *Loop7:* $P_{\max} - h_i - A_c - W_j - P_{\max}$, *Loop4:* $A_c - W_j - h_i - A_c$. *Loops 2 and 3 are identical to loop 1. Similarly, loop 5 and loop 6 resemble loop 7.* $h_i \left(i = c, p, f, \max\right)$ *respectively denote contact, plastic, residual and maximum depth of penetration. Likewise,* $W_j \left(j = S, T, E, P\right)$ *describe absolute, total, elastic and plastic energies dissipated during indentation respectively.*

$$H = K_{AF}^{-1} P_{\max}^{1-2\beta_{mat}} \tag{2.46}$$

where

$$K_E = \frac{\sqrt{\pi}}{2} \frac{K_P}{\sqrt{K_{AF}} K_{hF}^{\max} \left(K_P - 1\right)} \tag{2.47}$$

Symbols K_{AF}, K_P, and $K_{hF}^{\max}$ are proportionality constants appearing respectively in expressions like: $A_c = K_{AF} P_{\max}^{2\beta_{mat}}$; $h_{\max} = K_P h_P$; and $h_{\max} = K_{hF}^{\max} P_{\max}^{\beta_{mat}}$, where A_c, $P_{\max}$, $h_{\max}$, and h_P respectively describe the contact area, peak indentation load, maximum, and plastic depths. Note that Eq. (2.45) is obtained when aforementioned correlations are substituted in the fundamental equation relating initial unloading stiffness, contact area and reduced elastic modulus.

As mentioned earlier, the parameter β-material may be determined by fitting several experimental data set in the form specified in the unified correlations diagram. Alternatively, it may be approximated using total energy dissipated during loading by:

$$\beta_{mat} = \frac{1}{v_T - 1} \tag{2.48}$$

Eq. (2.48) overestimates the value of β-material by about 3%, 17% and 5% respectively for SiO_2, TiO_2 and Ta_2O_5 in comparison to that obtained by the curve fitting method. Jha et al. [64] performed a sensitivity analysis to examine the effect of changes in the β-material on the measured mechanical properties. For illustration, let β_0 and β_1, respectively, denotes the exact and approximate values of β-material. Then, the percentage error in the indentation modulus or hardness may be expressed in terms of $P_{\max}$ and $\Delta\beta = \beta_0 - \beta_1$ as:

$$\Delta E_r \text{ or } \Delta H = 1 - P_{\max}^{2\Delta\beta} \tag{2.49}$$

Figure 2.18 shows the plot of the expression given by Eq. (2.48). It is clear from the figure that even a small error in the value of β-material introduces a significant error in the

computed values of elastic modulus and hardness. For TiO_2, an error of 17% in β would mean nearly 80% errors in both elastic modulus and hardness. This error is found to be independent of the peak indentation load [64]. A method, based on the optimization of error in the mechanical properties, for the determination of β-material in described in Ref. [64].

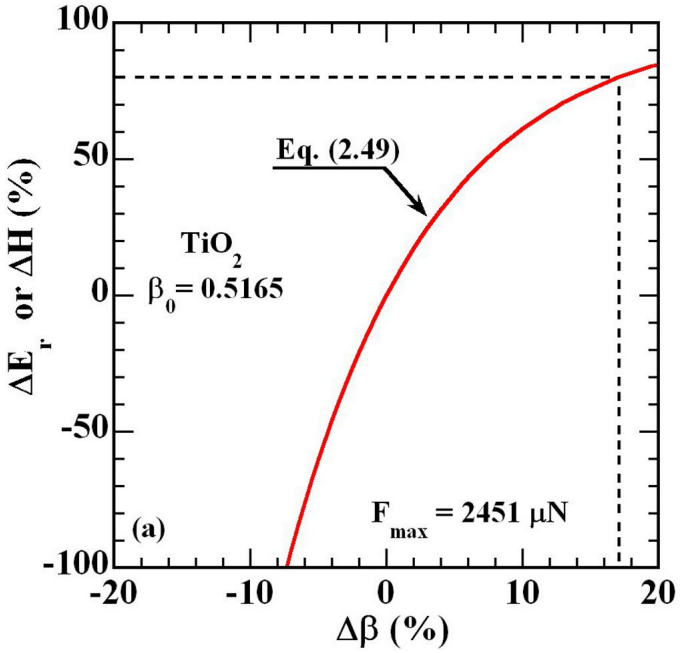

Figure 2.18: Error in the mechanical properties due to the change in β-material determined by Eq. (2.48) [64].

2.7 Representation of nanoindentation load-displacement curves

Analysis of indentation data requires representations for both loading and unloading curves. A material subjected to indentation deforms elasto-plastically and has non-uniform stress as well as displacement fields in the vicinity of contact. As a consequence, deriving analytical expressions for loading and unloading curves considering the elasto-plastic deformations is very difficult. Due to this reason, the experimental curves are often

represented by empirical equations. For instance, a power-law equation is used to describe an unloading curve. Other forms of equation, though less frequently used, are also considered as well [65, 66]. Similarly, a loading curve may be represented by the Meyer's power law given by $P = Ch^n$. The value of n depends on the indenter tip bluntness; it is equal to 2 for an ideally sharp indenter [40]. Note that when the exponent is 2, it is referred to as Kick's law. In general, this parameter decreases with the increase in the bluntness at the tip. A study by Zeng and Chiu [67] shows that the exponent of the loading curve changes from 1.5 to 2.0 when the peak indentation load reaches 30mN. A second order polynomial (Bernhardt formula) is also suggested for the loading curve [68]. Attaf [69] carried out a comparative study to examine the effectiveness of various formula (Kick's law, Bernhardt formula, Buckle's empirical equation, Meyer's power law and their modified and corrected forms) used to describe a loading curve. As a result, it has been found that all the approaches listed above are truncated forms of the Mayer's power law. In yet another study, Attaf [70] derived simple mathematical expressions capable of simulating the load-displacement responses, which is described in detail below.

If all the curves of a family intersect exactly at two points (both ends of the interval), then they can be represented by expressions having the following functional form:

$$\psi(x, p, q, r) = p\left(\frac{x}{q}\right)^r \tag{2.46}$$

where p, q are the ordinate and abscissa of the point lying on the right of the interval [0, ∞] and r is the exponent of the function. The exponent r is different for all curves of the family. In order to gain further insight, family of curves with $p = 2$, $q = 5$ and several values

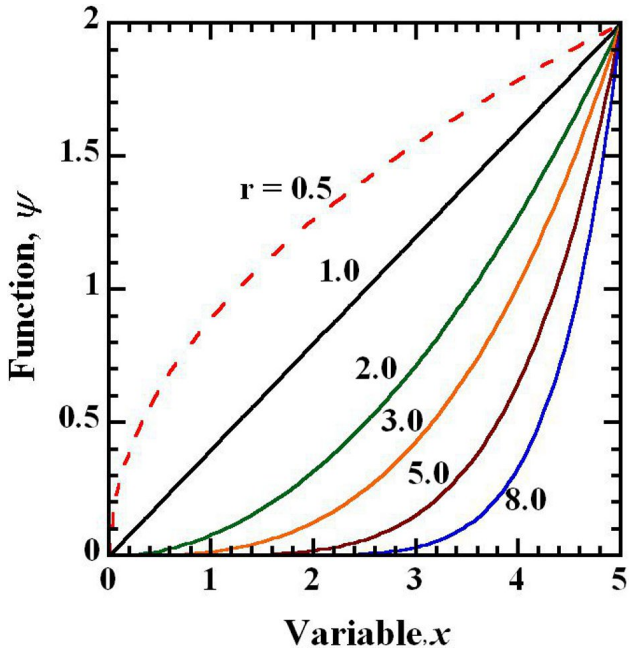

Figure 2.19: Example of a $\psi-$family of curves with $p=2, q=5$ and various values of r [70].

of r are plotted, as shown in figure 2.19. It can be inferred from the figure that a curve concaves upward if its exponent is greater than 1. A nanoindentation has two curves and intersects at two ends of the interval. Therefore, the functional given by Eq. (2.46) may be applied to the nanoindentation responses as well. The functional for loading and unloading curves may be written, respectively, as

$$\psi_L = P_{\max}\left(\frac{h}{h_{\max}}\right)^{r_L} \tag{2.47}$$

$$\psi_U = P_{\max}\left(\frac{h}{h_{\max}}\right)^{r_u} \tag{2.48}$$

The exponents r_L and r_U can be calculated from the consideration of the indentation energies. With the help of Eqs. (2.42) and (2.47), one may find $r_L = 2v_T - 1$. In a similar manner, the

unloading exponent is given by $(2v_E - 1)$. Hence, equations for the loading and unloading curves may finally be written finally as:

$$P = P_{\max}\left(\frac{h}{h_{\max}}\right)^{2v_T - 1} \tag{2.49}$$

$$P = P_{\max}\left(\frac{h}{h_{\max}}\right)^{2v_E - 1} \tag{2.50}$$

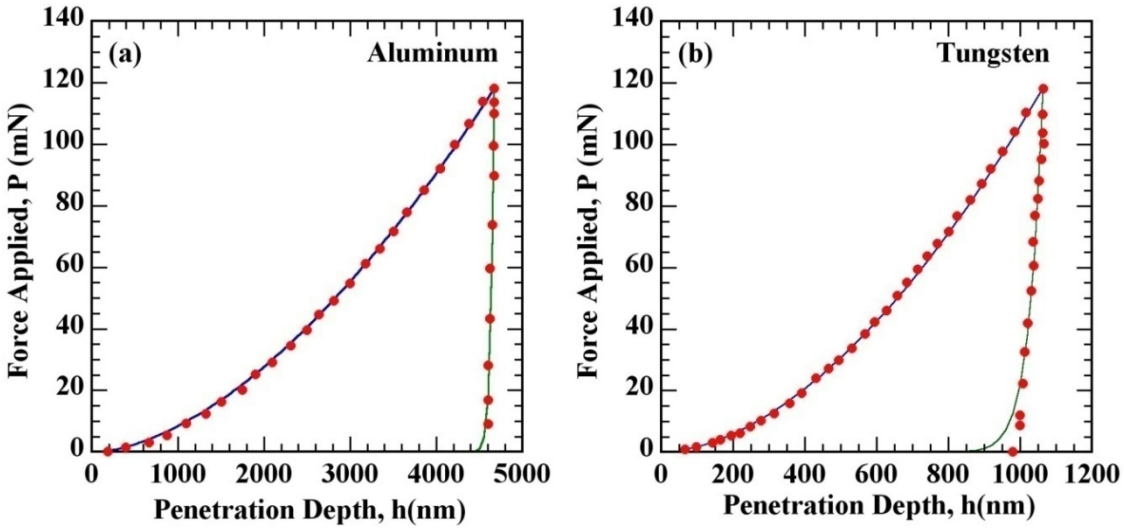

Figure 2.20: Modelling nanoindentaion load-displacement curvese using Eq. (2.47) and (2.48) : (a) aluminum; and (b) tungsten [71].

Note that above equations are valid only when v_T and v_E are equal to or greater than 1 for the same reason as mentioned above. The experimental load-displacement curves obtained with the help Eqs. (2.47) and (2.48) are shown in figure 2.20, where an excellent agreement between the experimental and theoretical curves could be seen. However, the approximating power of unloading curves depends on the type of material; for harder material, only initial portion can be modeled accurately [70-71].

2.8 Indentation analysis of heterogeneous materials

Analysis procedure presented so far is applicable to linear, isotropic and homogeneous materials, as the principle used relies on the self-similarity of the indentation test on an infinite half-space. A material at a length scale d is considered homogeneous if d is approximately equal to four times the maximum depth of penetration. This homogeneous space has the representative elementary volume (r.e.v.) whose characteristic length scale satisfies $\ell << d$. The material properties determined by nanoindentation correspond to the r.e.v. averaged over a structural volume $\propto d^3$ [72].

Constantinides and Ulm further hypothesized that if a material at length scale L contains n number of homogeneous phases of characteristic length scale such that $\ell << d << L$, and if the phases are perfectly distributed, the probability of indenting each phase is equal to the volume fraction of the phases present. It means, in addition to the average properties, the volume fraction of each phase can be determined by means of nanoindentation as:

$$f_J = \frac{N_J}{N}; \sum_{J=1}^{n} N_J = N \tag{2.51}$$

where N_J is the number of indentation on J^{th} material phase and f_J is the volume fraction of that phase. However, the application Eq. (2.51) requires a systematic approach particularly when the phases of a heterogeneous material are optically indistinguishable. The problem can be circumvented with the help of grid indentation [73, 74]. This approach consists of two steps: (1) indentation experiments at large number of points located on grid, as shown in figure 2.21; and (2) statistical analysis of the resulting data. The second step of this approach is carried out using the deconvolution technique, which is described below.

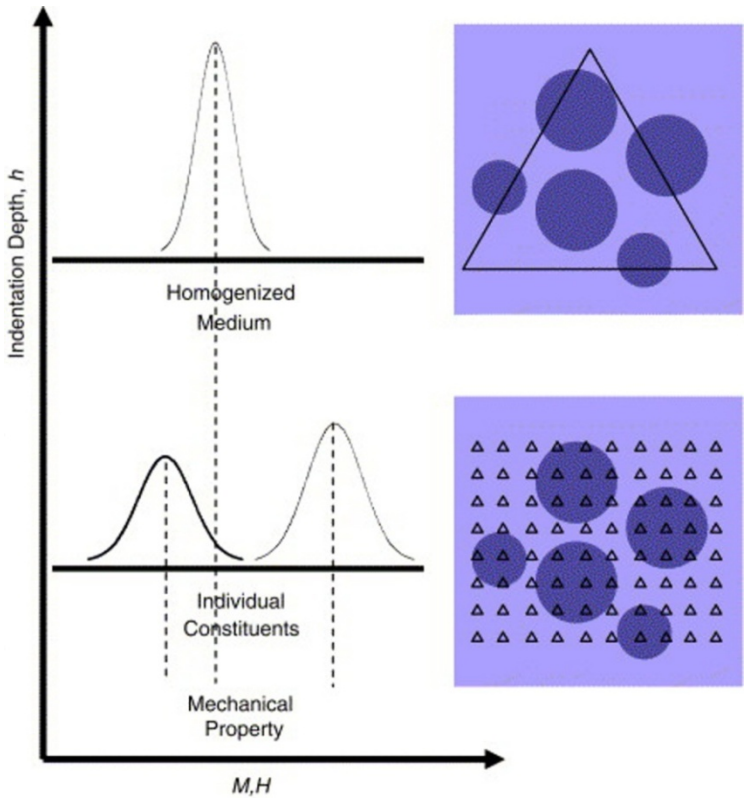

Figure 2.21: Principle of statistical analysis of nanoindentation results. Small indentation depths allow the determination of phase properties, while larger indentation depths lead to the response of the homogenized medium [74].

Let us assume that the mechanical property of interest, say x, for each phase follows normal distribution:

$$p_J(x) = \frac{1}{\sqrt{2\pi s_J^2}} \exp\left(-\frac{(x-\mu_J)^2}{2s_J^2}\right) \tag{2.52}$$

where μ_J and s_J denote the arithmetic mean and the standard deviation of x, which are evaluate from:

$$\mu_J = \frac{1}{N_J}\sum_{k=1}^{N_J} x_k \quad s_J^2 = \frac{1}{N_J - 1}\sum_{k=1}^{N_J}(x_k - \mu_J)^2 \tag{2.53}$$

The overall frequency distribution of the properties of interest pertaining to all mechanically non-interfering phases, which follow normal distribution individually, obeys the following theoretical probability density function:

$$P(x) = \sum_{J=1}^{n} f_J p_J(x) \tag{2.54}$$

where f_J is given by Eq. (2.51). The summation of all the volume fraction of the phases present in a heterogeneous material should satisfy the following compatibility condition:

$$\sum_{J=1}^{n} f_J = 1 \tag{2.55}$$

The above condition reduces the number of unknowns to $3n-1$, where n is the number of unknowns per phase. These unknowns are determined by minimizing the error between theoretical and experimental probability density functions

$$\begin{aligned} &\min \sum_{i=1}^{m} \frac{\left(P_i - P(x_i)\right)^2}{m} \\ &s.t: \quad \sum_{J=1}^{n} f_J = 1 \end{aligned} \tag{2.56}$$

where P_i is the observed probability density and m is the number of intervals chosen for the construction of the histogram. Eq. (2.56) must satisfy $3n-1 \le m < N$.

Constantinides and Ulm applied the deconvolution technique to the nanoindentation data from heterogeneous cementitious materials to determine the volume fractions and the average mechanical properties of different forms of C-S-H [74]. As a large number of indentations are required to perform such kind of statistical analysis, the efficiency of a method used to extract the mechanical properties becomes automatically a matter of concern.

2.9 References

[1] Sneddon, I.N. (1965). "The relation between load and penetration in the axisymmetric Boussinesq problem for a punch of arbitrary profile." *International Journal of Engineering Science*, 3, 47-57.

[2] Pharr, G.M., Oliver, W.C., and Brotzen. F.R. (1992). "On the generality of the relationship among contact stiffness, contact area, and elastic modulus during indentation." *Journal of Materials Research*, 7, 613-617.

[3] Fischer-Cripps, A.C. (2004). *Nanoindentation*. Second edition. Springer.

[4] Cheng, Y.T., and Cheng, C.M. (2004). "Scaling, dimensional analysis, and indentation measurements." *Materials Science and Engineering R*, 44, 91-149.

[5] Cheng, Y.T., and Cheng, C.M. (1999). "Can stress-strain relationships be obtained from indentation curves using conical and pyramidal indenters?" *Journal of Materials Research*, 14, 3493-3496.

[6] King, R.B. (1987). "Elastic analysis of some punch problems for a layered medium." *International Journal of Solids and Structures*, 23, 1657-1664.

[7] Oliver, W.C., and Pharr, G.M. (2004). "Measurement of hardness and elastic modulus by instrumented indentation: Advances in understanding and refinements of methodology." *Journal of Materials Research* 19, 3-20.

[8] Hendrix, B.C. (1995). "The use of shape correction factors for elastic indentation measurements." *Journal of Materials Research*, 10, 255-257.

[9] Strader J.H., Shim S., Bei, H., Oliver, W.C., and Pharr, G.M. (2006). "An experimental evaluation of the constant β relating the contact stiffness to the contact area in nanoindentation." *Philosophical Magazine*, 86, 5285-5298.

[10] Woirgard, J. (2006). "Some results on the indentation of an elastic half space." *Philosophical Magazine*, 86, 5199-5217.

[11] Cao, Y.P., Dao, M., and Lu, J. (2007). "A precise correcting method for the study of the superhard material using nanoindentation tests." *Journal of Materials Research*, 22, 1255-1264.

[12] Meza, J.M., Abbes, F., and Troyon, M. (2008). "Penetration depth and tip radius dependence on the correction factor in nanoindentation measurement." *Journal of Materials Research*, 23, 725-731.

[13] Hay, J.C., Bolshakov, A., and Pharr, G.M. (1999). "A critical examination of the fundamental relations used in the analysis of nanoindentation data." *Journal of Materials Research*, 14, 2296-2305.

[14] Xu, Z-H., and Li. X. (2008). "Effects of indenter geometry and material properties on the correction factors of Sneddon's relationship for nanoindentation of elastic and elastic-plastic materials." *Acta Materialia*, 56, 1399-1405.

[15] Troyon, M., and Lafaye, S. (2006). "About the importance of introducing a correction factor in the Sneddon relationship for nanoindentation measurement." *Philosophical Magazine*, 86, 5299-5307.

[16] Doerner, M.F., and Nix, W.D. (1986). "A method for interpreting the data from depth-sensing indentation instruments." *Journal of Materials Research*, 1, 601-609.

[17] Oliver, W.C., and Pharr, G.M. (1992). "An improved technique for determining hardness and elastic modulus using load and displacement sensing indentation experiments." *Journal of Materials Research*, 7, 1564-1583.

[18] Hainsworth, S.V., Chandler, H.W., and Page, T.F. (1996): "Analysis of nanoindentation load-displacement loading curves." *Journal of Materials Research*, 11, 1987-1995.

[19] Jha, K.K., Suksawang, N., and Agarwal, A. (2010). "Analytical method for the determination of indenter constants used in the analysis of nanoindentation loading curves." *Scripta Materialia*, 63, 281-284.

[20] Malzbender, J., de With, G., and den Toonder, J. (2000). "The P-h^2 relationship in indentation." *Journal of Materials Research*, 15, 1209-1212.

[21] Troyon, M., and Martin, M. (2003). "A critical examination of the P-h^2 relationship in nanoindentation." *Applied Physics Letters*, 83, 863-865.

[22] Tuck, J.R., Korsunky, A.M., Bull, S.J., and Davidson, R.I. (2001). "On the application of the work-of-indentation approach to depth-sensing indentation experiments in coated system." *Surface & Coating Technology*, 137, 217-224.

[23] Cheng, Y.T., and Cheng, C.M. (1998). "Relationships between hardness, elastic modulus, and the work of indentation." *Applied Physics Letters*, 73, 614-616.

[24] Oliver, W.C. (2001). "Alternative technique for analyzing instrumented indentation data." *Journal of Materials Research*, 16, 3202-3206.

[25] Troyon, M. and Huang, L. (2005). "Critical examination of the two-slope method in nanoindentation." *Journal of Materials Research*, 20, 2194-2198.

[26] Woirgard, J., and Dargenton, J.-C. (1997). "An alternative method for penetration depth determination in nanoindentation measurements." *Journal of Materials Research*, 12, 2455-5458.

[27] Pharr, G.M., and Bolshakov, A. (2002). "Understanding nanoindentation loading curve." *Journal of Materials Research*, 17, 2227-2234.

[28] Martin, M., and Troyon, M. (2002). "Fundamental relations used in nanoindentation: Critical examination based on experimental measurements." *Journal of Materials Research*, 17, 2660-2671.

[29] Troyon, M., and Huang, L. (2005). "Correction factor for contact area in nanoindentation measurements." *Journal of Materials Research*, 20, 610-617.

[30] Pharr, G.M. (1998). "Measurement of mechanical properties by ultra-low load indentation." *Material Science & Engineering A*, 253, 151-159.

[31] Cheng, Y.T., and Cheng, C.M. (2005). "Relationship between initial unloading slope, contact depth, and mechanical properties for spherical indentation in linear viscoelastic solids." *Material Science & Engineering A*, 409, 93-99.

[32] Sawa, T. and Tanaka, K. (2001). "Simplified method for analyzing nanoindentation data and evaluating performance of nanoindentation instruments." *Journal of Materials Research*, 16, 3084-3096.

[33] Gong, J., Miao, H., and Peng, Z. (2004). "Analysis of the nanoindentation data measured with a Berkovich indenter for brittle materials: Effect of the residual contact stress." *Acta Materialia*, 52, 785-793.

[34] Briscoe, B.J., and Sebastian, K.S. (1996). "The elastoplastic response of Poly (Methyl Methacrylate) to indentation." *Proceeding of The Royal Society A*, 452, 439-457.

[35] Tranchida, D., and Piccarolo, S. (2005). "On the use of the nanoindentation unloading curve to measure Young's modulus of polymers on nanometer scale." *Macromolecular Rapid Communications*, 26, 1800-1804.

[36] Jha, K.K., Suksawang, N., Lahiri, D., and Agarwal, A. (2012): "Energy-based analysis of nanoindentation curves for cementitious materials." *ACI Materials Journal,* 109, 81-90.

[37] Gong, J., Peng, Z., and Miao, H. (2005). "Analysis of the nanoindentation load-displacement curves measured on a high-purity fine grained alumina." *Journal of the European Ceramic Society*, 25, 649-654.

[38] Marx, V., and Balke, H. (1997). "A critical investigation of the unloading behavior of sharp indentation." *Acta Materialia*, 45, 3791-3800.

[39] VanLandingham, M.R., Villarrubia, J.S., Guthrie, W.F., and Meyers, G.F. (2001). "Nanoindentation of polymers: An overview." Macromol. Symp. 167, 15-44.

[40] Cheng, Y.T., and Cheng, C.M. (1998). "Analysis of indentation loading curves obtained using conical indenters." *Philosophical Magazine Letters*, 77, 39-47.

[41] Sun, Y., Zheng, S., Bell, T., and Smith, J. (1999). "Indenter tip radius and load frame compliance calibration using nanoindentation loading curves." *Philosophical Magazine Letters*, 79, 649-658.

[42] Gong, J., Miao, H. and Peng, Z. (2004). "On the contact area for nanoindentation tests with Berkovich indenter: case study on soda lime glass." *Materials Letters*, 58, 1349-1353.

[43] Stilwell, N.A., and Tabor, D. (1961). "Elastic recovery of conical indenters" Proceedings of the Physical Society, 78, 169-179.

[44] Tuck, J.R., Korsunky, A.M., Bull, S.J., and Davidson, R.I. (2001). "On the application of the work-of-indentation approach to depth-sensing indentation experiments in coated systems." *Surface and Coating Technology*, 137, 217-224.

[45] Beegan, D., Chowdhury, S., Laugier, M.T. (2005). "Work of indentation methods for determining copper film hardness." *Surface & Coating Technology*, 192, 57-63.

[46] Khan, M.K., Hainsworth, S.V., Fitzpatrick, M.E., and Edwards, L. (2009). "Application of the work of indentation approach for the characterization of aluminum 2024-T351 and Al cladding by nanoindentation" *Journal of Materials Science*, 44, 1006-1015.

[47] Zhou, L., and Yao, Y. (2007). "Single crystal bulk material micro/nano indentation hardness testing by nanoindentation instrument and AFM." *Material Science & Engineering A*, 460-461, 95-100.

[48] Kusano, Y., and Hutchings, I.M. (2003). "Analysis of nano-indentation measurements on carbon nitride films." *Surface and Coatings Technology*, 169-170, 739-742.

[49] Venkatesh, T.A., Van Vliet, K.J., Giannakopoulos, A.E., and Suresh, S. (2000). "Determination of elasto-plastic properties by instrumented sharp indentation: guidelines for property extraction." *Scripta Materialia*, 42, 833-839.

[50] Dao, M., Chollacoop N., Van Vliet, K.J., Venkatesh, T.A., and Suresh, S. (2001). "Computational modeling of the forward and reverse problems in instrumented sharp indentation." *Acta Materialia*, 49, 3899-3918.

[51] Malzbender, J. and de With, G. (2002). "Indentation load-displacement curve, plastic deformation and energy." *Journal of Materials Research,* 17, 502-511.

[52] Ni, W., Cheng, Y-T., Cheng, C.M., and Grummon, D.S. (2004). "An energy-based method for analyzing instrumented spherical indentation experiments." *Journal of Materials Research,* 19, 149-157.

[53] Malzbender, J. (2004). "The energy dissipated during spherical indentation." *Journal of Materials Research,* 19, 1605-1607.

[54] Ma, D. Ong, C.W., and Wong S.F. (2005). "New relationship between Young's modulus and nonideally sharp parameters." *Journal of Materials Research,* 20, 1498-1506.

[55] Choi, Y., Lee, H-S., and Kwon D. (2004). "Analysis of Sharp-tip-indentation load-depth-curve for contact area determination taking into account pile-up and sink-in effect into account." *Journal of Materials Research,* 19, 3307-3315.

[56] Malzbender, J. (2005). "Comment on the determination of mechanical properties from the energy dissipated during indentation." *Journal of Materials Research,* 20, 1090-1092.

[57] Alkorta, J., Martinez-Esnaola, J.M. and Sevillano, J. (2005). "Absence of one-to-one correspondence between elastoplastic properties and sharp-indentation load-penetration data." *Journal of Materials Research,* 20, 432-437.

[58] Alkorta, J., Martinez-Esnaola, J.M. and Sevillano, J. (2005). "Erratum: Absence of One-to-one correspondence between elastoplastic properties and sharp-indentation load-penetration data." *Journal of Materials Research,* 20, 1369-1369.

[59] Alkorta, J., Martinez-Esnaola, J.M., and Sevillano, J. (2006). "Comments on "Comment on the determination of mechanical properties from the energy dissipated during indentation" by J. Malzbender [J. Mater. Res. 20, 1090 920050]." *Journal of Materials Research,* 21, 302-305.

[60] Sakai, M. (1993). "Energy principle of the indentation-induced inelastic surface deformation and hardness of brittle materials." *Acta Metallurgica et Materialia*, 41, 1751-1758.

[61] Attaf, M.T. (2003). "New ceramics related investigation of the indentation energy concept." *Material Letters*, 57, 4684-4693.

[62] Attaf, M.T. (2003). "A unified aspect of power-law correlations for berkovich hardness testing of ceramics." *Material Letters*, 57, 4627-4638.

[63] Attaf, M.T. (2004). "New formulation of the nanomechanical quantities using the β-material concept and the indentation function." *Material Letters*, 58, 889-894.

[64] Jha, K.K., Suksawang, N. and Agarwal, A. (2011). "The sensitivity of β-material parameters and its determination based on optimization of error in the mechanical properties." *Computational Materials Science*, 50, 2891-2897.

[65] Gubicza, J., Juhasz, A., and Lendvai, J. (1996). "A new method for hardness determination from depth sensing indentation tests." *Journal of Materials Research,* 11, 2964-2967.

[66] Gong, J., Miao, H., and Peng, Z. (2003). "Simple method for determining the initial unloading slope for ceramics nanoindentation test." *Journal of Materials Science Letters*, 22, 267-268.

[67] Zeng, K., and Chiu, C.H. (2001). "An analysis of load-penetration curves from instrumented indentations." *Acta Materialia*, 49, 3539-3551.

[68] Cheng, Y.T., and Cheng, C.M. (1998). "Further analysis of indentation loading curves: Effects of tip rounding on mechanical properties." *Journal of Materials Research*, 13, 1059-1064.

[69] Attaf, M.T. (2004). "Connection between the loading curve models in elastoplastic indentation." *Material Letters*, 58, 3491-3498.

[70] Attaf, M.T. (2004). "Step by step building of a model for the Berkovich indentation cycle." *Material Letters*, 58, 507-512.

[71] Jha, K.K., Suksawang, N., and Agarwal, A. (2011). "Analytical Approach for the Determination of Nanomechanical Properties for Metals." MEMS and Nanotechnology, Proceedings of conference of the Society for Experimental Mechanics Series, Uncasville, CT, 4, 65-71.

[72] Constantinides, G., Ulm, F.-J., and Van Vliet K. (2003). "On the use of nanoindentation on cementitious materials." *Materials and Structures*, 36, 191-196.

[73] Constantinides, G., Ravi Chandran, K.S., Ulm, F.-J., and Van Vliet K. (2006). "Grid indentation analysis of composite microstructure and mechanics: Principles and validation." *Materials Science & Engineering A*, 430, 189-202.

[74] Constantinides, G., and Ulm, F.-J. (2007). "The nanogranular nature of C-S-H." *Journal of the Mechanics and Physics of Solids*, 55, 64-90.

CHAPTER 3

CHARACTERIZATION OF THE LOAD-DISPLACEMENT CURVES

3.1 Introduction

Nanoindentation has been established as a reliable experimental means for small scale mechanical characterization of a large array of materials. Its application, initially limited to linear, isotropic and homogenous materials such as metals and ceramics, has been extended to more complex polymeric, biological and cementitious materials. In this technique, a probe of specified geometry and known mechanical properties is indented on to the surface of a material to record the response in terms of load-penetration history. The response obtained is subsequently analyzed to extract meaningful nanomechanical properties such as Young's modulus, hardness [1], yield strength, the strain hardening exponent [2], fracture toughness [3] etc. However, the accuracy with which these properties are evaluated largely depends on how well the response to indentation is understood and interpreted. Indentation is a complex elasto-plastic phenomena resulting in a non-uniform displacement as well as stress fields in the vicinity of contact, which complicates the analytical derivation of a load-displacement relationship. As a consequence, much of our understanding concerning the response of a material to indentation has been gained empirically [4].

Although significant advancement and refinement of our knowledge has been made over the last two decades, understanding the experimental load-displacement data is still enigmatic. We begin our discussion with the representation of the load-displacement curves acquired with pyramidal indenters. In general, an experimental loading curve obtained with a pyramidal indenter may be described by a power law: $P = Ch^n$. The exponent n primarily

depends on the type and geometry of the indenter; it is usually equal to 2 for an ideally sharp pyramidal indenter [5]. A value of 2 is also obtained when the depth of penetration is very large as compared to the indenter tip radius. Zeng and Chiu [7] found that n changes from 2 to 1.5 when the peak indentation load becomes smaller than 30mN even for an ideally sharp indenter. Thus, whether an indenter is actually sharp or blunt cannot be decided based on the exponent. Note that the determination of indenter tip radius (or blunt height) is an important endeavor in the nanomechanical analysis [8, 9]. However, the power law description of the loading curve is still relevant; it may be used to examine whether an indenter is behaving like a sharp one, a prerequisite for some mechanical property evaluation procedures [8, 10-11]. On the other hand, in addition to the indenter geometry, the coefficient C also depends on the material properties. Despite its relevancy in the determination of the elastic modulus and yield strength, materials response characterization using C is difficult. Cheng and Cheng [12], using dimensional analysis and finite element simulations, showed that a loading curve may be better represented by a second order polynomial and its coefficients can be used to determine the indenter tip radius. However, the radius determined in this way lacks consistency.

As far as unloading response is concerned, according to Oliver and Pharr [1], it is represented by another power law in the form: $P = A_0 \left(h - h_f \right)^m$, where h_f is the final depth of penetration, A_0 is the coefficient and m is the exponent. These quantities are determined by a least squares curve fitting procedure. Punch geometry may be characterized on the basis of the exponent: $m = 1$ for flat punch, $m = 1.5$ for solid of revolution and $m = 2.0$ for conical indenters. According to Oliver and Pharr, the exponent determined by curve fitting of the

experimental unloading curve obtained using a Berkovich indenter is slightly material dependent and fall in the range 1.20-1.60. However, the exponent greater than 2 is frequently reported in the literature, and it can neither be justified by the "effective indenter shape" nor by "residual stress" theories [1, 13]. In addition, it is possible that the two different materials can have the same exponent value [14], or the same material can have two different values of this exponent. Discrepancies in the values of fitting parameters are generally ascribed to the amount of data used in the process [14, 15]. On the basis of these observations, one may state that neither the indenter geometry nor the material response to indentation can be characterized using the power law parameters. Therefore, identification of parameters that can serve the purpose of analytical representation of the load-displacement curves, characterization of both indenter as well as material and the derivation of required nanomechanical quantities simultaneously is paramount.

Indentation energies or their ratios are frequently employed to analyze the material response to indentation [16-18]. The relation between the energy dissipated and the ratio of hardness to reduced elastic modulus has been a basis for many nanomechanical property evaluation procedures [17]. Several quantities such as peak indentation load, area of contact, penetration depth and their ratios, etc., may be related to the indentation energies [16, 19]. Moreover, Attaf [18] introduced two energy ratios – named total and elastic energy constants – and showed that they can even be used to describe the experimental load displacement curves. Again, the depth along which the contact is made by the indenter with the specimen can be computed from the elastic energy constant [20-22]. Except for these uses, little is known about their physical meaning, influencing factors, variation range, realm of applications, etc., and such is the subject of this study. The load-displacement curves obtained as a result of

elastic and elasto-plastic finite element simulations are analyzed to gain further understanding of their characteristics and uses.

3.2 Theoretical background

In this section, a brief review of the mathematical representation of load-displacement data and the definition of the energy constants is presented. When an elastic half-space is indented by an ideally sharp conical indenter, the resulting load(P) vs. the displacement(h) relationship is described according to the Sneddon's solution [23], which is given by:

$$P = \frac{2E_s \tan\alpha}{\pi\left(1-\nu_s^2\right)} h^2 \tag{3.1}$$

where, E_s is Young's modulus of the elastic-half space, ν_s is Poisson's ratio and α is the half-included angle of the indenter. A theoretical solution capable of describing the $P-h$ relation is not available for a Berkovich (pyramidal) indenter. Finite element simulations of Berkovich indentation showed, however, that a parabolic relation between indentation load and penetration depth still holds, albeit in a slightly different form [24]. More recently, Poon et al. [25] showed that the indenter tip rounding has a great influence on the load-displacement curves. Their numerical simulations of indentation on linear elastic solids resulted in the following expression.

$$\begin{aligned} P &= f\left(\nu\right)\frac{2E_s \tan(70.3^0)}{\pi\left(1-\nu^2\right)} h\left(h+g\left(R\right)\right) \\ f\left(\nu\right) &= a_1\nu_s^2 + a_2\nu_s + a_3 \\ g\left(R\right) &= c_1R^2 + c_2R \end{aligned} \tag{3.2}$$

where, $f(\nu)$ and $g(\nu)$ are known as multiplicative and additive factors, respectively, and R is the indenter tip radius. Note that a Berkovich equivalent conical indenter has a half-included angle of 70.3^0. Constants a_1, a_2, a_3, c_1 and c_2 appearing in Eq. (3.2) are fitting parameters and are equal to -0.062, -0.156, 1.12, $1.50\text{x}10^{-5}$ nm^{-1} and 0.117, respectively. For spherical indentation, the load-displacement relation is expressed as follows [26]:

$$P = \frac{4}{3}\sqrt{R}E_r h^{3/2} \tag{3.3}$$

where E_r is known as the reduced modulus and is related to the elastic modulus and Poisson's ratios of the material (E_s, ν_s) and the indenter (E_i, ν_i) by:

$$\frac{1}{E_r} = \frac{1-\nu_s^2}{E_S} - \frac{1-\nu_i^2}{E_i} \tag{3.4}$$

For elasto-plastic indentation, no closed form solution is available as such and therefore, they are usually represented by algebraic expressions obtained by fitting the experimental curves. A typical load displacement diagram is shown in figure 3.1. The areas under the loading and unloading curves signify energy dissipated and recovered upon complete withdrawal of load, respectively. In any indentation experiment, the maximum energy dissipation takes place when the $P-h$ relation is linear, which, according to Attaf [18], is termed as absolute work of indentation. Several energy-based parameters can be defined using absolute work as reference energy. Two of them are given by:

$$v_T = \frac{W_S}{W_T}; \quad v_E = \frac{W_S}{W_E} \tag{3.5}$$

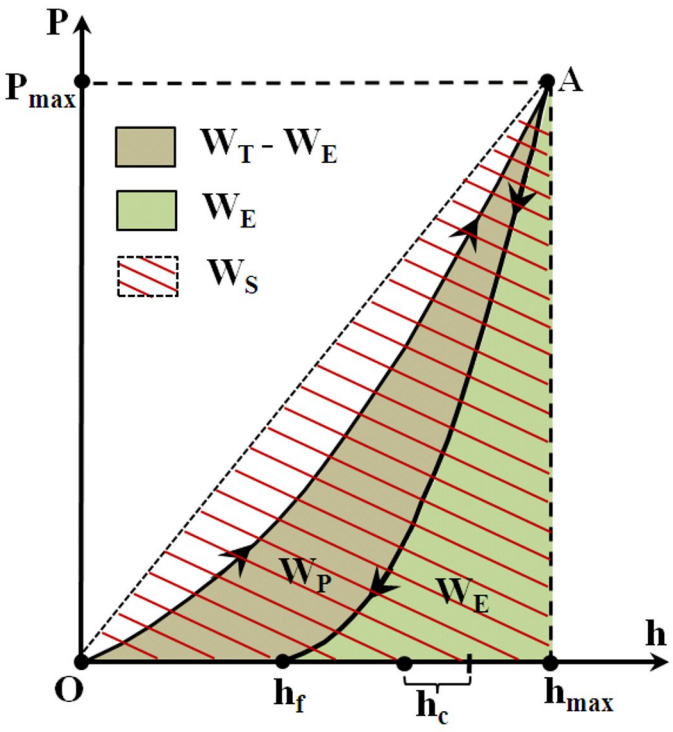

Figure 3.1: Schematic representation of load-displacement curves showing terminology used.

where, the ratios v_T and v_E are respectively described as the total and elastic energy constants. Similarly, terms W_S, W_T and W_E are referred to as the absolute, total and elastic works of indentation, respectively. Note that v_T and v_E are equal in the case of elastic indentation. When evaluated using Eq. (3.1), one may obtain v_T equal to 1.5, for an ideally sharp indenter, irrespective of the elastic modulus and half-included angle of the indenter. The corresponding value for the spherical indenter is 1.25. When Eq. (3.2) is used to determine v_T, the effect of the tip radius becomes apparent; it decreases with the increase in the tip radius. At this stage, we may conclude that the total energy constant is a function of the indenter type and geometry, not the material properties as has been assumed, as long as

the indentation is elastic. It should be noted that both v_T and v_E has a minimum value of 1, which corresponds to the linear load-displacement relation.

Total and elastic energy constants may be used to describe the indentation load-displacement curves. Attaf [27], based on functional analysis, derived the following power functions to represent the loading and unloading curves, respectively:

$$P_{load} = P_{\max}\left(\frac{h}{h_{\max}}\right)^{2v_T-1}$$
$$P_{unload} = P_{\max}\left(\frac{h}{h_{\max}}\right)^{2v_E-1} \tag{3.6}$$

where $P_{\max}$ is the peak indentation load and $h_{\max}$ is the corresponding maximum depth of penetration. In general, an experimental loading curve can be fitted more accurately than an unloading curve with the help of Eq. (3.6). Approximation of an unloading response by Eq. (3.6) is very much dependent on the elastic recovery ratio, a fraction of the depth recovered after the indenter is completely withdrawn, of a material; a better fit is obtained when the recovery is very small. It should be noted that only the initial portion of the unloading response is of great importance in the analysis of indentation data. The elastic energy constant may also be used to determine the depth along which the contact is made between the material and the specimen which is given by [28]:

$$h_c = \frac{2\left(v_E - 1\right)}{\left(2v_E - 1\right)} h_{\max} \tag{3.7}$$

The validity of Eq. (3.7) has been confirmed in several studies. It is reported that the above equation reasonably estimates the contact depth for many materials with an accuracy of

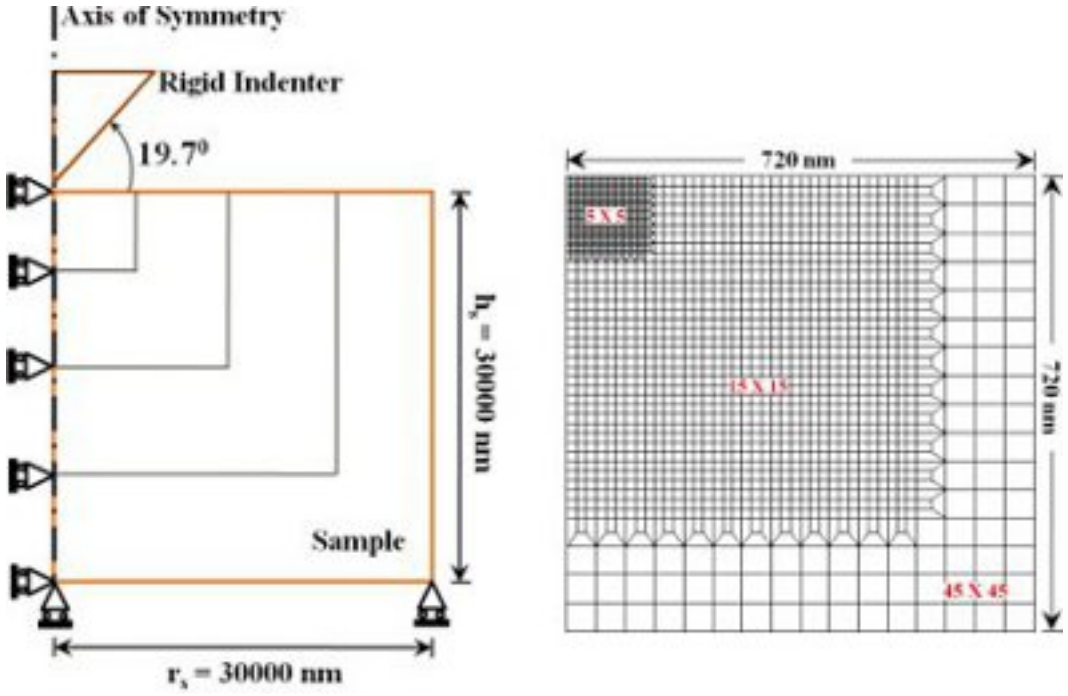

Figure 3.2: The axisymmetric mesh used in finite element simulations: (a) overall mesh showing specimen dimensions and boundary conditions and (b) details of mesh in the region of contact near the indenter tip.

better than 5%. In order to gain further insight on v_T and v_E, load-displacement curves from a wide range of materials are required, which can be acquired through finite element simulations of indentation. Application of the finite element method in the study of indentation phenomenon has long been in use as it allows systematic variations of the parameters involved [3, 5, 24, 29-34].

3.3 Finite element modeling

In this study, the commercially available finite element based software ABAQUS/Standard is used to acquire the nanoindentation load-displacement curves. The axisymmetric finite element model with large-strain features is employed. To comply with

the chosen model, a pyramidal Berkovich indenter is modeled as an equivalent conical indenter with a half-included angle of 70.3^0, which has the same area-to-depth ratio as the former one. Selection of the specimen size is one of the most important steps in the modeling, as it governs the accuracy of the simulations. Poon et al. [17] showed that accurate load-displacement curves may be obtained if the specimen size satisfies the following convergence condition:

$$\frac{r_s}{h_s} \geq 1; \quad \frac{h_s}{h_{\max}} \geq 100 \tag{3.8}$$

Table 3.1: Summary of the parameters used in the finite element simulations of nanoindentation load-displacement curves.

Parameters (Unit)	**Value / Range of Values**
Elastic Modulus (GPa)	70.00
Poisson's Ratio	0.05:0.20:0.45
Yield Strength (GPa)	0.4 - 70
Hardening Parameter	0; $10\sigma_y$
Friction coefficient	0.40
Indenter angle (deg)	70.3^0
$R / h_{\max}$	0-15

where r_s and h_s are described as the radius and height of the cylindrical specimen, respectively, and are taken to be 30000nm; this is large enough to acquire an accurate load-displacement curve up to the penetration depth of 300nm, as per the condition given by Eq. (3.8). To exploit the advantage offered by the axisymmetric conditions, only half of the cross-section is considered. The entire domain is discretized using 4-node quadrilateral

elements, with the highest mesh density in the vicinity of contact to account for large local deformation beneath the indenter similar to one adopted in Ref. [30]. Progressively coarser mesh, as shown in figure 3.2, is used as we move away from the contact, resulting in 4000 elements and 4299 nodes.

The specimen is modeled as elastic as well as elasto-plastic deformable materials, which are assumed to obey the following stress-strain relations:

$$\sigma = \begin{cases} E_s \varepsilon & \text{for } \varepsilon \le \sigma_y / E_s \\ \sigma_y + E_p \left(\varepsilon - \sigma_y / E \right) & \text{for } \varepsilon > \sigma_y / E_s \end{cases} \tag{3.9}$$

where, σ_y is the yield strength and E_P is the work hardening parameter. While Young's modulus of the solid is fixed (70.0 GPa), the yield strength, Poisson's ratio and the hardening parameters are varied in the majority of simulations, as summarized in Table 3.1. This combination of mechanical properties covers many metals, ceramics and polymers. In some cases, other values of the elastic modulus are also used to ascertain the effect of elastic parameters on the total and elastic energy constants. The indenter is modeled as an analytically rigid surface with the $R / h_{\max}$ ratio varied systematically. When the tip radius to the maximum penetration depth ratio is very large, a conical indenter behaves like a spherical one. As such, simulations involving the analytically rigid spherical indenter have also been carried out to illustrate the transition between these two kinds of indenters. Roller boundary conditions are considered along the axis of symmetry and the bottom of the specimen as shown in figure 3.2. The contact between the indenter and the specimen is assumed to be frictional with the coefficient of friction 0.4. Indentations were carried out in the displacement-controlled mode, in which the indenter was pushed up to a specified depth.

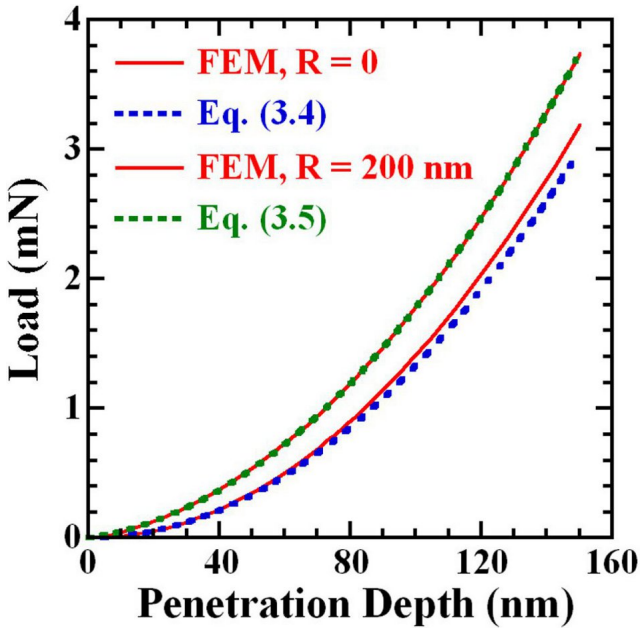

Figure 3.3: Comparison of the load-displacement curves obtained from finite element simulations with that from Eqs. (3.1) and (3.2).

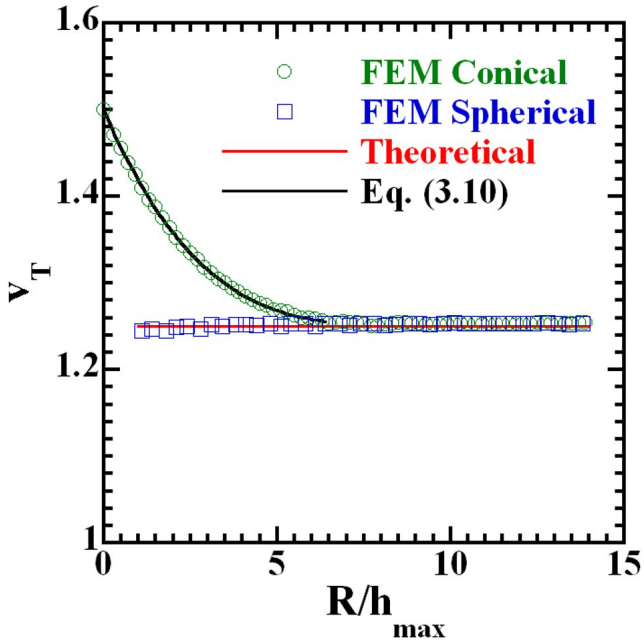

Figure 3.4: Plot showing the variation of total energy constant v_T with R/h_{max} for conical and spherical indenters.

3.4 Results and Discussion

At the outset, indentations on elastic solids with $E = 70\,GPa$ and $\nu = 0.25$ were performed using both the blunt and sharp indenter to examine the adequacy of the meshing scheme adopted in the finite element (FE) simulations. Figure 3.3 shows that the plots of load-displacement curves obtained by FE analysis are in very good agreement with those obtained from Eqs. (3.1) and (3.2) for both types of indenters, and thus confirms that the meshing used is appropriate.

Next, we performed several simulations using conical indenters with the ratio of the indenter tip radius to the maximum depth of penetration $\left(R / h_{\max}\right)$ varying between 0 and 10 for the same values of the elastic modulus and Poisson's ratio. These simulations were repeated using spherical indenter as well. The total energy constant determined from the simulated load-displacement curves are plotted against $R / h_{\max}$, as shown in figure 3.4. It is evident from the plot that, for conical, v_T varies as a function of the $R / h_{\max}$ ratio of up to a certain value and thereafter remains constant. For the spherical indenter, as expected, v_T remains the same irrespective of the $R / h_{\max}$ ratio. It is interesting to note here that when $R / h_{\max}$ is approximately 6.4, the total energy constants for both the blunt conical and spherical indenter are equal implying that the load-displacement curves corresponding to both of these indenters are the same. This is evident from the figure 3.5 that loading curves obtained as a result of FEM simulations corresponding to the blunt conical and spherical indenters coincide with that obtained by Eq. (3.6) with $v_T = 1.25$.

The variation of v_T with the $R / h_{\max}$ ratio can be fitted with a fourth-degree polynomial as:

$$v_T = \sum_{i=0}^{4} M_i \left(\frac{R}{h_{\max}} \right)^i \tag{3.10}$$

where M_i are the coefficients of the polynomial equations and are given by: $M_0 = 1.50$, $M_1 = -0.088711$, $M_2 = 0.006994$, $M_3 = -0.00043217$ and $M_4 = 0.00011582$. By solving Eq. (3.10) for a given value of v_T, the indenter tip radius may be calculated. Poon et al. [25] determined the indenter radius R using the following relation:

$$c_1 R^2 + c_2 R = \frac{p_1}{p_2} \tag{3.11}$$

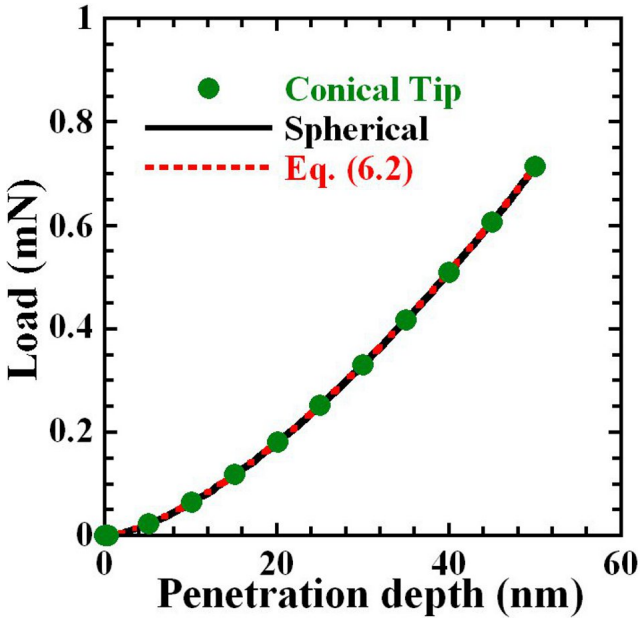

Figure 3.5: Comparison of the elastic $P-h$ curves obtained by finite element simulations.

where, p_2 and p_2 are the coefficients of the second order polynomial in P and h is used to represent the experimental load-displacement curves. Similarly, based on dimensional

analysis and FE simulations, Cheng and Cheng [12] developed the following expression to calculate the tip radius:

$$R = \frac{p_1}{2p_2}\left(\frac{1}{\sin\theta} - 1\right)^{-1} \tag{3.12}$$

Table 3.2 summarizes the tip radius given by Eqs. (10) – (12). Their comparison shows that the method presented in this study predicts R more precisely and consistently than the other two methods described above.

Table 3.2: Comparison of indenter tip radius obtained from three different methods using elastic response; input radius is 200nm.

h_{max} (nm)	R/h	This Study		p_1	p_2	Poon et al. R (nm)	C&C R (nm)
		v_T	R (nm)				
50	4.00	1.286	202.00	0.003548	0.000146	202.35	195.35
100	2.00	1.358	200.80	0.003768	0.000141	222.76	215.60
150	1.33	1.396	199.80	0.003706	0.000141	217.82	210.69
200	1.00	1.418	199.80	0.003629	0.000142	212.36	205.27

The load-displacement response obtained from a material that deforms elasto-plastically during indentation depends on several factors, such as Young's modulus, Poisson's ratio, yield strength, the work hardening parameter, the indenter type and geometry, the coefficient of friction, etc. A sensitivity analysis was first performed to examine which of these parameters significantly affects the determination of energy constants. Elasto-plastic simulations with different values of coefficient of friction revealed that its effect on the load-displacement curves is insignificant – a fact, which is also corroborated by Wang et al. [32]. Due to this reason, a value of 0.4 was used for the coefficient of frictions in all simulations.

Similarly, test simulations were carried out to assay which of the mechanical properties has a greater influence on the energy constants. For this purpose, three different sets of elastic moduli and yield strengths were chosen in such a way that their ratio remained the same; Poisson's ratio and the work hardening parameter were kept equal to 0.25 and 0,

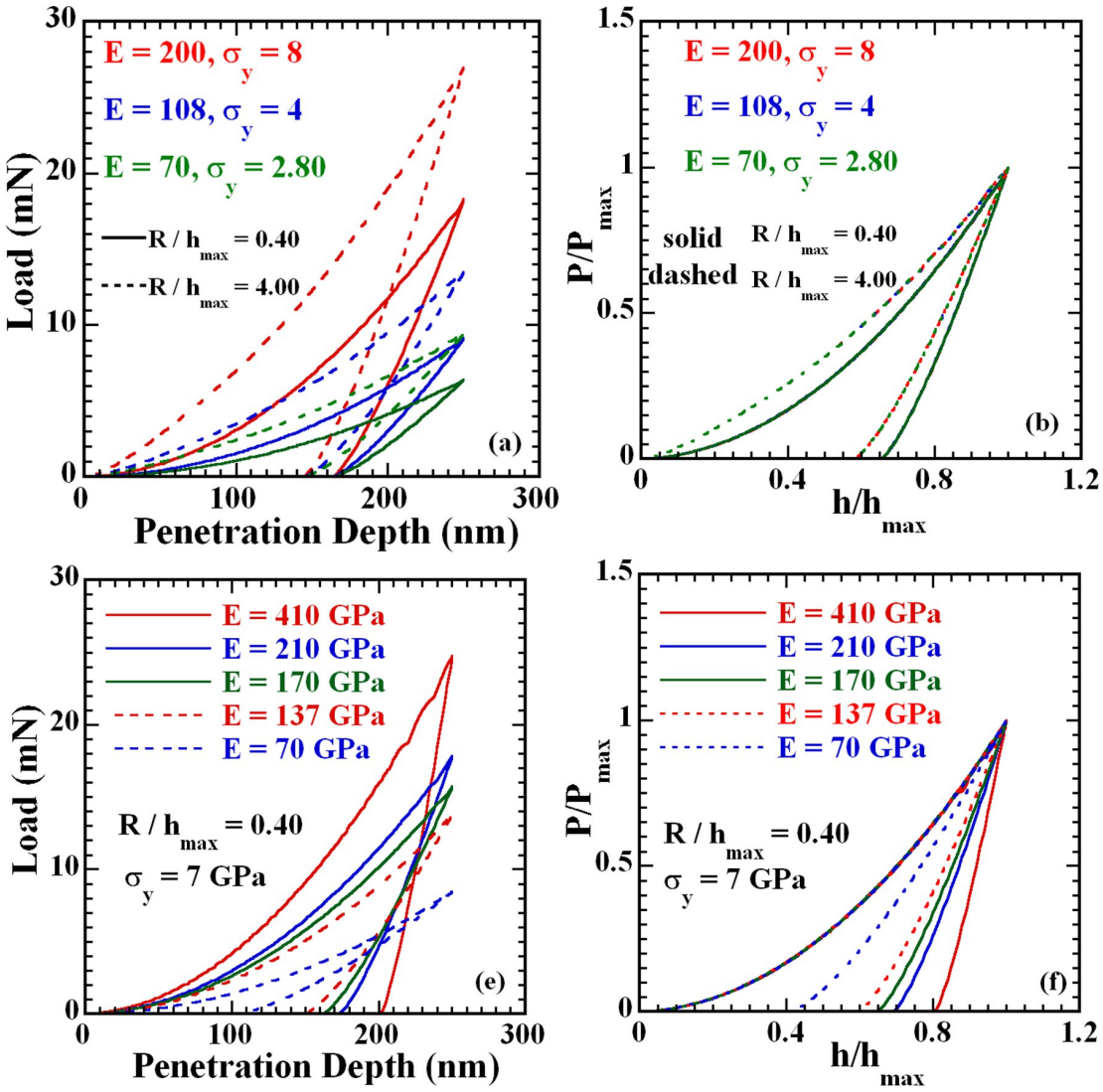

Figure 3.6: Plots of load-displacement curves showing: (a) & (b) effect of E/σ_y and R/h_{max} ratios on the load-displacement curves and normalized responses, respectively (c) & (d) effect of elastic modulus on the load-displacement curves and normalized responses, respectively.

respectively. The load-displacement curves so obtained for two values of the $R/h_{\max}$ ratio are displayed in figure 3.6a, where, as expected, the effects of material properties and the radius-to-depth ratio are evident. Although such results are mundane in nanoindentation studies, two interesting observations could be made. First, if the elastic modulus-to-yield strength ratio is constant, the resulting residual depths of impression are equal, irrespective of the $R/h_{\max}$ ratio. The second observation is that if the load and displacement are respectively normalized with their maximum values, for a given $R/h_{\max}$ ratio, the resulting load-displacement curves exactly coincide, as shown in figure 3.6b. These two observations imply that the load-displacement curves corresponding to the identical E/σ_y ratio yield similar values for both v_T and v_E , provided the $R/h_{\max}$ ratios are also equal.

In yet another experiment, the elastic modulus was varied in the range 70-410 GPa, keeping all other parameters constant. The resulting load-displacement curves after normalization follow almost the same loading path but have different unloading paths (as shown in figures 3.6c and 3.6d) thereby implying that only the unloading curve is susceptible to the modulus values. Due to this reason, the elastic modulus was kept constant and all other parameters were varied, as mentioned in Table 3.1. The total energy constant evaluated from all such simulations is against the $R/h_{\max}$ ratio as shown in figure 3.7. It is evident from the figure that v_T is independent of material properties and varies in a way similar to that obtained in the elastic case whenever the $R/h_{\max}$ ratio is less than 2. Thereafter, its dependence on the modulus-to-yield stress ratio is apparent, which may be attributed to the effect of sphericity of the indenter tip. It should be noted here that v_T eventually becomes

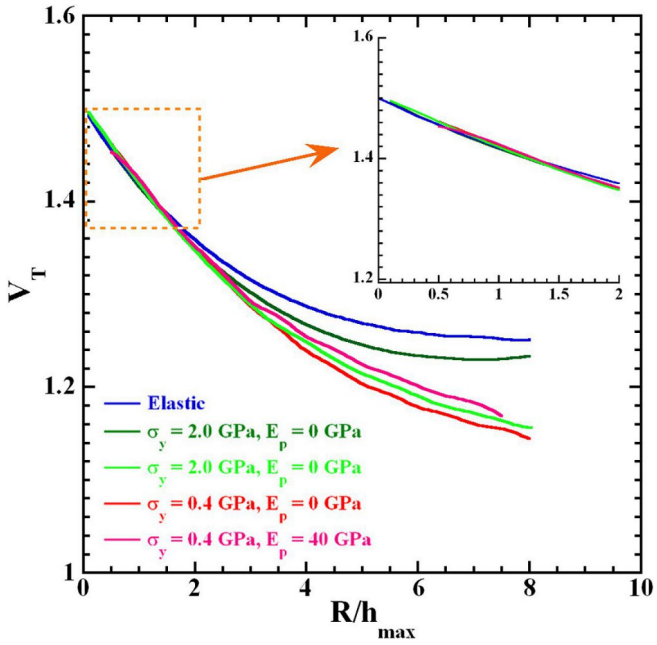

Figure 3.7: Variation of v_T on E/σ_y and $R/h_{\max}$ ratios for elasto-plastic indentation.

constant when the radius of the Berkovich tip is such that it behaves as a spherical indenter. Cheng and Cheng suggested that a blunt conical indenter behaves like a spherical one when the $R/h_{\max}$ ratio is 13.7 when the half-included angle is 68^0. However, the distinction between them diminishes well below this theoretical value. As far as the variation of elastic energy constant is concerned, it is affected by both material properties as well as indenter geometry, as shown in figure 3.8a. However, when normalized with respect to the v_E value determined for the ideally sharp indenter the entire curve falls on the same line, as shown in figure 3.8b, thereby implying that the rate at which the elastic energy constant decreases is independent of the material properties. On the basis of these observations, one may conclude that the total and elastic energy constants characterize the indenter geometry and material response to the Berkovich indentation, respectively.

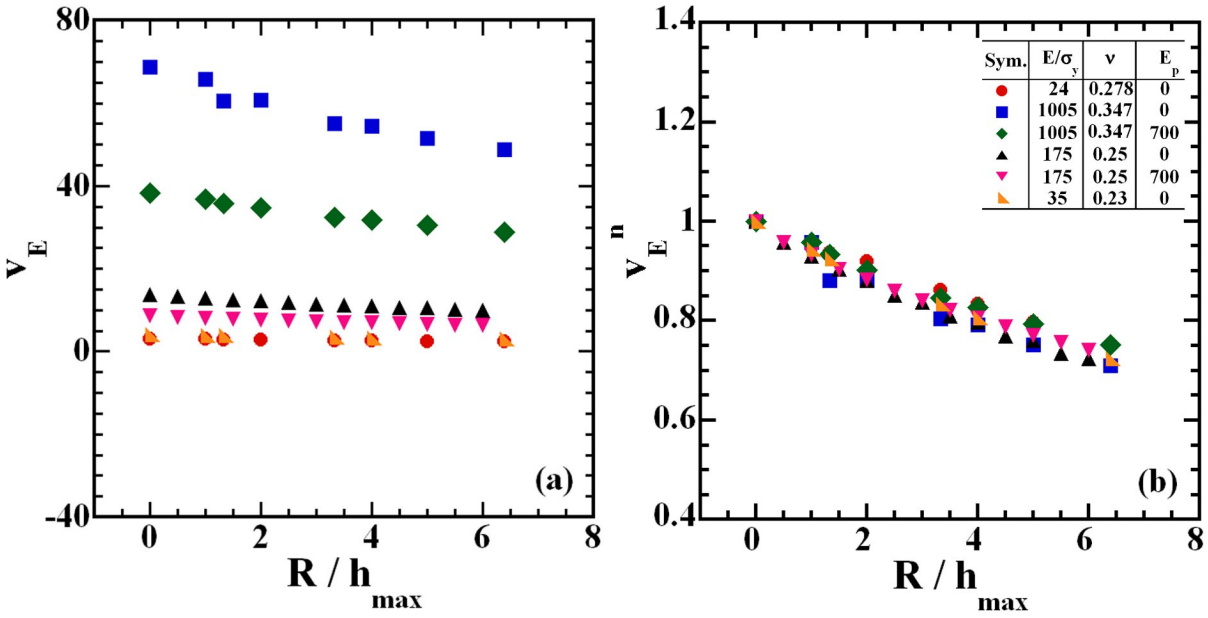

Figure 3.8: (a) Plot showing the variation of v_E with the radius-to-depth ratio and material properties; (b) Variations in v_E normalized with its value corresponding to a sharp conical indenter with the radius-to-depth ratio.

As discussed, v_T is independent of material properties, and Eq. (3.10) used in the determination of the indenter tip radius can be applied in the case of elasto-plastic indentation as well, if $R/h_{\max}$ is less than 2. Reasonable agreement between the input value and the calculated indenter tip radius validates the proposed method, as shown in Table 3.3. Note that the method by Poon et al. is applicable to the elastic indentation only. The accuracy of the proposed method, however, depends on v_T; better accuracy in R is obtained when v_T is greater than 1.4. Thus, while calibrating the indenter tip, the test material (say aluminum) should be indented to a maximum depth of penetration such that the resulting v_T is greater than or equal to 1.4. The total energy constant may also be used to determine the nominal hardness of a material. The nominal hardness of a material is defined as the indentation load

divided by the indenter area evaluated at the maximum depth of penetration [35], which may be written, for an ideally sharp conical indenter, as:

$$H_n = \frac{P_{\max}}{A_{\max}} = \frac{P_{\max}}{24.56 h_{\max}^2} \tag{3.13}$$

Table 3.3: Comparison of indenter tip radius obtained in this study with that from Cheng and Cheng method using elasto-plastic response; input radius is 200nm.

σ_y (GPa)	h_{max} (nm)	R/h	This Study		p_1	p_2	C&C R (nm)
			v_T	R (nm)			
2	50	4.00	1.245	543.10	0.002716	7.43E-05	294.0
	100	2.00	1.339	240.50	0.002384	8.17E-05	234.6
	150	1.33	1.391	211.35	0.002288	8.30E-05	221.8
	200	1.00	1.419	197.00	0.002222	8.35E-05	214.0
8	50	4.00	1.267	254.95	0.003784	0.000128	238.5
	100	2.00	1.349	218.60	0.003747	0.000128	235.5
	150	1.33	1.393	206.25	0.003588	0.000130	221.8
	200	1.00	1.412	199.00	0.003462	0.000131	212.2

For a non-perfect pyramidal indenter, Ma et al. [36] expressed the indenter area in the following form:

$$A_{\max} = 24.497 h^2 + \sum_{i=1}^{7} C_i h^{1/2^n} \tag{3.14}$$

where terms within the summation account for the bluntness in the tip of the indenter. The form of Eq. (3.14) suggests that Ma et al. evaluated the maximum area in a manner similar to that used for the determination of contact area in the standard Oliver and Pharr method.

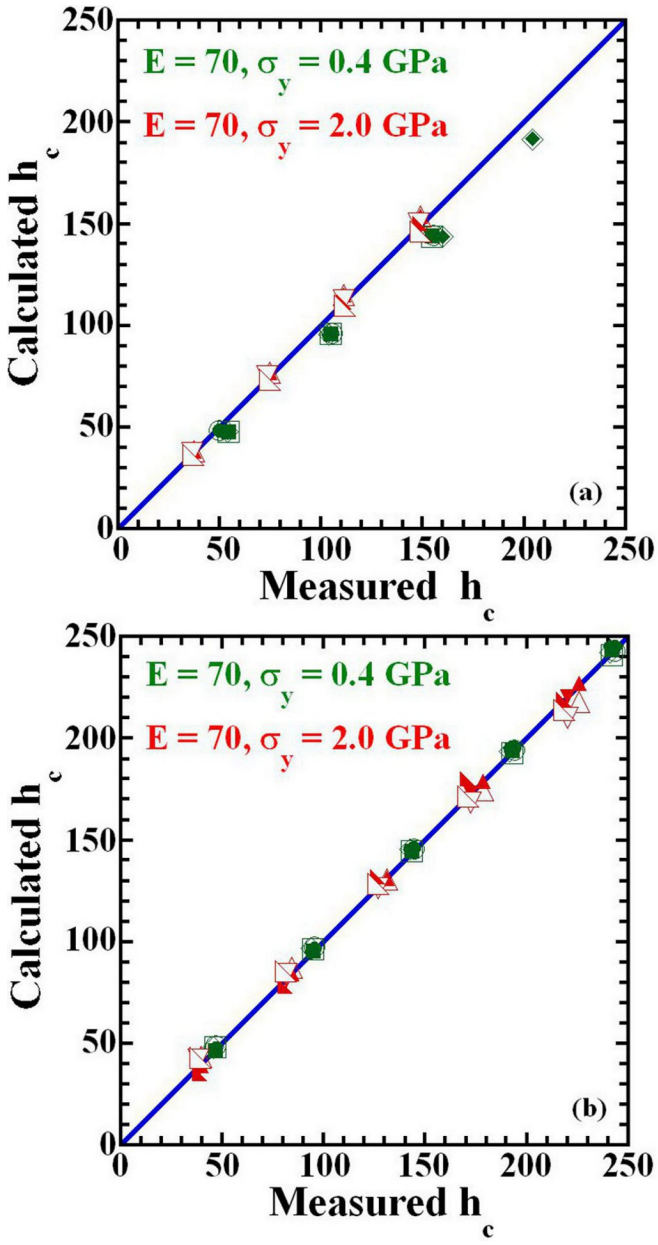

Figure 3.9: Comparison of the contact depth determined using Eq. (7) with that obtained by the Oliver and Pharr method (a) Berkovich; and (b) spherical indenters. Solid marker: individual value, and hollow marker: average value.

Therefore, area functions corresponding to the contact depth and the maximum depth of penetration may have common limitations. Employing the indentation work [37], we propose the following expression for the determination of nominal hardness:

$$H_n = \frac{v_T^2 P_{\max}}{2.25 h_{\max}^2} \tag{3.15}$$

Values of H_n calculated from Eq. (3.15) for aluminum, steel and fused silica are in excellent agreement with that obtained by Ma et al. as summarized in Table 3.4. The accuracy of the proposed method ensures that the effect of tip bluntness can be quantified using the elastic energy constant.

Table 3.4: Calculation for the nominal hardness values for aluminum, steel and fused silica: Experimental data from Ma et al. [34].

Material	**h_{max} (nm)**	**A_{max} (x 10^7 nm^2)**	**H_n* GPa**	**P_{max} (mN)**	**v_T**	**H_n** GPa**
Aluminum single crystal	2000.7	9.97	0.256	25.5	1.411	0.226
	2003.6	10.00	0.255	25.5		0.225
	1990.0	9.86	0.259	25.5		0.229
	2023.1	10.19	0.250	25.5		0.221
	1938.1	9.36	0.272	25.5		0.240
GCr15 bearing steel	1923.7	9.22	7.156	660.0	1.462	6.91
	1941.5	9.39	7.026	660.0		6.78
	1938.5	9.36	7.048	660.0		6.80
	1962.3	9.59	6.880	660.0		6.64
	1936.4	9.34	7.063	660.0		6.82
Fused Silica	1996.8	9.93	4.632	460.0	1.484	4.60
	1998.8	9.95	4.623	460.0		4.59
	1996.7	9.93	4.633	460.0		4.60
	1996.2	9.92	4.635	460.0		4.61
	1996.4	9.93	4.634	460.0		4.60

*by Ma et al. method; **this study

Finally, we would like to comment on the determination of contact depth from the elastic energy constant using Eq. (3.7). Attaf [28] calculated the contact depth using the best fit value of v_E obtained from the plot between the absolute and elastic works corresponding to different peak indentation loads. This may lead to the erroneous contact depth, especially when the material is softer, as shown in figure 9a. Thus, we recommend calculating h_c using the elastic energy constant obtained from the individual unloading response. Errors resulting from the use of the average value can be minimized if the correction due to ratio is applied to the elastic energy constant according to the variation trend shown in figure 3.8b. When the spherical indenter is employed in the indentation, the contact depth is generally obtained as an average value of the maximum depth of penetration and the residual depth of penetration as:

$$h_{cs} = \frac{\left(h_{\max} + h_f\right)}{2} \tag{3.16}$$

The calculated contact depths from Eqs. (3.7) and (3.16) are compared, as shown in figure 3.9b. Excellent agreement between them ensures the effectiveness of the elastic energy constant in the determination of contact depth through Eq. (3.7). However, the level of accuracy remains the same, even if the average value of elastic energy constants evaluated at different peak indentation is used in this case.

3.5 References

[1] Oliver, W.C., and Pharr, G.M. (1992). "An improved technique for determining hardness and elastic modulus using load and displacement sensing indentation experiments." *Journal of Materials Research*, 7, 1564-1583.

[2] Dao, M., Chollacoop N., Van Vliet, K.J., Venkatesh, T.A., and Suresh, S. (2001). "Computational modeling of the forward and reverse problems in instrumented sharp indentation." *Acta Materialia*, 49, 3899-3918.

[3] Phar, G.M. (1998). "Measurement of mechanical properties by ultra-low load indentation." *Material Science & Engineering A*, 253, 151-159.

[4] Pharr, G.M., and Bolshakov, A. (2002). "Understanding nanoindentation unloading curves." *Journal of Materials Research*, 17, 2660-2671.

[5] Cheng, Y.T., and Cheng, C.M. (1998). "Analysis of indentation loading curves obtained using conical indenters." *Philosophical Magazine Letters*, 77, 39-47.

[6] Hainsworth, S.V., Chandler, H.W., and Page, T.F. (1996): "Analysis of nanoindentation load-displacement loading curves." *Journal of Materials Research*, 11, 1987-1995.

[7] Zeng, K., and Chiu, C.H. (2001). "An analysis of load-penetration curves from instrumented indentations." *Acta Materialia*, 49, 3539-3551.

[8] Malzbender, J., de With, G., and den Toonder, J. (2000). "The P-h^2 relationship in indentation." *Journal of Materials Research*, 15, 1209-1212.

[9] Meza, J.M., Abbes, F., and Troyon, M. (2008). "Penetration depth and tip radius dependence on the correction factor in nanoindentation measurement." *Journal of Materials Research*, 23, 725-731.

[10] Jha, K.K., Suksawang, N., and Agarwal, A. (2010). "Analytical method for the determination of indenter constants used in the analysis of nanoindentation loading curves." *Scripta Materialia*, 63, 281-284.

[11] Giannakopoulos, A.E., and Suresh, S. (1999): "Determination of elastoplastic properties by instrumented sharp indentation." *Scripta Materialia*, 40, 1191-1198.

[12] Cheng, Y.T., and Cheng, C.M. (1998). "Further analysis of indentation loading curves: Effects of tip rounding on mechanical property measurements." *Journal of Materials Research*, 13, 1059-1064.

[13] Gong, J., Miao, H., and Peng, Z. (2004). "Analysis of the nanoindentation data measured with a Berkovich indenter for brittle materials: effect of the residual contact stress." *Acta Materialia*, 52, 785-793.

[14] Marx, V., and Balke, H. (1997). "A critical investigation of the unloading behavior of sharp indentation." *Acta Materialia*, 45, 3791-3800.

[15] Sawa, T. and Tanaka, K. (2001). "Simplified method for analyzing nanoindentation data and evaluating performance of nanoindentation instruments." *Journal of Materials Research*, 16, 3084-3096.

[16] Sakai, M. (1993). "Energy principle of the indentation-induced inelastic surface deformation and hardness of brittle materials." *Acta Metallurgica et Materialia*, 41, 1751-1758.

[17] Cheng, Y.T., and Cheng, C.M. (1998). "Relationships between hardness, elastic modulus, and the work of indentation." *Applied Physics Letters*, 73, 614-616.

[18] Attaf, M.T. (2003). "New ceramics related investigation of the indentation energy concept." *Material Letters*, 57, 4684-4693.

[19] Attaf, M.T. (2003). "A unified aspect of power-law correlations for berkovich hardness testing of ceramics." *Material Letters*, 57, 4627-4638.

[20] Attaf, M.T. (2004). "New formulation of the nanomechanical quantities using the β-material concept and the indentation function." *Material Letters*, 58, 889-894.

[21] Uzun, O., Guclu, N., Kolemen, U., and Sahin, O. (2008). "Analysis of data on indentation load against penetration depth for bulk MgB_2 crystal using nanoindentation work and Oliver-Pharr approaches." *Materials Chemistry and Physics*, 112, 5 -10.

[22] Jha, K.K., Suksawang, N., Lahiri, D., and Agarwal, A. (2012): "Energy-based analysis of nanoindentation curves for cementitious materials." *ACI Materials Journal,* 109, 81-90.

[23] Sneddon, I.N. (1965). "The relation between load and penetration in the axisymmetric Boussinesq problem for a punch of arbitrary profile." *International Journal of Engineering Science*, 3, 47-57.

[24] Larson, P.L., Giannakopoulos, A.E., Soderlund, E., Rowcliffe, D.J., Vstergaard, R. (1996). "Analysis of Berkovich indentation" *International Journal of Solids and Structures*, 33, 221-248.

[25] Poon, B., Rittel, D., and Ravichandran, G. (2008). "An analysis of nanoindentation in linearly elastic solids." *International Journal of Solids and Structures*, 45, 6018-6033.

[26] Basu, S.A., Moseson, A., and Barsoum, M.W. (2006). "On the determination of spherical nanoindentation stress–strain curves." *Journal of Materials Research*, 21, 2628-2637.

[27] Attaf, M.T. (2004). "Step by step building of a model for the Berkovich indentation cycle." *Material Letters*, 58, 507-512.

[28] Bhattacharya, A.K., and Nix, W.D. (1991). "Finite element analysis of cone indentation." *International Journal of Solids and Structures*, 27, 1047-1058.

[29] Knapp, J.A., Follstaedt, D.M., Myres, S.M., Barbour, J.C., and Friedmann, T.A. (1999). "Finite-element modeling of nanoindentation." *Journal of Applied Physics*, 85, 1460-1474.

[30] Hay, J.C., Bolshakov, A., and Pharr, G.M. (1999). "A critical examination of the fundamental relations used in the analysis of nanoindentation data." *Journal of Materials Research*, 14, 2296-2305.

[31] Xu, Z-H., and Li. X. (2008). "Effects of indenter geometry and material properties on the correction factors of Sneddon's relationship for nanoindentation of elastic and elastic-plastic materials." *Acta Materialia*, 56, 1399-1405.

[32] Wang, T.H., Fang, T.-H., and Lin, Y.-C. (2007). "A numerical study of factors affecting the characterization of nanoindentation on silicon." *Material Science & Engineering A*, 447, 244-253.

[33] Poon, B., Rittel, D., and Ravichandran, G. (2008). "An analysis of nanoindentation in elasto-plastic solids." *International Journal of Solids and Structures*, 45 (2008) 6399-6415.

[34] Ma, D., Ong, C.W., and Zhang, T. (2009). "An instrumented indentation method for Young's modulus measurement with accuracy estimation." *Experimental Mechanics*, 49, 719-729.

[35] Cao, Y., Xue, Z., Chen, X., and Raabe, D. (2008). "Correlation between the flow stress and the nominal indentation hardness of soft metals." *Scripta Materialia* 59, 518-521.

[36] Tuck, J.R., Korsunky, A.M., Bull, S.J., and Davidson, R.I. (2001). "On the application of the work-of-indentation approach to depth-sensing indentation experiments in coated systems." *Surface and Coating Technology*, 137, 217-224.

CHAPTER 4

DETERMINATION OF CONTACT STIFFNESS

4.1 Introduction

The experimental load-displacement curves obtained by probing the surface of a material in a nanoindentation experiment are analyzed to evaluate the reduced modulus of a material according to the fundamental relation given by [1]

$$S_u = \beta \frac{2}{\sqrt{\pi}} E_r \sqrt{A_c} \tag{4.1}$$

where S_u is initial unloading stiffness or contact stiffness, A_c is the projected area of elastic contact, E_r is the reduced modulus of a material and β is the correction factor that takes the lack of axial symmetry of the pyramidal indenter into account. The contact stiffness is defined as the slope of the unloading curve evaluated at the maximum depth of penetration. The area of contact is either measured independently from the hardness impression or derived using the contact stiffness according to the procedure developed by Oliver and Pharr [2]. To evaluate the slope, one needs the complete description of the unloading response, which is difficult to obtain analytically owing to the complexities involved in the indentation process. The unloading response is usually described by an algebraic function established by curve fitting.

In the most widely used Oliver and Pharr method (OP method), the unloading curve obtained using a Berkovich indenter is represented by a power law whose parameters are determined by least square fitting. The exponent of the power law, according to Oliver and Pharr, is slightly material dependent and may take a value in the range 1.2-1.6, which led

them to conclude that the shape of a Berkovich indenter closely approximates a parabola of revolution. This observation was unexpected, as a Berkovich indenter was believed to be approximated by a conical indenter for which the exponent is usually 2. Later, Pharr and Bolshakov [3] justified the variation in the exponent by introducing the concept of "effective indenter shape." However, uncertainties exist in their determination; power law parameters depend on the fraction of the unloading data used in the curve-fitting process [4-5]. It should be noted here that power law parameters are usually determined using the initial 30% of the unloading response in the OP method. They are also liable to the initial guess and are very sensitive to the residual depth of indentation, thereby making the fitting process very cumbersome.

Furthermore, the power law parameters are remarkably different if they are determined at different peak indentation loads, even for the same material. Gong et al. [6], using experimental data on the oxide of ceramics, argued that the unloading response acquired with the help of a Berkovich indenter indeed resembles that from the conical indenter, provided appropriate correction for residual stress that arises during indentation is applied. They suggested a modified form of power law, having exponent 2 with an additional term accounting for the residual stress effect. Their assumption appears reasonable from the viewpoint that the loading curves obtained by both Berkovich and the conical indenters are represented by parabola [7]. Unknown parameters of this modified power law are determined by the hit and trial method, which is again equally cumbersome. There are, however, many cases where the values of the exponent well above 2 have been observed [8-10], a fact that cannot be explained on the basis of the theories mentioned above. Moreover, instances where the power law poorly fits have also been reported; VanLandimgham et al. [11] showed that

the spline curve fit provides a better approximation of the unloading responses from polymers they studied. Thus, uncertainties in their values, lack of clear physical meaning, and amount of computational effort needed warrant the development of an alternative method for the evaluation of the contact stiffness.

Energies measured in a nanoindentation experiment, or their ratios, are often employed for the nanomechanical analysis of the response of a material [12-17]. Quantities such as the peak indentation load, penetration depths, contact area, hardness and reduced modulus can be correlated to the indentation energies. One of the important applications of the indentation energies is that they can be used to represent the load-displacement curves. Attaf [16] has shown that the total and elastic energy constants—defined with respect to reference indentation energy—can be used to model the loading and unloading indentation responses. However, the analytical differentiation of the unloading power function evaluated at the maximum penetration depth is usually overestimated, even in the case where this function perfectly models the experimental unloading curve. The intent of this study is to develop an efficient contact stiffness evaluation procedure using the derivative of the energy-based power function by considering the unloading responses of materials having a wide range of elastic recovery capabilities.

4.2 Background theory

In the following section, we briefly review the procedure used to determine the contact stiffness and depth in the standard OP method for the sake of comparison. Several terminologies that are relevant in this study and used in the characterization of the indentation response are also explained.

4.2.1 Overview of the Oliver and Pharr method

In the OP method, the initial unloading stiffness (or contact stiffness, S_{OP}) is usually obtained by evaluating the differential of the power law at the maximum depth of penetration $\left(h_{\max}\right)$ as:

$$S_{OP} = mA_0\left(h_{\max} - h_f\right)^{m-1} \tag{4.2}$$

where A_0, m and h_f are the parameters determined by the least square fitting of the initial 30% of the unloading portion of the load-displacement curves. Initial unloading stiffness so obtained is then used to determine the contact depth $\left(h_c\right)$ as:

$$h_c = h_{\max} - \varepsilon\frac{P_{\max}}{S_{OP}} \tag{4.3}$$

4.2.2 Elastic recovery and energy constants

Response of a material to indentation is often characterized by a dimensionless elastic recovery ratio [18-19]. This parameter is a measure of a fraction of the deformation, which behaves elastically and is generally expressed either in terms of depth $\left(\eta_h\right)$ or work $\left(\eta_h\right)$ recovery ratios as:

$$\eta_h = \frac{h_{\max} - h_f}{h_{\max}} \tag{4.4}$$

$$\eta_w = \frac{W_E}{W_T} \tag{4.5}$$

where W_T is the total work done and W_E is elastic work recovered upon the complete withdrawal of the indenter. These quantities are determined from the area of the loading and

unloading curves, respectively, as shown in figure 4.1. Depth and work recovery ratio are equal in magnitude and may fall in the range 0-1 in which lower and upper limits represent the elastic and fully plastic materials, respectively. It has been found that the depth and work recovery ratio are approximately equal.

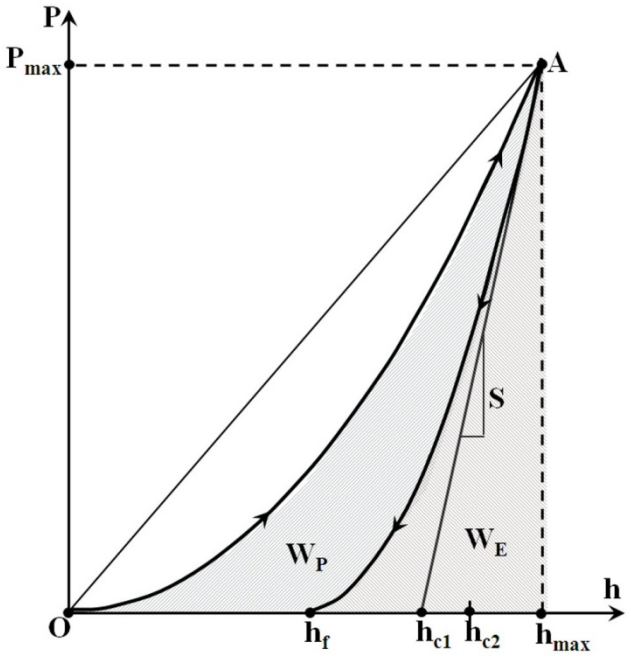

Figure 4.1: Schematic illustration of load-displacement curves showing associated terminology used in this study. Points h_{c1} *and* h_{c2} *are contact depths corresponding to* $\varepsilon = 1.0$ *and* $\varepsilon = 0.75$*, respectively.*

Attaf [13] introduced several energy-based parameters by assuming the absolute work, maximum possible energy that could be dissipated in an indentation experiment, as datum. Based on nanoindentation results on ceramics, they found that the absolute work (W_S) is proportional to both total and elastic work done respectively, such that

$$v_T = \frac{W_S}{W_T}; \quad v_E = \frac{W_S}{W_E} \tag{4.6}$$

The absolute work is given by: $W_S = 0.5 P_{\max} h_{\max}$. Ratios v_T and v_E are known as the total and elastic energy constants, respectively. Value for the total energy constant, which primarily depends on the indenter geometry, falls in the range 1.0-1.50, the upper limit corresponding to perfectly sharp conical indenter. On the other hand, v_E may vary in the range 1 to ∞, depending on the type of material with extremes denoting, like the energy recovery ratio, elastic and perfectly plastic materials, respectively. We have shown elsewhere [10] that v_T and v_E are evaluated in a slightly different way when the experimental load-displacement curves also feature a dwelling portion.

The energy constants defined above may be used to represent nanoindentation curves for a material. Attaf [16] derived the following expressions, on the basis of functional analysis, to represent the loading and unloading curves, respectively.

$$P = P_{\max} \left(\frac{h}{h_{\max}} \right)^{2v_T - 1} \tag{4.7}$$

$$P = P_{\max} \left(\frac{h}{h_{\max}} \right)^{2v_E - 1} \tag{4.8}$$

It is generally found that Eq. (4.7) can model the loading curve very accurately for all levels of loads. The approximating power of Eq. (4.8), however, depends on the type of material; this is more accurate in the case of materials that recover less upon unloading [20]. For harder materials, only the initial portion of the unloading curve can be approximated, which is good enough to evaluate the slope at the maximum depth of penetration analytically. The differentiation of Eq. (4.8) at $h = h_{\max}$ leads to the following expressions for the slope $\left(S_E \right)$.

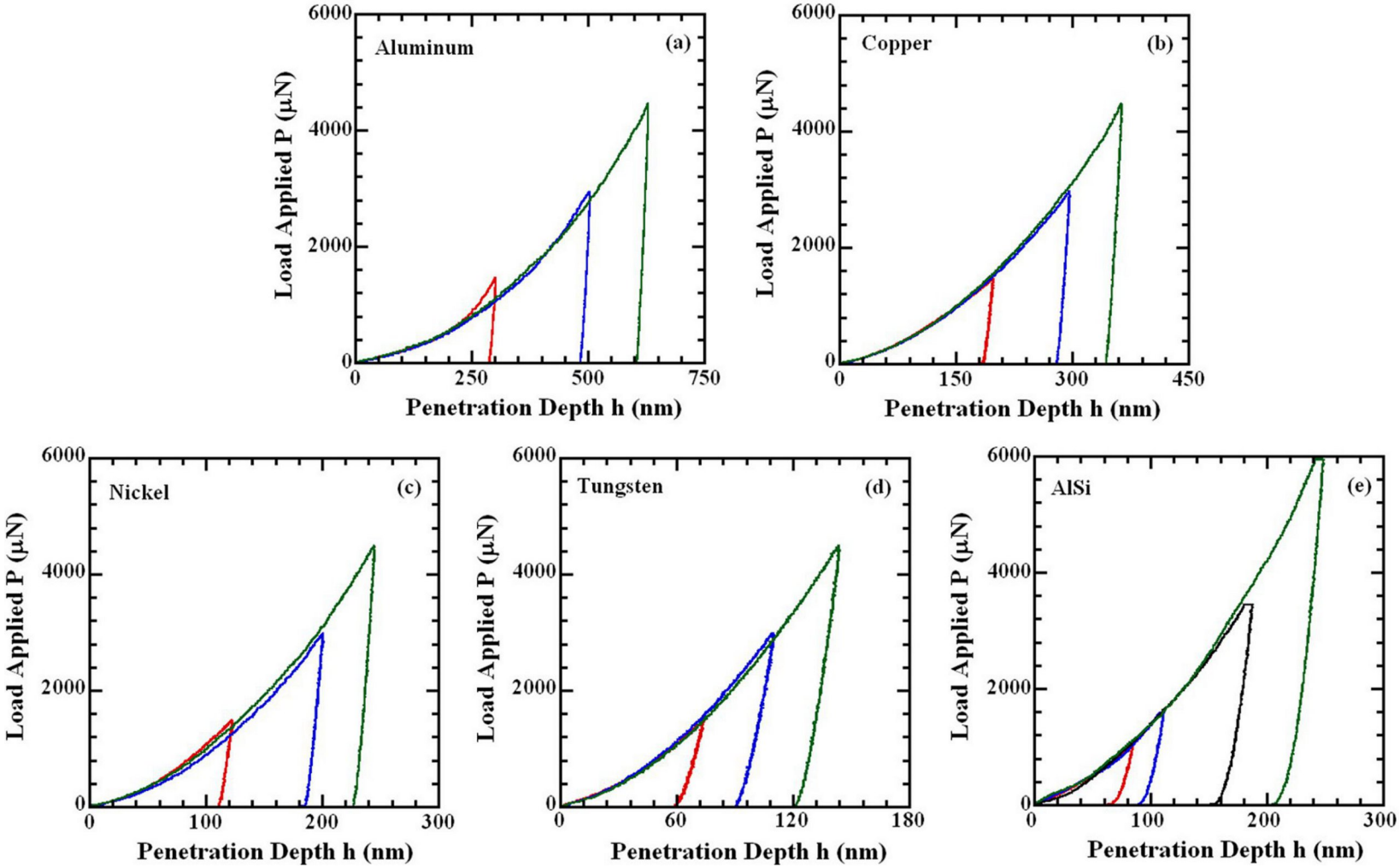

Figure 4.2: Representative load-displacement curves obtained in a nanoindentation experiment with a Berkovich indenter for materials tested in this study.

$$S_E = \left.\frac{dP}{dh}\right|_{h=h_{\max}} = \left(2\nu_E - 1\right)\frac{P_{\max}}{h_{\max}} \tag{4.9}$$

The S_E determined by Eq. (4.9) should in principle match the S_{OP} obtained by Eq. (4.1). Finally, Attaf [17] derived an expression for the contact depth $\left(h_c^E\right)$ using Eq. (4.9) in the following form:

$$h_c^E = \frac{2\left(\nu_E - 1\right)}{\left(2\nu_E - 1\right)} h_{\max} \tag{4.10}$$

The validity of the above equation has been confirmed in many studies. Eq. (4.10) implies that the difference between h_c^E and $h_{\max}$ becomes smaller as we move from harder to softer materials. As will be discussed, the proximity between these two quantities has important bearing on the accuracy of initial unloading stiffness determined by Eq. (4.9).

4.3 Experimental

Nanoindentation experiments are conducted in the load controlled mode using a Hysitron Triboindenter fitted with a Berkovich indenter at room temperature on four metal samples: single crystal aluminum, and copper; and polycrystalline nickel and tungsten. A triangular loading history with loading and unloading times each equal to 10s is considered with three different peak indentation loads of magnitudes approximately equal to 1500 μN, 3000 μN and 4500 μN. A total of nine indents are made corresponding to each peak indentation load on every polished sample having a surface roughness less than 100 Å. Representative load-displacement curves obtained from nanoindentation experiments for copper are shown in figure 4.2. The area function was established according to the OP method using a standard

Table 4.1: Measured values (mean) of mechanical properties and other nanomechanical quantities, for Al and Cu measured in this study. Values in parenthesis are standard deviations.

Materials	**P_{max} (μN)**	**H_{max} (nm)**	**H_f (nm)**	**v_E**	**E_r (GPa)**	**H (GPa)**
Al	1456.3 (1.4)	304.9 (5.4)	288.8 (5.8)	32.5 (3.1)	78 .0 (1.6)	0.50 (0.02)
	2941.4 (0.4)	499.8 (5.9)	476.3 (6.6)	33.4 (2.5)	64.2 (1.4)	0.39 (0.01)
	4447.7 (0.5)	631.3 (6.5)	603.1 (5.9)	34.4 (2.3)	59.3 (1.9)	0.38 (0.01)
Cu	1472.1 (1.1)	196.5 (3.1)	183.9 (3.1)	18.8 (1.3)	129.3 (4.4)	1.20 (0.04)
	2964.9 (0.9)	299.9 (2.7)	282.5 (2.7)	22.5 (1.9)	122.6 (3.4)	1.08 (0.02)
	4470.5 (0.8)	367.9 (2.2)	346.3 (2.0)	22.5 (0.9)	122.3 (4.3)	1.09 (0.01)

Table 4.2: Measured values (mean) of mechanical properties and other nanomechanical quantities, for Ni and W measured in this study. Values in parenthesis are standard deviations.

Materials	**P_{max} (μN)**	**H_{max} (nm)**	**H_f (nm)**	**v_E**	**E_r (GPa)**	**H (GPa)**
Ni	1483.3 (1.1)	131.6 (6.3)	119.9 (6.4)	15.0 (1.6)	210.8 (13.2)	2.81 (0.28)
	2979.1 (1.8)	192.1 (7.1)	175.6 (7.8)	15.5 (1.5)	216.3 (7.9)	2.67 (0.21)
	4480.5 (1.1)	242.9 (6.3)	223.2 (7.0)	15.8 (0.9)	205.4 (5.6)	2.52 (0.14)
W	1490.9 (1.1)	73.6 (3.5)	58.6 (4.5)	6.6 (0.6)	316.9 (14.9)	9.20 (0.89)
	2987.7 (0.5)	110.2 (0.5)	89.2 (1.0)	7.0 (0.3)	314.4 (8.5)	8.75 (0.06)
	4489.4 (0.7)	140.8 (5.0)	116.5 (6.2)	7.2 (0.5)	306.3 (6.1)	8.13 (0.67)

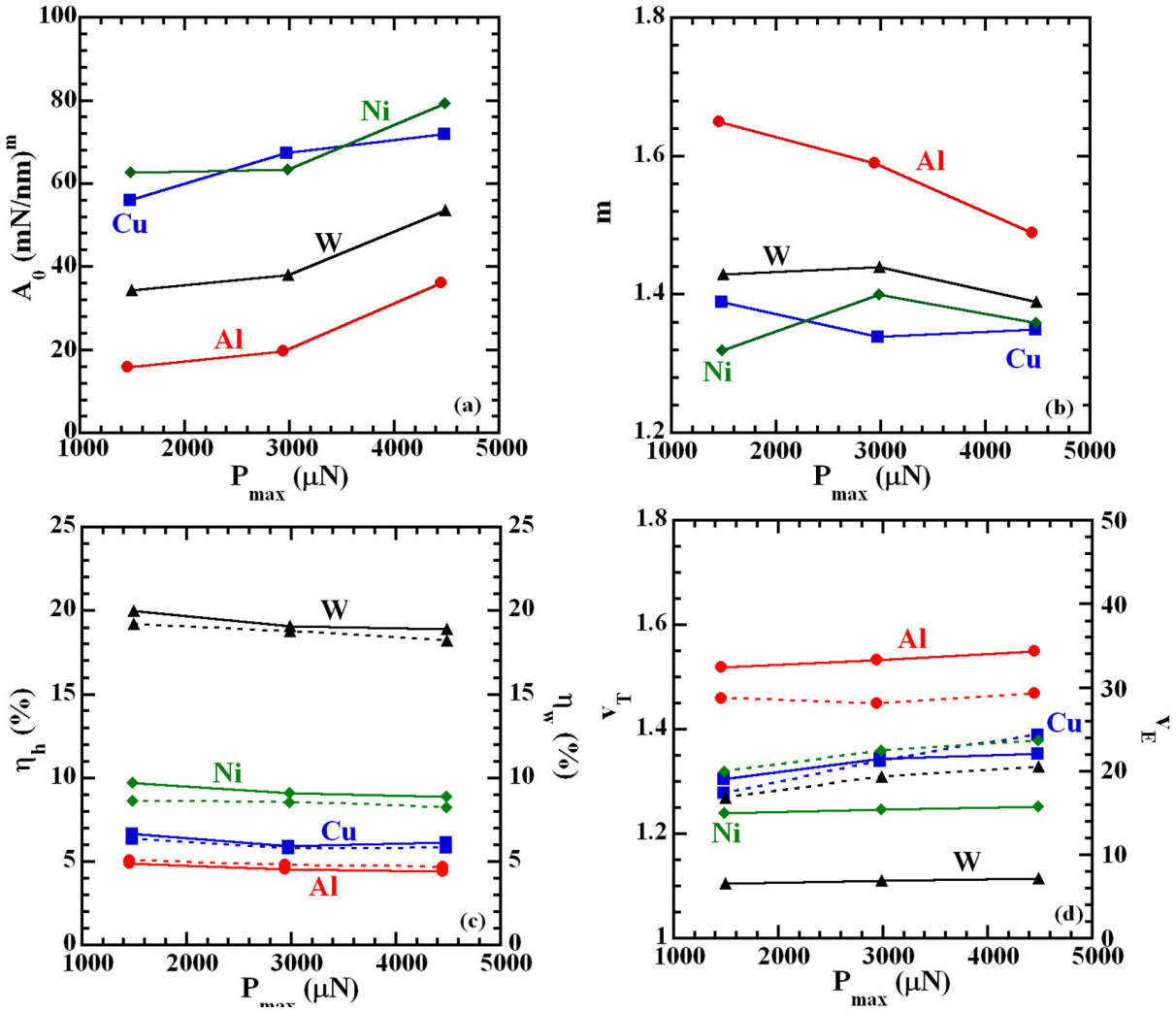

Figure 4.3: Plots showing the variations of (a) power-law coefficient; (b) power-law exponent; (c) elastic depth (dashed lines) and work recoveries (solid lines); and (d) total (dashed lines) and elastic (solid lines) energy constants with the peak indentation load for aluminum, copper, nickel and tungsten.

fused quartz sample. Table 4.1 summarizes mean and standard deviation of the reduced modulus and hardness for all these metals, which accord well with those reported in the literature.[21] Previously conducted indentation tests on plasma sprayed Al-12 wt. % Si (*referred as Al-Si hereafter)* coating are also used in this study [22]. An Al-Si sample was

subjected to a trapezoidal load history with loading, dwelling and unloading times respectively equal to 10s, 2s and 10s. Similarly, experimental data on SiO_2, TiO_2 and Ta_2O_5 are selected from Ref. [15] to constitute a set of materials that has a wide range of percentage elastic recovery and an elastic energy constant. The load-displacement curves for coating and oxides of ceramics mentioned are acquired by employing four different peak indentation loads of a magnitude less than 10mN. Finally, experimental data reported in the literature [2, 18, 23] are used to validate the proposed method for the evaluation of initial unloading stiffness when the peak indentation load is in excess of 100mN.

4.4 Results and discussions

4.4.1 Determination of nanomechanical quantities

Experimental load-displacement curves are analyzed to determine various nanomechanical quantities such as depth and work elastic recovery ratios, energy constant, contact depth and initial unloading stiffness, as described in section II. Figure 4.3 shows the variations in power-law parameters, recovery ratios and energy constants with the peak indentation load. It is evident that, unlike power-law parameters, recovery ratios and energy constants remain practically the same with respect to the peak indentation load for all these metals. Figure 4.4 compares initial unloading stiffness determined by Eq. (4.2) and Eq. (4.9) for all the materials considered in this study where significantly large deviations in the stiffness values are apparent. As can be seen, the error depends on the type of materials; it is greater for the materials which recovers less. The average percentage error for W, Ni, Cu and Al falls in the range of 60% -120%, in which cases Eq. (4.8) models unloading curves very accurately. Contact depths determined by Eq. (4.10) compare well with those measured

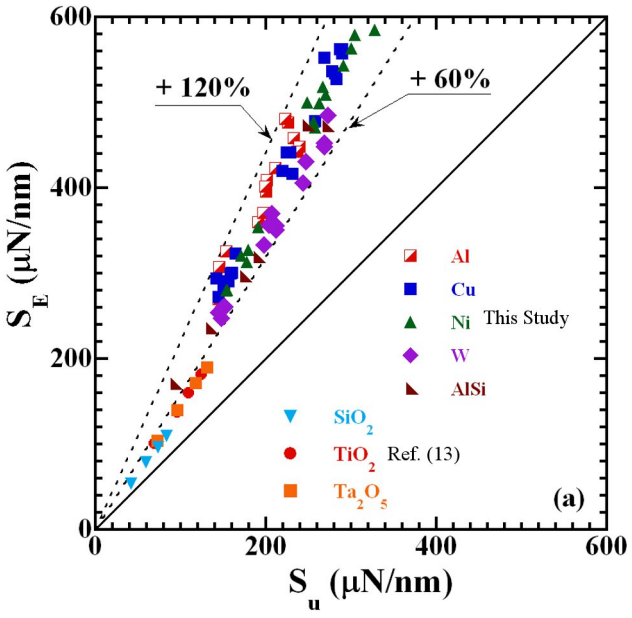

Figure 4.4: Comparison of calculated initial unloading stiffness using Eq. (4.9) with that obtained by the Oliver and Pharr method using Eq. (4.2).

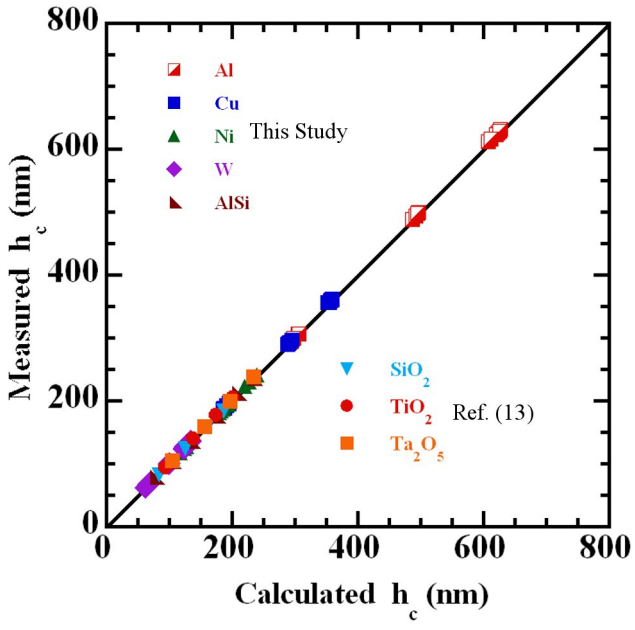

Figure 4.5: Comparison of calculated contact depths using Eq. (4.10) with that obtained by the Oliver and Pharr method using Eq. (4.3).

with a relative error better than 5%, as depicted in figure 4.5 for all the materials. At this point, a question arises as to why Eq. (4.9) yields erroneous stiffness while Eq. (4.10), derived using Eq. (4.9), predicts reasonable contact depth. This can be explained with reference to figure 4.1. The actual contact depth lies somewhere between h_{c1} and h_{c2}, which corresponds to geometric factor, ε, equal to 1.0 and 0.75, respectively. Point h_{c1} is referred to as plastic depth and is determined by extending the tangent to the unloading curve with slope $S_{OP}\left(S_E\right)$ to the h-axis [24], which is exactly followed by Attaf to derive Eq. (4.10) from Eq. (4.9). This means that h_c^E actually is the plastic depth $\left(h_{c1}\right)$, not the contact depth $\left(h_c\right)$. However, the fact that $h_c^E \approx h_c$ and the initial unloading stiffness are always overestimated indicates that the energy-based power function given by Eq. (4.8) has larger curvature as compared to the power-law at the maximum depth of penetration. The tangent to the unloading power function happens to pass through the actual contact depth, not the plastic depth ostensibly due to large curvature. This warrants an appropriate correction to Eq. (4.10).

4.4.2 Proposed method to evaluate the contact stiffness

In the OP method, as discussed previously, contact depth is evaluated from the initial unloading stiffness. Since the contact depth is known as a function of the elastic energy constant in advance, it may be used to evaluate the initial unloading stiffness in a reverse manner. To do this, Eq. (4.3), by substituting $h_c = h_c^E$ and replacing S_{OP} by S_E, may be rearranged in the following form:

$$S_E = \varepsilon \frac{P_{\max}}{h_{\max} - h_c^E} \tag{4.11}$$

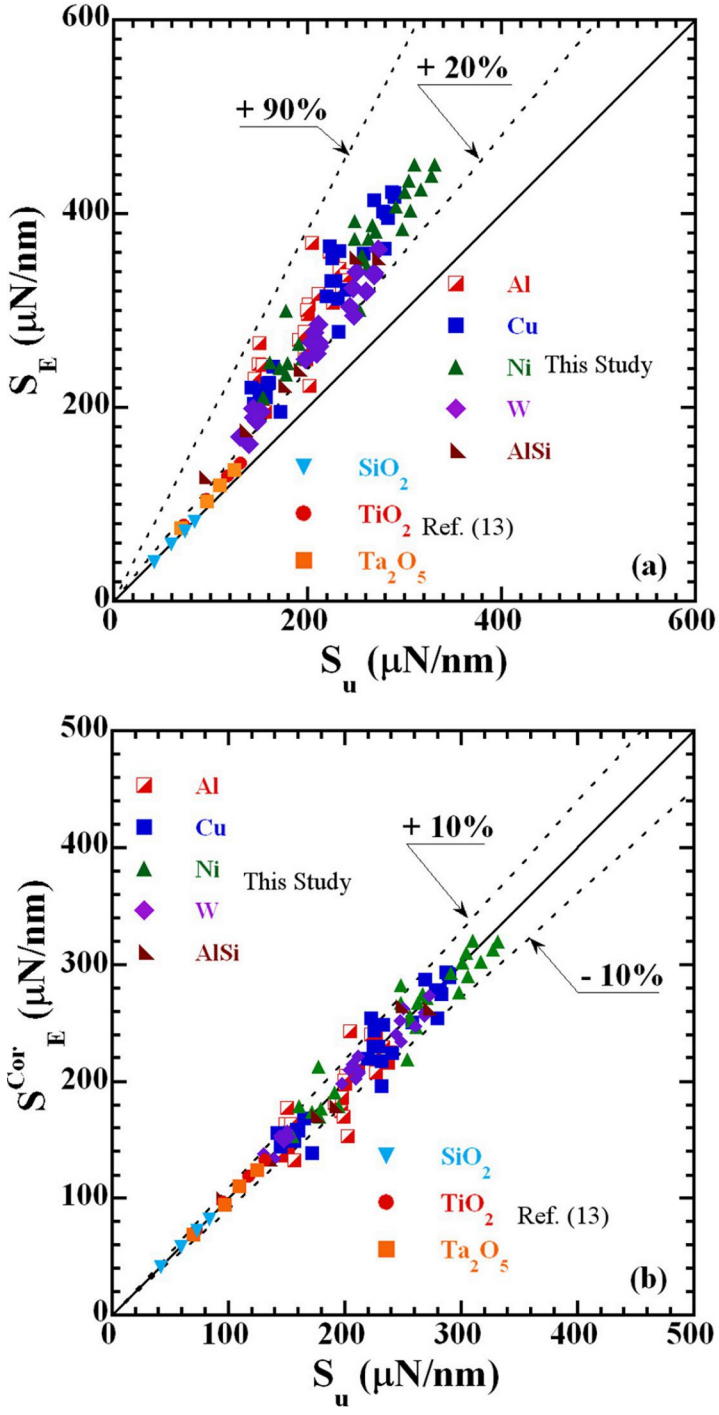

Figure 4.6: Comparison of corrected initial unloading stiffness when correction due to (a) curvature; and (2) proximity between contact and maximum penetration depths with that obtained by the Oliver and Pharr method.

which may be written in terms of the elastic energy constant as:

$$S_E = \varepsilon\left(2v_E - 1\right)\frac{P_{\max}}{h_{\max}} \tag{4.12}$$

From Eq. (4.9) and (4.12), it is evident that the error in the initial unloading stiffness may be reduced by 25% by multiplying it with the geometry factor $\varepsilon = 0.75$. Comparison between S_E calculated by Eq. (4.12) with that obtained by Eq. (4.11), as shown in figure 6a, indicates that Eq. (4.12) yields a reasonably accurate value in the case of SiO_2 only. Note that SiO_2 has the maximum elastic recovery among the materials considered in this study. For the rest of the materials, the error in the initial unloading stiffness is still very large and increases with the decrease in the percentage elastic recovery. For example, the average error in S_E determined by Eq. (4.14) or Eq. (4.15) is about 58% for aluminum, which has the least percentage elastic recovery in the list of materials considered. Note that the corresponding error in the contact depth h_c^E is only 0.84%. After careful examination, we found this is a computational error which arises due to the proximity of the contact and maximum penetration depth. This can be explained with the help of a numerical example in one of the indentation tests on aluminum, where we found $P_{\max} = 1497.0$ μN, $h_{\max} = 311.80$ nm, $h_c =$ 304.7 nm, $h_{cE} =$ 307.30 nm.

Using the values of h_c and h_{cE} successively in Eq. (4.14), we found S_u and S_E, respectively, equal 156.6μN/nm and 241.2μN/nm. Clearly, the discrepancy between S_u and S_E arises due to a large difference in the denominator of Eq. (4.14) when evaluated using h_c and h_c^E. For the set of data considered above, the difference between $\left(h_{\max} - h_c\right)$ and

$\left(h_{\max} - h_c^E\right)$ is about 36%. This error is more pronounced when the $h_{\max}$ and h_c (or h_{cE}) values are very close to each other. On the basis of this observation, one may conclude that significantly different initial unloading stiffnesses are obtained if the contact and maximum depth of penetration are very close to each other, no matter how accurately Eq. (4.10) determines the contact depth. For materials whose maximum depth of penetration and contact depth are considerably apart, this error becomes insignificant.

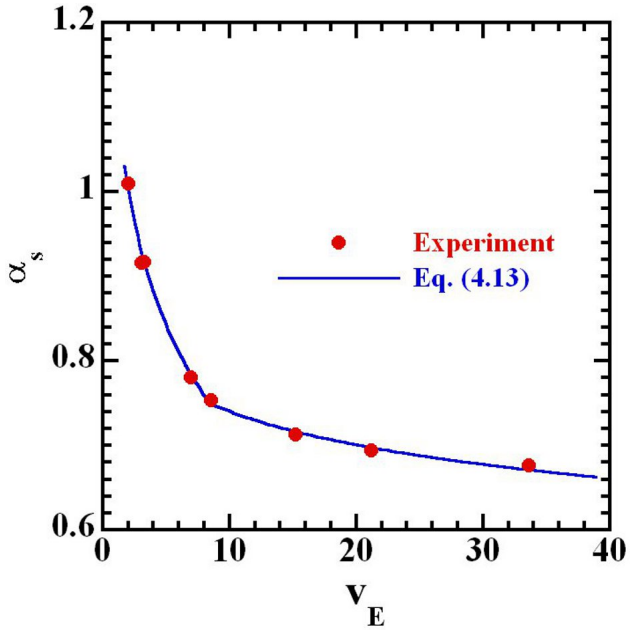

Figure 4.7: Plot showing the variations of stiffness correction factors with the elastic energy constant.

Dependency of this error on the elastic recovery of a material indicates that a correlation between the error due to proximity in the contact and maximum penetration depths and elastic energy constant may exist. To establish a possible correlation between them, the ratio of stiffness calculated by the OP method to that by Eq. (4.12) for each material is plotted as a

function of their elastic energy constant, as shown in figure 4.7. As can be seen, the ratio decreases as the elastic energy constant increases. The correlation may be fitted with the piecewise logarithmic equations as:

$$\alpha_s = \begin{cases} A_1 - B_1 \log(v_E) & v_E \le 8.50 \\ A_2 - B_2 \log(v_E) & v_E > 8.50 \end{cases} \tag{4.13}$$

where $\alpha_s = S_u / S_E$ is termed as the stiffness correction factor, and A_1, A_2, B_1 and B_2 are constants equal to 1.124, 0.873, 0.404 and 0.132, respectively. Thus, a corrected expression for the initial unloading stiffness may be written as:

$$S_E = \alpha_s \varepsilon (2v_E - 1) \frac{P_{\max}}{h_{\max}} \tag{4.14}$$

The initial unloading stiffness evaluated from Eq. (4.14) is once again compared with that obtained by the OP method, as shown in figure 6b, where excellent agreement could be seen between them. The proposed method is further validated with the help of nanoindentation data available in the literature, which were acquired with a peak indentation load equal to or greater than 100 mN. For illustration, we consider the nanomechanical data pertaining to the fused silica mentioned in ref. [2] as $P_{\max} = 118.43$ mN, $h_{\max} = 1045.0$ nm, $h_f = 540.40$ nm, $A_0 = 0.050$, and $m = 1.24$. The reduced modulus (E_r) and hardness (H) of this material are reported to be 69.60 and 8.40 GPa, respectively. With these input parameters, unloading stiffness is calculated using both the power law and Eq. (4.14), and are found to be equal to 296.0 μN/nm and 300.0 μN/nm, respectively, which are very close to each other. This

quantity can also be back-calculated from the known peak indentation load, reduced elastic modulus and hardness (obtained by substituting $P_{\max} / H$ for A_c in Eq. (4.1)).

$$S_u = \frac{2}{\sqrt{\pi}} E_r \sqrt{\frac{P_{\max}}{H}} \tag{4.15}$$

Table 4.3: Comparison of the initial unloading stiffness calculated using Eq. (4.14) with that obtained by the Oliver and Pharr method for materials subjected to the peak indentation load equal to or greater than 100mN.

Materials	**P_{max} (mN)**	**η_h (%)**	**ν_E**	**α_s**	**S_E^{cor}**	**S_u**	**% Error**
Aluminum	118.32	1.70	79.31	0.622	1.881	1.906	1.3
Quartz	118.48	51.30	2.33	0.976	0.388	0.412	5.8
Soda lime glass	118.37	39.60	3.02	0.930	0.373	0.364	-2.5
Fused Silica	118.50	48.30	2.31	0.977	0.300	0.296	-1.4
Sapphire	118.43	40.90	3.09	0.926	0.819	0.795	-3.0
Tungsten	118.43	7.50	18.55	0.705	2.103	1.998	-5.3
Copper	100.00	5.90	24.87	0.689	1.181	1.227	3.7
1070 Steel	100.00	23.60	4.95	0.843	0.837	0.788	-6.2
Silicon Nitride	100.00	44.30	2.94	0.935	0.632	0.598	-5.7

Eq. (4.15) yields $S_u = 295.0$ μN/nm and thus confirms that the error due to digitization of the data from the literature is negligibly small. Similar calculations for materials like aluminum, quartz, soda lime glass, sapphire, tungsten, copper, 1070 steel and SiN_4 were carried out.

Excellent agreement, with accuracy better than 6% between the values evaluated by the two methods, was obtained for each material, as summarized in Table 4.3.

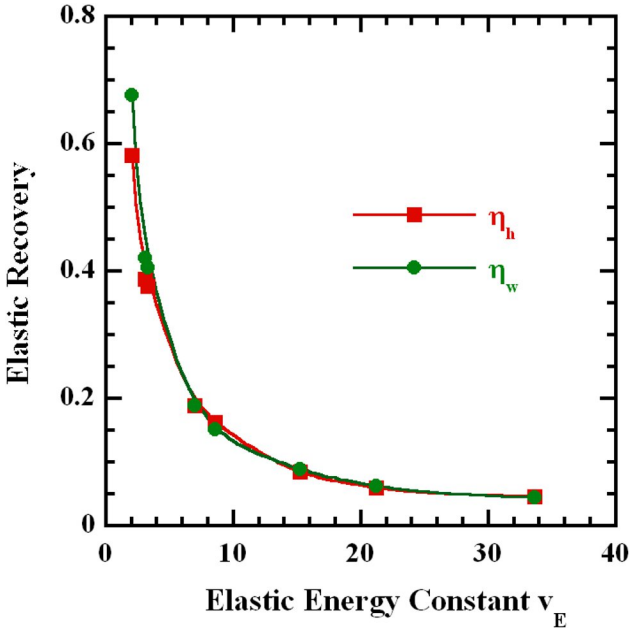

Figure 4.8: Plot showing the correlation between elastic depth and work recoveries with the elastic energy constant.

4.4.3 Further simplification

The method described in the previous section to determine initial unloading stiffness can further be simplified by employing the relationship between the elastic recovery ratios and elastic energy constant, and the information contained in the loading curve. For this purpose, depth and work recovery ratios are plotted as a function of the elastic energy constant for SiO_2, TiO_2, Ta_2O_5, Al-Si, W, Ni, Cu and Al, as shown in figure 4.8. It is clear from the figure that recovery ratios decrease with the increase in the elastic energy constant. This relationship allows us to calculate the elastic energy constant without evaluating the elastic

work done. Thus, the determination of initial unloading stiffness requires peak indentation load, maximum depth of penetration and residual depth as input parameters; all can be readily obtained from the nanoindentation load displacement curves and thus require less computational effort, as compared to that applied in the conventional OP method.

If S_E corresponding to one set of $P^1_{\max}$ and $h^1_{\max}$ is known, then it may be scaled for the other set $P^2_{\max}$ and $h^2_{\max}$ without analyzing the unloading curve obtained corresponding to the peak indentation load $P^2_{\max}$, provided the indentation response is free from any residual stress effect.[25] Such a combination of peak indentation load and maximum depth of penetration may be obtained from Eq. (4.7) as:

$$P^2_{\max} = P^1_{\max}\left(\frac{h^2_{\max}}{h^1_{\max}}\right)^{2v_T-1} \tag{4.16}$$

This eliminates the need for analyzing the unloading curve corresponding to each indentation. The proposed method may be used to quantify the effect of the substrate on the mechanical properties of thin coatings.

4.5 References

[1] Pharr, G.M., Oliver, W.C., and Brotzen, F.R. (1992). "On the generality of the relationship among contact stiffness, contact area, and elastic modulus during indentation." *Journal of Materials Research*, 7, 613-617.

[2] Oliver, W.C., and Pharr, G.M. (1992). "An improved technique for determining hardness and elastic modulus using load and displacement sensing indentation experiments." *Journal of Materials Research*, 7, 1564-1583.

[3] Pharr, G.M., and Bolshakov, A. (2002). "Understanding nanoindentation unloading curves." *Journal of Materials Research*, 17, 2660-2671.

[4] Marx, V., and Balke, H. (1997). "A critical investigation of the unloading behavior of sharp indentation." *Acta Materialia*, 45, 3791-3800.

[5] Sawa, T. and Tanaka, K. (2001). "Simplified method for analyzing nanoindentation data and evaluating performance of nanoindentation instruments." *Journal of Materials Research*, 16, 3084-3096.

[6] Gong, J., Miao, H., and Peng, Z. (2004). "Analysis of the nanoindentation data measured with a Berkovich indenter for brittle materials: effect of the residual contact stress." *Acta Materialia*, 52, 785-793.

[7] Giannakopoulos, A.E., and Suresh, S. (1999): "Determination of elastoplastic properties by instrumented sharp indentation." *Scripta Materialia*, 40, 1191-1198.

[8] Briscoe, B.J., and Sebastian, K.S. (1996). "The elastoplastic response of Poly (Methyl Methacrylate) to indentation." *Proceeding of The Royal Society A*, 452, 439-457.

[9] Tranchida, D., and Piccarolo, S. (2005). "On the use of the nanoindentation unloading curve to measure Young's modulus of polymers on nanometer scale." *Macromolecular Rapid Communications*, 26, 1800-1804.

[10] Jha, K.K., Suksawang, N., Lahiri, D., and Agarwal, A. (2012): "Energy-based analysis of nanoindentation curves for cementitious materials." *ACI Materials Journal,* 109, 81-90.

[11] VanLandingham, M.R., Villarrubia, J.S., Guthrie, W.F., and Meyers, G.F. (2001). "Nanoindentation of polymers: An overview." Macromol. Symp. 167, 15-42.

[12] Sakai, M. (1993). "Energy principle of the indentation-induced inelastic surface deformation and hardness of brittle materials." *Acta Metallurgica et Materialia*, 41, 1751-1758.

[13] Attaf, M.T. (2003). "New ceramics related investigation of the indentation energy concept." *Material Letters*, 57, 4684-4693.

[14] Malzbender, J. (2005). "Comment on the determination of mechanical properties from the energy dissipated during indentation." *Journal of Materials Research*, 20, 1090-1092.

[15] Attaf, M.T. (2003). "A unified aspect of power-law correlations for berkovich hardness testing of ceramics." *Material Letters*, 57, 4627-4638.

[16] Attaf, M.T. (2004). "Step by step building of a model for the Berkovich indentation cycle." *Material Letters*, 58, 507-512.

[17] Attaf, M.T. (2004). "New formulation of the nanomechanical quantities using the β-material concept and the indentation function." *Material Letters*, 58, 889-894.

[18] Hainsworth, S.V., Chandler, H.W., and Page, T.F. (1996): "Analysis of nanoindentation load-displacement loading curves," *Journal of Materials Research*, 11, 1987-1995.

[19] Milman, Y.V. (2008): "Plasticity characteristic obtained by indentation." *Journal of Physics D: Applied Physics* 41, 074013.

[20] Jha K.K., Suksawang N, Agarwal A. "Analytical approach for the determination of nanomechanical properties for metals." In: MEMS and Nanotechnology, Volume 4, Conference proceedings of the Society for Experimental Mechanics, Uncasville, CT, 2011.

[21] Lee, H., Ko, S., Han, Park, J.H. and Hwang, W. (2005): "Novel analysis for nanoindentation size effect using strain gradient plasticity." *Scripta Materialia*, 53, 1135-1139.

[22] Bakshi, S.R., Singh, V., Seal, S. and Agarwal, A. (2009). "Aluminum composite reinforced with multiwalled carbon nanotubes from plasma spraying of spray dried powders." *Surface and Coating Technology*, 203, 1544-1554.

[23] Jayaraman, S., Hahn, G.T., Oliver, W.C., Rubin, C.A. and Bastias, P.C. (1998). "Determination of monotonic stress-strain curve of hard materials from ultra-low-load indentation tests." *International Journal of Solids and Structures*, 35, 365-381.

[24] Doerner, M.F., and Nix, W.D. (1986). "A method for interpreting the data from depth-sensing indentation instruments." *Journal of Materials Research*, 1, 601-609.

[25] Suresh, S., and Giannakopoulos, A.E. (1998). "A new method for estimating residual stresses by instrumented sharp indentation." *Acta Materialia*, 46, 5755-5767.

CHAPTER 5

MODIFIED WORK-OF-INDENTATION APPROACH

5.1 Introduction

Small scale mechanical properties of a material such as hardness, elastic modulus, yield stress, strain hardening exponent, fracture toughness, etc. may be determined conveniently and reliably by an experimental technique called nanoindentation. In this method, a smooth surface of a material is indented with a probe of a specified geometry and known mechanical properties to record load vs. penetration depth curves. The data so obtained generally provides information on curvatures, contact stiffness (initial unloading stiffness), indentation energies, maximum depth of penetration, peak indentation load, etc., which may be used in conjunction with the theory of contact mechanics to evaluate the mechanical properties [1]. For instance, contact stiffness may be used in the Sneddon's solution for indentation of the elastic half-space by a rigid axial indenter to determine the elastic modulus, provided the area of contact or hardness of the material is known.

The mechanical property that we are interested in determining first is the hardness of a material – defined as a ratio of the peak indentation load to projected contact area, which is computed according to a procedure called the area function technique [2]. This procedure essentially consists of establishing an area function, expressed in terms of contact depth, using a test material with a known elastic modulus. The area function established in this way is used subsequently in the evaluation of mechanical properties of unknown materials. the unloading curve obtained as a result of the indentation on a material under consideration is analyzed to ascertain the contact depth, which is eventually used to calculate contact area and

hardness. Accuracy better than 5% is obtained if the hardness is evaluated by the method just explained. However, an erroneous contact area may be obtained if the pile-up around the hardness impression is significant [3]. The area function technique is also found to be unsuitable for the material that is viscoelastic and/or heterogeneous [4-5]. Although attempts have been made to calculate the corrected contact area, no dramatic improvement in the accuracy of the computed value is realized. This limitation of the Oliver and Pharr (OP) method has led to the development of various nanomechanical property evaluation procedures that do not require the calculation of the contact area at all [5-9]. These procedures, however, have their own limitations and their accuracy remains a concern in the material science community. Furthermore, the area function is calibrated using the same fundamental relation described above, which needs to be corrected due to both the lack of axial symmetry of the indenter and the improper boundary condition used in its derivation, even when the contact depth is precisely known. Correction factors that account for these effects depend on the indenter geometry, Poisson's ratio of the material, maximum penetration depth, etc., but their precise measurement is still debated [10-13]. Omission of these correction factors has more serious consequences on the accuracy of contact area (or hardness) than on the reduced elastic modulus [10].

The work-of-indentation approach, as proposed by Tuck et al. [9], offers a convenient way to determine the hardness of a material, and is the most promising among the methods that do not require the computation of the contact area. This approach employs the total work done during indentation, which can be evaluated very precisely as compared to the area function, even if the pile-up is significant. Varying conclusions regarding its accuracy could be found in the literature. It is reported that this approach works well when it is applied to the

indentation data from soft materials [9, 14-15]. On the other hand, studies on harder materials indicate that it gives erroneous results [16-17]. Such a comparison, however, is not justified, as the hardness values determined by the OP method and the WI approach are fundamentally different. While the hardness determined in the OP is based on the contact depth, the maximum depth of penetration is used in the WI approach.

The WI approach, in its existing form, is limited to the case where an indenter is considered to be ideally sharp. In recent times, nanoindentation tests are routinely carried out in the load range below 10 mN due to the restriction imposed by the sample size and type. The effectiveness of the work-of-indentation approach is largely unexplored in this load range. As the indenter tip bluntness is more pronounced at a small indentation load [6], it is imperative to further investigate the viability of this approach in this load range. Thus, the objectives of this study are to: (1) improve the existing WI approach by accounting for the effect of tip bluntness ; (2) investigate if and how hardness values of a material evaluated by these two methods could be related; and (3) examine how such correlation is affected by the tip bluntness. The study presented here is of great significance from the viewpoint of the development of a method to determine Young's modulus from the loading curve, where the knowledge of conventional hardness is *a priori* [6-8].

5.2 Theoretical background

The link between the hardness values determined by the OP method and WI approach can be established using parameters that are obtainable from the load-displacement curves. To facilitate understanding, the definitions of elastic recovery ratios and energy constants used

in this study followed by a short description of the hardness determination by the OP method are given below.

5.2.1 Definition of terms

Typical load-displacement curves obtained in a nanoindentation experiment are shown schematically in figure 5.1. Certain nanomechanical quantities derived from such curves may be utilized to characterize the indenter geometry and material's response to indentation. For instance, whether a material is elastic or perfectly plastic can be ascertained with the help of elastic recovery. It is usually expressed either in terms of the depth recovery ratio (η_h) or energy (η_w) recovery ratios, respectively as:

$$\eta_h = \frac{h_{\max} - h_f}{h_{\max}} \times 100\%$$
$$\eta_w = \frac{W_E}{W_T} \times 100\% \qquad (5.1)$$

where $h_{\max}$ is the maximum depth of penetration, h_f is the residual depth, W_T is the total energy dissipated and W_E is the elastic energy recovered after the complete withdrawal of the load. The total and elastic energies are usually evaluated, respectively from the areas under the loading and unloading curves. Values of both depth as well as energy recovery ratios fall in the range 0–1; their upper and lower limits correspond to the elastic and perfectly plastic materials, respectively. Although elastic recovery ratios also depend on the half-included angle and tip radius, the condition of the indenter (whether it is ideally sharp or blunt) cannot be decided based on their magnitude.

On the other hand, the characterization of the indenter geometry and material response to indentation can be effectively done with the help of energy constants. Attaf [18] introduced several energy constants, which have important implications in the analysis of load-displacement data. Three of them are relevant to this study and may be expressed mathematically as:

$$v_T = \frac{W_S}{W_T}; \quad v_P = \frac{W_S}{W_P}; \quad v_E = \frac{W_S}{W_E} \tag{5.2}$$

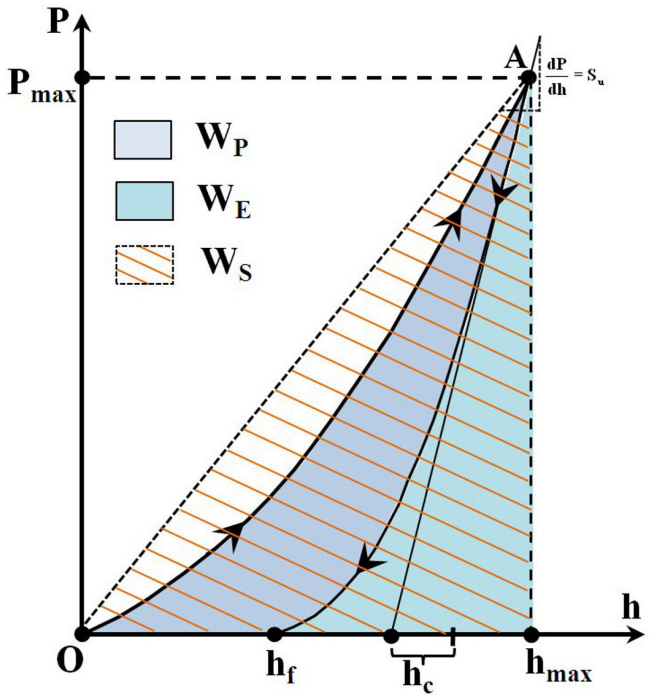

Figure 5.1: Typical load-displacement curves obtained from nanoindentation and the terminologies used.

Ratios v_T, v_E and v_P are known as total, elastic and plastic energy constants, respectively. The absolute work (energy), denoted by W_S in Eq. (5.2), is the maximum possible work done by the indenter in any indentation experiment and is evaluated as the area of the triangle $OAh_{\max}$,

as shown in figure 5.1. The energy absorbed as a result of plastic deformation is given by the difference between the total and elastic energies: $W_P = W_T - W_E$. These three ratios satisfy the following condition for a given indenter geometry:

$$\frac{1}{v_T} = \frac{1}{v_E} + \frac{1}{v_P} \tag{5.3}$$

Constant v_T depends primarily on the indenter geometry which may take the value in the range of 1.0-1.5, where the maximum value corresponds to an ideally sharp conical indenter; it decreases with the increase in the tip bluntness. Likewise, the elastic energy constant quantifies the portion of the deformation recovered upon complete unloading. It varies in the range of 1.0 - ∞; the end values represent elastic and perfectly plastic materials, respectively. We have shown elsewhere that the total energy constant is independent of the material properties if the indenter tip to maximum depth of penetration $\left(R / h_{\max}\right)$ ratio is less than 2 [19]. The elastic energy constant, on the other hand, depends on both material properties as well as the $R / h_{\max}$ ratio. However, the rate at which it decreases with respect to $R / h_{\max}$ is independent of the material properties. Due to this reason, these quantities may be used as index parameters wherever the material's response to indentation and the condition of the indenter need to be quantified.

5.2.2 Determination of hardness by the Oliver and Pharr method

Conventionally, the hardness of a material is defined as the average pressure divided over the projected contact area as:

$$H_{OP} = \frac{P_{\max}}{A_c} \tag{5.4}$$

where A_c denotes the contact area at the peak indentation load $P_{\max}$. In the OP method [2], the contact area is expressed as a function of the depth (h_c) along which the contact is made, which has the following form:

$$A_c = C_0 h_c^2 + \sum_{i=1}^{8} C_i h_c^{2-i} \tag{5.5}$$

The above expression is called the area (shape) function and is usually established with the help of a test material whose elastic modulus is precisely known. Note that the leading term C_0 describes an ideally sharp Berkovich indenter and the rest of the constants C_i take the indenter tip bluntness into account. The contact depth is estimated from the unloading portion of the load-displacement curves according to:

Table 5.1: Typical values of the mechanical properties and other quantities for metals tested in this study.

Material	**P_{max} (μN)**	**h_{max} (nm)**	**h_c (nm)**	**H_{OP} (GPa)**	**E_r (GPa)**
Al	2941.37	499.77	488.8	0.39	64.2
Cu	2964.88	299.89	290.05	1.08	121.9
Ni	2979.05	192.05	183.11	2.67	216.3
W	2987.72	110.19	99.23	8.92	314.4

$$h_c = h_{\max} - \varepsilon \frac{P_{\max}}{S_u} \tag{5.6}$$

The symbol S_u is the initial unloading stiffness obtained as the derivative of the power law evaluated at the maximum depth of penetration, and ε is a constant, which depends on the indenter geometry; a value of 0.75 is used for a Berkovich tip. The OP method yields an accurate value of hardness for all those materials for which the ratio η_h is less than 0.3 [3].

5.3 Experimental data

Nanoindentation tests were carried out on polished samples from polycrystalline tungsten and nickel, and single crystals of copper and aluminum using a Triboindenter fitted with a Berkovich tip. Three different peak indentation loads of magnitudes approx. 1500, 3000 and 4500 μN were selected. A total of 27 indents were made on each sample; 9 correspond to each peak indentation load. Using the OP method, the reduced modulus and hardness values for all these metals were evaluated as summarized in Table 5.1. Besides these data, the indentation result on ceramics (SiO_2, TiO_2 and Ta_2O_5) from the literature [18] is also included in this study. Indentations on ceramics were also carried out using a Berkovich indenter, but with peak indentation loads of the approximate magnitudes of 2500, 5000, 7500 and 10000μN. These materials constitute a set in which the percentage elastic recovery varies from 4% (Aluminum) to 58% (SiO_2).

In order to examine the validity of the proposed model over a wide range of peak indentation loads, data available in the literature, other than that which is mentioned above, are also used. Nominal hardness determined by the WI approach is verified using the data from the microhardness test on aluminum, steel and fused silica as reported in Ma et al. [20].

Similarly, nanoindentation results on aluminum, copper, glass and sapphire acquired at the peak indentation load of 30mN, reported by Sawa and Tanaka [20], are also considered for verification. Finally, the load-displacement curves pertaining to aluminum, tungsten, quartz, fused silica, sapphire, soda lime glass [1], copper [6], 1070 steel and Si_3N_4 [21] acquired with peak indentation loads greater than 100mN are also used.

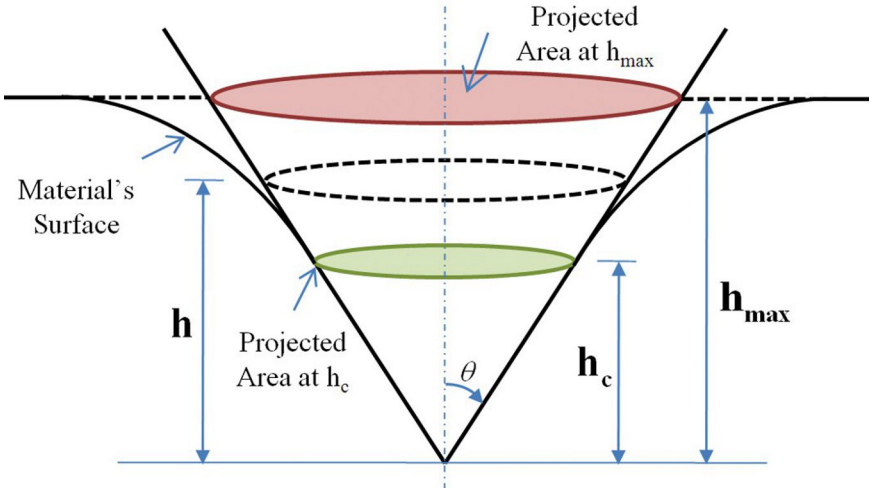

Figure 5.2: Schematic of indentation by a conical indenter and the concept of projected areas at contact and maximum depth of penetrations.

5.4 Modified work-of-indentation approach

Referring to figure 5.2, the projected area of the conical indenter at a height h from the apex is given by $k^{-1}h^2$. Let us define a fictitious hardness as:

$$H_W = \frac{P_{\max}}{k^{-1}h^2} \tag{5.7}$$

where k is a constant which depends on the indenter geometry and is equal to 0.0408 and 0.0378 for Berkovich and Vickers indenters, respectively. If h is replaced by h_c in Eq. (5.7),

the resulting expression will exactly match the definition of hardness commonly used for an ideally sharp indenter (Eq. 5.5) with A_c containing only the first term). Note that k^{-1} and C_0 are equal. If h is taken as the maximum depth of penetration, then Eq. (5.7) will have the following form:

$$H_W = \frac{P_{\max}}{24.56 h_{\max}^2} \tag{5.8}$$

The hardness given by Eq. (5.8) is sometimes referred to as the "nominal" hardness of a material obtained by an ideally sharp indenter [19, 22]. The total work done (or energy dissipated) while indenting a material to a depth of $h_{\max}$ is given by:

$$W_T = \int_0^{h_{\max}} P(h)\, dh \tag{5.9}$$

It has been shown that, for an ideally sharp conical indenter, the experimental loading curve may be described using a parabolic equation in the form: $P = Ch^2$ [6,9]. Thus, the total work done by a sharp indenter is always given by

$$W_T = \frac{1}{3} P_{\max} h_{\max} \tag{5.10}$$

Using Eq. (5.8) and (5.10), one can immediately write

$$H_W = \frac{k P_{\max}^3}{9 W_T^2} \tag{5.11}$$

The work-of-indentation approach employs Eq. (5.11) to calculate the hardness of a material. Beegan et al. [14] stated that the total work done in the above equation should be replaced by

the plastic work if the hardness is considered to be a function of plastic deformation alone. It is clear from the above derivation that the hardness evaluated from total work done is simply nominal hardness and is fundamentally different than that obtained by the OP method. This subtlety has been ignored while reporting a comparison between nominal and conventional hardness in the previous studies. In view of the definition of the total energy constant, Eq. (5.11) may be rewritten as:

$$H_W = \frac{k v_T^2 P_{\max}}{2.25 h_{\max}^2} \tag{5.12}$$

Since v_T depends on the ratio, it allows us to quantify the effect of tip bluntness on the nominal hardness of a material. Therefore, the work-of-indentation approach, which is heretofore applicable only to the sharp indenter, can be applied to the blunt indenter as well. The expressions for nominal and conventional hardness differ in the choice of penetration depth and may be correlated if a relation between the contact depth and maximum depth of penetration is known. An expression that relates these two depths is derived by Attaf [23] as:

$$h_c = \frac{2\left(v_E - 1\right)}{\left(2v_E - 1\right)} h_{\max} \tag{5.13}$$

Eq. (5.5), (5.8) and (5.13) allow us to establish a connection between the conventional and nominal hardness values in the following form:

$$\frac{H_{OP}}{H_W} = \frac{\left(2v_E - 1\right)^2}{4\left(v_E - 1\right)^2} = K_N \tag{5.14}$$

Figure 5.3 shows the plot of hardness ratio K_N as a function of the elastic energy constant. It is evident from the figure that H_{OP} and H_W are almost equal for a material that has a

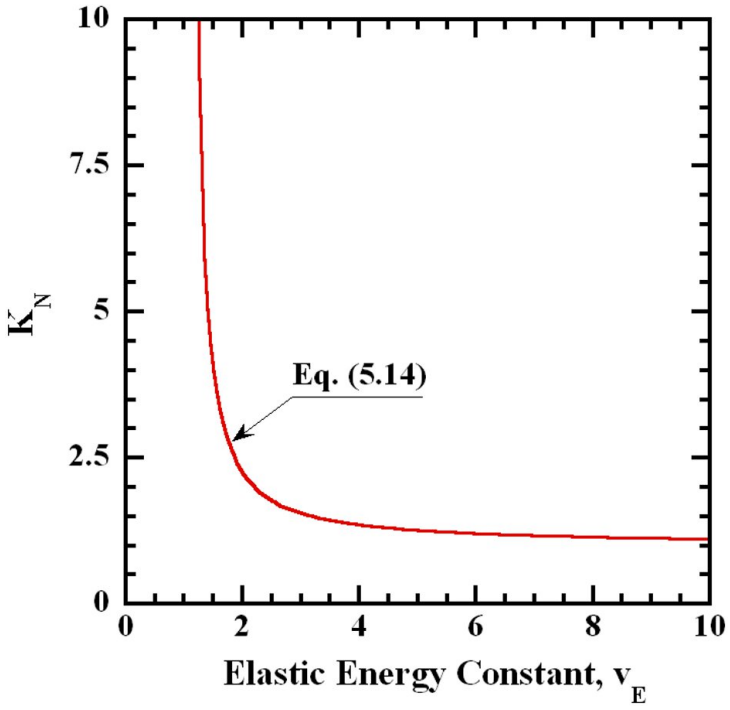

Figure 5.3: Plot showing the variation in the hardness ratio with the elastic energy constant.

relatively large value of v_E. With the help of Eqs. (5.1) and (5.2), Eq. (5.14) may be written in terms of the energy recovery ratio as:

$$K_N = \frac{\left(2v_T - \eta_w\right)^2}{4\left(v_T - \eta_w\right)^2} \tag{5.15}$$

The effectiveness of the modified work-of-indentation approach in the determination nominal as well as conventional hardness of a material will be examined next.

5.5 Results and Discussion

5.5.1 Nominal hardness by the work-of-indentation approach

Figure 5.4 shows a comparison between the hardness values determine by the OP method and the work-of-indentation approach for copper and TiO_2. Both the total and plastic works of indentation are used to determine the nominal hardness. As can be seen, all three hardness values are comparable for copper but differ significantly for TiO_2. For copper, the nominal hardness values are smaller by 10% and greater by 15% as compared to H_{OP}, if they are evaluated using the total work done and plastic work, respectively. The corresponding deviations in the hardness values are found to be 33% and 105% for TiO_2. These observations suggest that the discrepancies among the hardness values determined by the WI approach (using both W_T and W_P) and by the OP method diminish for the material that recovers less upon the withdrawal of load. Note that the percentage elastic recoveries for copper and TiO_2 are 4% and 36%, respectively. The reason for the observed discrepancies could be explained as follows. The total work done and plastic work are equal if a material has little or no recovery upon unloading, and thus provides nearly the same nominal harness values if used in Eq. (5.11). Likewise, for a perfectly plastic material, the difference between the contact depth and the maximum depth of penetration is negligibly small. As a result, equal values for the nominal and conventional hardness will be obtained for such materials. This is certainly not the case with harder materials; h_c and $h_{\max}$ are considerably apart.

As explained earlier, the maximum projected contact area is needed to evaluate the nominal hardness of a material. Ma et al. [19] showed that the required area can be determined from an area function, which is similar in form of that used in the OP method.

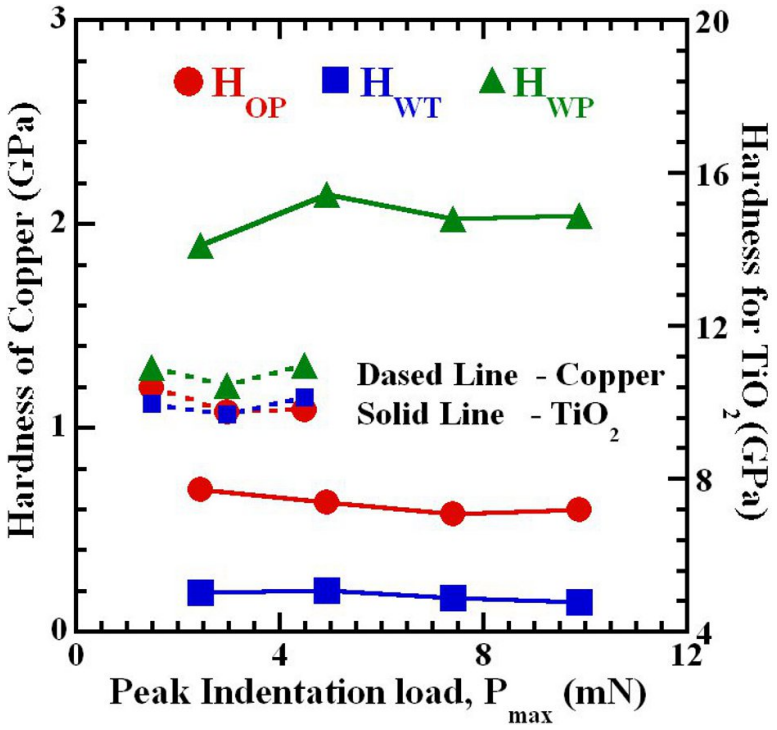

Figure 5.4: Plots showing the difference between nominal and conventional hardness values, respectively, obtained by the work-of-indentation approach and the OP method for TiO2 and single crystal copper.

The objective of constructing an area function is to take the effect of tip bluntness into account. To examine how practical the total energy constant is in the quantification of the effect of tip bluntness, we evaluated the nominal hardness for aluminum, steel and fused silica using Eq. (5.12). The total energy constants are found to be 1.43, 1.46, and 1.48 for these materials, respectively. Nominal hardness values so obtained are summarized in Table 1. It is clear from the table that the nominal hardness values determined by Eq. (5.12) differ by a maximum of 10% from that obtained by Ma et al. for the materials considered. Based on the accuracy obtained, one may conclude that the quantification of the effect of tip bluntness can be done conveniently and efficiently using the total energy constant.

5.5.2 Conventional hardness by the modified WI approach: Ideally sharp indenter

The modified work-of-indentation approach presented in the previous section is applied to evaluate the conventional hardness of materials considered in this study. To begin with, the nominal hardness values for aluminum, steel and fused silica are determined by the modified work-of-indentation approach given by Eq. (5.12). Corresponding conventional

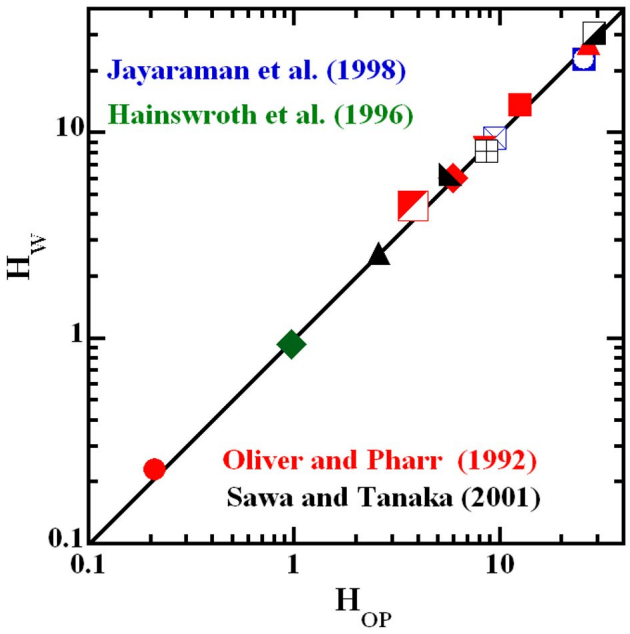

Figure 5.5: Comparison of conventional hardness values determined by the OP method and modified work-of-indentation approach using correction factors K_N given by Eq. (14) and $v_T = 1.50$, when the peak indentation load is greater than 25mN.

hardnesses are then obtained by multiplying the nominal one with conversion factor K_N. Calculations are summarized in Table 5.2. The conventional hardnesses so obtained appear to be in excellent agreement with those commonly known for these materials. Zeng and Chiu [25] suggested that the experimental loading curve may be described by a parabola if the

peak indentation load is greater than 30mN. If this condition prevails, a value of 1.5 may be used for v_T. To validate this assumption, the proposed approach is applied to the load–displacement data given in the literature mentioned earlier, which has the peak indentation in the load reason 30mN-120mN. Figure 5.5 shows a comparison between the conventional hardnesses determined by the OP method and modified WI approach. Excellent agreement between them confirms the efficacy of the work-of-indentation approach in the computation of the conventional hardness of a material when it is probed with an ideally sharp indenter. When the penetration depth is very large, a blunt indenter behaves like a sharp indenter, and thus Eq. (5.12) is highly suitable for the microhardness test.

5.5.3 Conventional hardness by the modified WI approach: Blunt indenter

The nanoindentation load-displacement curve is very much affected by the magnitude of bluntness at the tip of the indenter. The total work done by a blunt indenter is always greater than that by a sharp one, when the specimen is indented to the same maximum depth of penetration. It means that the total energy constant decreases with the increase in the tip bluntness. As such the conversion factor K_N used for sharp indenter may not be applicable when the tip bluntness is more pronounced. This could be explained on the basis of Eq. (5.15). Plots of K_N vs. percentage energy recovery ratio for different values of v_T are shown in figure 5.6. From the figure, it can be immediately inferred that the tip bluntness has no effect on K_N if the percentage elastic recovery is less than 10% approximately. The effect becomes gradually apparent, as it passes the threshold limit. The conversion factor may be affected significantly when η_w is in the excess of 60%. Obtaining a closed form solution for

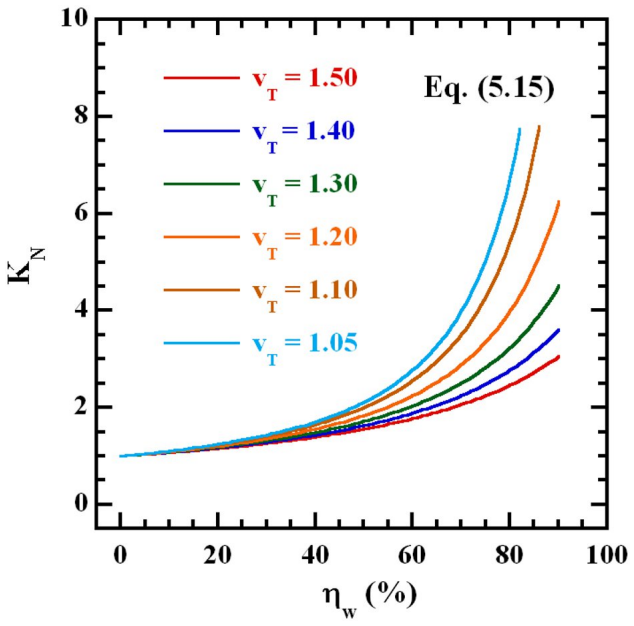

Figure 5.6: Plots showing the variations of the conventional to nominal hardness ratio with percentage energy elastic recovery for different values of total energy constants.

K_N for a blunt indenter is a difficult task, as expressions for both, the area function and total work, contain additional terms, and thus the relation between the conventional and nominal hardness values could only be developed empirically. For this purpose, the hardness ratios (conversion factors) $\left(H_{OP}/H_{WT} \text{ and } H_{OP}/H_{WP}\right)$ are plotted as a function of elastic recovery ratios (both depth and energy) and elastic as well as plastic energy constants separately, as shown in figure 5.7. Both the total and plastic conversion factors have been found to follow specific variation patterns with respect to each of these parameters. For instance, they vary linearly with the percentage recovery (depth and elastic) ratios which may be approximated by the following equations:

$$\begin{aligned} K_{HT}^{h} &= 0.83 + 0.017\eta_h \\ K_{HP}^{h} &= 0.92 - 0.012\eta_h \end{aligned} \tag{2.16}$$

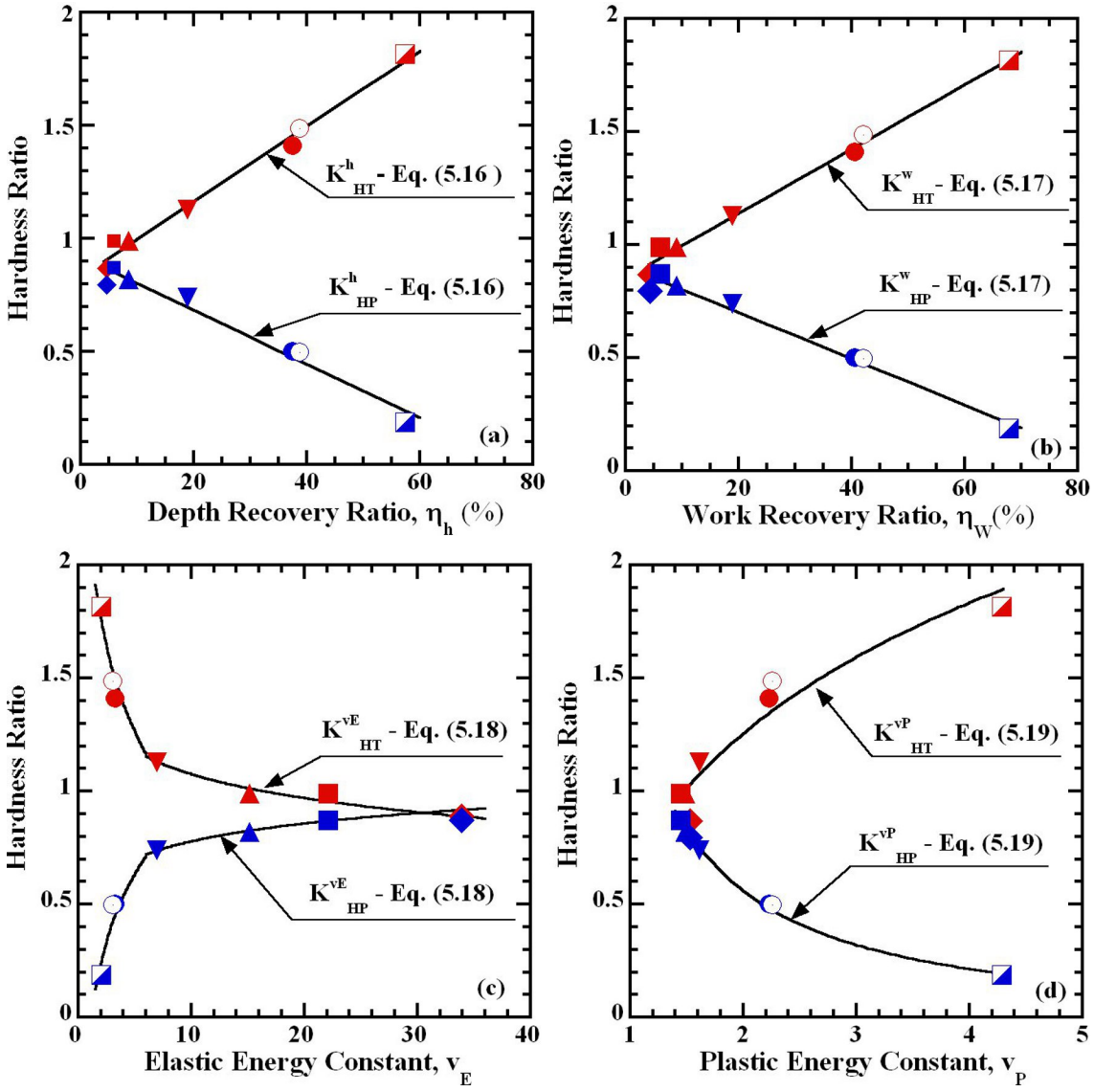

Figure 5.7: Variations of H_{OP}/ H_{WT} and H_{OP}/ H_{WP} Ratios with (a) depth recovery ratio; (b) energy recovery ratio; (c) elastic energy constants; and (d) plastic energy constant, when the peak indentation load is less than 10mN. Red and blue markers are used total and plastic hardness ratios respectively.

and

$$K^w_{HT} = 0.86 + 0.014\eta_w$$
$$K^w_{HP} = 0.90 - 0.010\eta_w \qquad (17)$$

Similarly, the relationship between the hardness ratios and v_E may be described logarithmically. The variation pattern is, however, different for the ceramics oxides and metals considered in this study. Accordingly, we employed two logarithmic functions to obtain the best fit as:

$$K_{HT}^{v_E} = \begin{cases} 2.13 - 1.24\log(v_E) & for\ v_E \le 5.90 \\ 1.43 - 0.35\log(v_E) & Otherwise \end{cases}$$
$$K_{HP}^{v_E} = \begin{cases} -0.047 + 0.98\log(v_E) & for\ v_E > 5.90 \\ 0.52 - 0.261\mathrm{og}(v_E) & Otherwise \end{cases} \tag{18}$$

Finally, the empirical relationship between the hardness ratios H_{OP} / H_{Wj} and plastic energy constant may be describes as:

$$K_{HT}^{v_p} = 0.68 + 1.92\log(v_P)$$
$$K_{HP}^{v_p} = 1.45 v_P^{-1.37} \tag{19}$$

In view of the above phenomenological correction factors, an expression to determine material's conventional hardness using the modified work-of-indentation approach may be succinctly written as:

$$H_{Wj} = \frac{K_{Hj}^{i} k v_j^2}{2.25} \frac{P_{\max}}{h_{\max}^2} \tag{20}$$

where $K_{Hj}^{i}\left(= H_{OP} / H_{Wj}\right)$ is the hardness ratio with $j = T, P$ and $i = h, w, v_E$ and v_P. Letters T and P stand for the total and plastic works, respectively. Depending on the choice of indentation works and parameters, conventional hardness may be evaluated by eight different ways using Eq. (5.20). Computed hardness values for metals and ceramic oxides using Eq. (5.20) are compared with those obtained by the OP method and is displayed in figure 5.8,

where a close agreement between the computed and measured values can be realized. The performance of the phenomenological correction factors is also examined by evaluating the hardnesses for the other two sets of materials. As a consequence, the hardnesses determined using these empirical factors well accord with their respective experimental values, as shown in figures 5.9 and 5.10. Thus, the proposed empirical are also applicable when the peak indentation load is such that the tip bluntness is less pronounced.

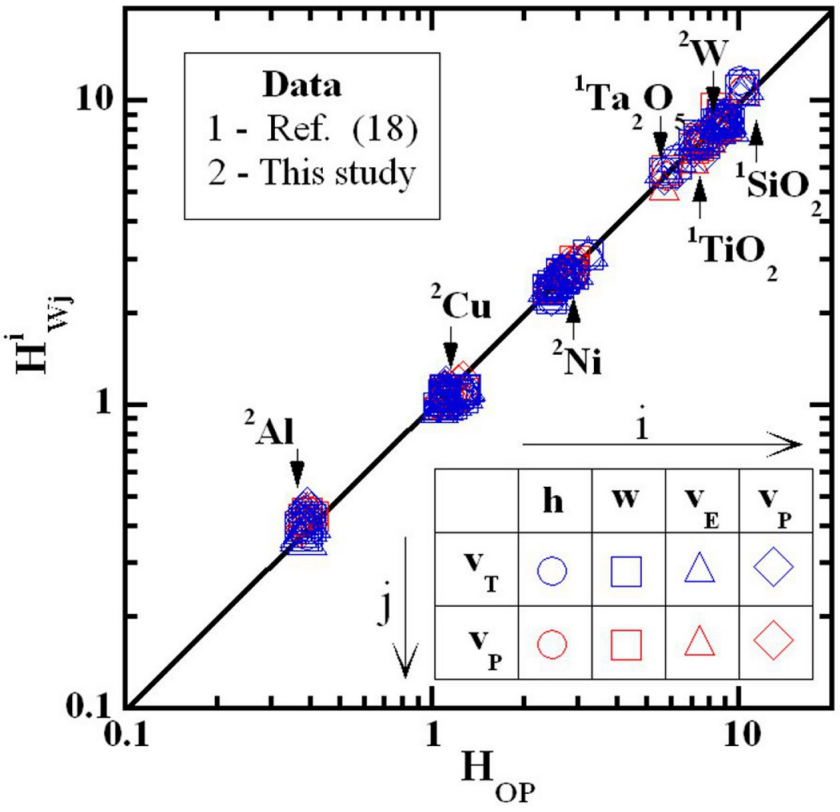

Figure 5.8: Comparison of conventional hardness values determined by the OP method and modified work-of-indentation approach using correction factors given by Eqs. (5.16) – (5.19), when the peak indentation load is less than 10mN.

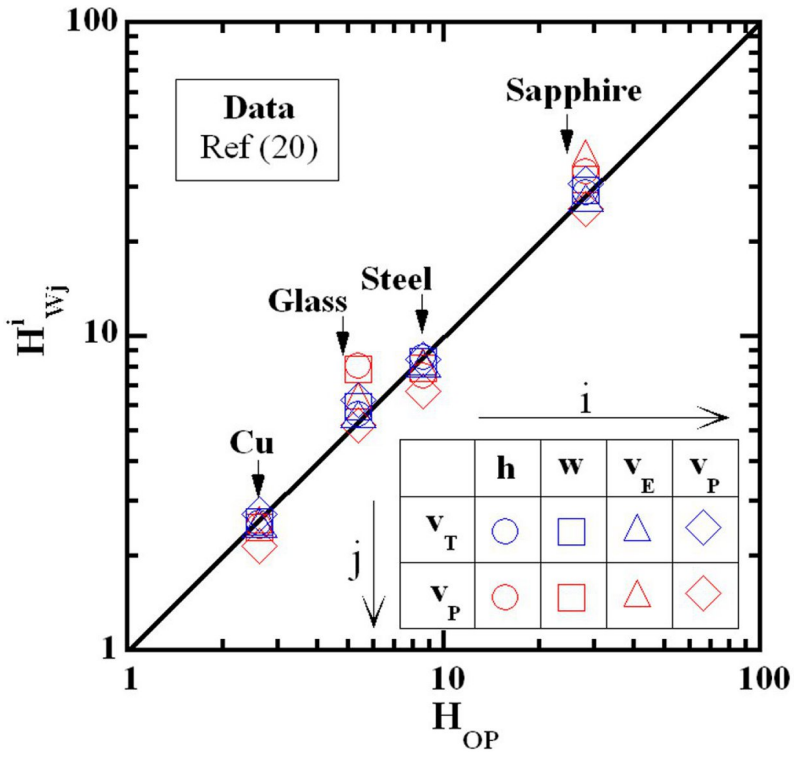

Figure 5.9: Comparison of conventional hardness values determined by the OP method and modified work-of-indentation approach using correction factors given by Eqs. (5.16) – (5.19), when the peak indentation load is 30mN.

Finally, we comment on the choices of indentation works and other parameters. Total works should be a preferred choice in the determination of hardness, as the expression containing it has some mathematical basis, at least for an ideally sharp indenter. The inclusion of the plastic work in this study is just for the purpose of illustration. If a nanoindentation loading curve is well describable by a parabolic relation, then K_N should be evaluated either from Eq. (5.14) or Eq. (5.15). Off all the empirical correction factors discussed, one which involves the use of depth recovery ratio is recommended, as it can be readily obtained from the load-displacement curves. Further experimental study is required to validate the proposed method when both pile-up and percentage elastic recovery are significant.

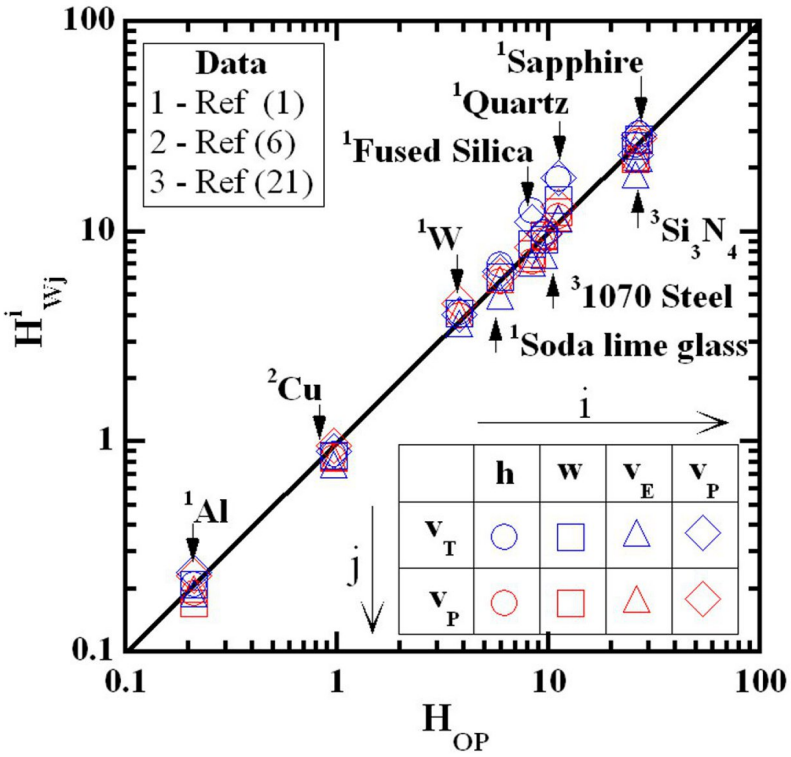

Figure 5.10: Comparison of conventional hardness values determined by the OP method and modified work-of-indentation approach using correction factors given by Eqs. (16) – (19), when the peak indentation load is in the range 100-120mN.

5.6 References

[1] Oliver, W.C., and Pharr, G.M. (1992). "An improved technique for determining hardness and elastic modulus using load and displacement sensing indentation experiments" *Journal of Materials Research*, 7, 1564-1583.

[2] Oliver, W.C., and Pharr, G.M. (2004). "Measurement of hardness and elastic modulus by instrumented indentation: Advances in understanding and refinements of methodology." *Journal of Materials Research* 19, 3-20.

[3] Phar, G.M. (1998). "Measurement of mechanical properties by ultra-low load indentation." *Material Science & Engineering A*, 253, 151-159.

[4] Cheng, Y.T., and Cheng, C.M. (2005). "Relationship between initial unloading slope, contact depth, and mechanical properties for spherical indentation in linear viscoelastic solids." *Material Science & Engineering A*, 409, 93-99.

[5] Oliver, W.C. (2001). "Alternative technique for analyzing instrumented indentation data." *Journal of Materials Research*, 16, 3202-3206.

[6] Hainsworth, S.V., Chandler, H.W, and Page, T.F. (1996). "Analysis of nanoindentation load-displacement loading curves" *Journal of Materials Research*, 11, 1987-1995.

[7] Malzbender, J., de With, G., and den Toonder, J. (2000). "The P-h^2 relationship in indentation." *Journal of Materials Research*, 15, 1209-1212.

[8] Jha, K.K., Suksawang, N., and Agarwal, A. (2010). "Analytical method for the determination of indenter constants used in the analysis of nanoindentation loading curves." *Scripta Materialia*, 63, 281-284.

[9] Tuck, J.R., Korsunky, A.M., Bull, S.J., and Davidson, R.I. (2001). "On the application of the work-of-indentation approach to depth-sensing indentation experiments in coated systems." *Surface and Coating Technology*, 137, 217-224.

[10] Hay, J.C., Bolshakov, A., and Pharr, G.M. (1999). "A critical examination of the fundamental relations used in the analysis of nanoindentation data." *Journal of Materials Research*, 14, 2296-2305.

[11] Strader J.H., Shim S., Bei, H., Oliver, W.C., and Pharr, G.M. (2006). "An experimental evaluation of the constant β relating the contact stiffness to the contact area in nanoindentation." *Philosophical Magazine*, 86, 5285-5298.

[12] Xu, Z-H., and Li. X. (2008). "Effects of indenter geometry and material properties on the correction factors of Sneddon's relationship for nanoindentation of elastic and elastic-plastic materials." *Acta Materialia*, 56, 1399-1405.

[13] Meza, J.M., Abbes, F., and Troyon, M. (2008). "Penetration depth and tip radius dependence on the correction factor in nanoindentation measurement." *Journal of Materials Research*, 23, 725-731.

[14] Beegan, D., Chowdhury, S., Laugier, M.T. (2005). "Work of indentation methods for determining copper film hardness." *Surface and Coating Technology*, 192, 57-63.

[15] Khan, M.K., Hainsworth, S.V., Fitzpatrick, M.E., and Edwards, L. (2009). "Application of the work of indentation approach for the characterization of aluminum 2024-T351 and Al cladding by nanoindentation" *Journal of Materials Science*, 44, 1006-1015.

[16] Zhou, L., and Yao, Y. (2007). "Single crystal bulk material micro/nano indentation hardness testing by nanoindentation instrument and AFM" *Material Science & Engineering A*, 460-461, 95-100.

[17] Uzun, O., Guclu, N., Kolemen, U., and Sahin, O. (2008). "Analysis of data on indentation load against penetration depth for bulk MgB2 crystal using nanoindentation work and Oliver-Pharr approaches." *Materials Chemistry and Physics*, 112, 5 -10.

[18] Attaf, M.T. (2003). "New ceramics related investigation of the indentation energy concept." Material Letters, 57, 4684-4693.

[19] Ma, D., Ong, C.W., and Zhang, T. (2009). "An instrumented indentation method for Young's modulus measurement with accuracy estimation" *Experimental Mechanics*, 49, 719-729.

[20] Sawa, T., and Tanaka, K. (2001). "Simplified method for analyzing nanoindentation data and evaluating performance of nanoindentation instruments" *Journal of Materials Research*, 16, 3084-3091.

[21] Jayaraman, S., Hahn, G.T., Oliver, W.C., Rubin, C.A. and Bastias, P.C. (1998). "Determination of monotonic stress-strain curve of hard materials from ultra-low-load indentation tests." *International Journal of Solids and Structures*, 35, 365-381.

[22] Cao, Y., Xue, Z., Chen, X., and Raabe, D. (2008). "Correlation between the flow stress and the nominal indentation hardness of soft metals" *Scripta Materialia* 59, 518-521.

[23] Attaf, M.T. (2004). "New formulation of the nanomechanical quantities using the β-material concept and the indentation function" *Material Letters*, 58, 889-894.

[24] Zeng, K., and Chiu, C.H. (2001). "An analysis of load-penetration curves from instrumented indentations" *Acta Materialia*, 49, 3539-3551.

CHAPTER 6

NANOINDENTATION ON CEMENTITIOUS MATERIALS

6.1 Introduction

Recent years have seen an upsurge of interest in studying the mechanical behavior of cementitious materials at a very small scale using nanoindentation. A number of articles have appeared in the literature, beginning with the work reported by Velez et al. [1] on pure cement clinkers. Since then, the outcome of this technique has been used in: the characterization and identification of different forms of Calcium Silicates Hydrates (C-S-H) [2-5]; the mapping of the mechanical properties [6-8]; the study of time-dependent properties of C-S-H [9-12]; and multi-scale modeling as input parameters [13]. All of these studies are concerned with the determination of mechanical properties from the nanoindentation load-displacement data. As cementitious materials exhibit heterogeneity at all levels of length scales, the protocols adopted for materials like metals and ceramics in their testing and analysis of results may require modifications in order to be applicable for this class of materials. For example, the statistical nanoindentation technique, which is found to be useful for composites such as cementitious materials, bones, etc., is absolutely redundant for materials like metals. Evaluation of mechanical properties such as elastic modulus and hardness for cementitious materials by nanoindentation involves four different steps: (1) surface preparation; (2) indentation testing; (3) analysis of load-displacement data; and (4) statistical indentation analysis. While protocols concerning steps (1), (2) and (4) are well established, the methods used in the analysis of the load-displacement data from linear, isotropic and homogeneous materials may not be applicable for those from heterogeneous

materials. Note that the accuracy of such methods rely on empirical observations, which may sometimes be material specific, due to our poor understanding regarding the complex elasto-plastic deformation processes that occur during indentation [14].

The most widely used method for the load-displacement data analysis to evaluate the elastic modulus and hardness is that proposed by Oliver and Pharr [15-17]. The method relies on the principle of elastic punch theory, which is applied to the unloading portion of the load-displacement curves. Besides that, three other quantities, namely the area of contact between the indenter and the specimen, the slope of the unloading curve (initial unloading stiffness) evaluated at peak indentation load, and reasonable estimate of Poisson's ratio, are also required. The initial unloading stiffness is usually obtained by evaluating the differentiation of the power law representing an unloading curve at peak indentation load. The exponent of the power law is supposed to have its value in the range 1.2 to 1.6 for most of the materials [15]. However, as will be seen, analysis of the load-displacement data from cementitious materials revealed that the exponent can take a value that falls well beyond this range. Such a variation in the exponent of the power law can be explained neither on the basis of the "effective indenter shape" nor on the basis of the "residual stress" theories [14, 17-18]. Again, the contact area evaluated according to the Oliver and Pharr method is found to be inaccurate for materials that show excessive pile-up during indentation, viscoelastic and heterogeneous materials. Furthermore, establishing an area function is an iterative process and needs to be carried out at regular intervals to account for the bluntness at the tip of the indenter that may deteriorate continuously during the course of indentation. This is particularly cumbersome when grid indentation is required to be performed–an essential step in nanoindentation testing on cementitious materials.

On the other hand, energies dissipated during indentation are found to be useful parameters in determining the mechanical properties of a material [19, 20-22]. For example, the ratio of elastic work to the total work is equal to the ratio of hardness to the indentation modulus for elastic perfectly plastic material. A good account of this kind of relationship is given in reference [21]. Similarly, Sakai [22] found that the energy dissipated during the indentation cycle bears a specific relationship to quantities such as hardness, peak indentation load, and volume of the indentation impression. Recently, Attaf [23-26] has shown that various forms of energy (readily obtainable from the load-displacement curves) and their ratios have important applications in modeling the load-displacement curves. Total, elastic, and plastic energy constants are defined with respect to the absolute energy. This form of energy is defined as the maximum energy that may be dissipated during the indentation on the surface of a material. The total and elastic energy constants are related to the curvatures of the loading and unloading curve, respectively, and are independent of the indentation size for a given geometry. Using nanoindentation data on certain kinds of ceramics, Attaf [23, 25] found that the work-of-indentation can be correlated with other nanomechanical quantities obtained from the indentation experiment. For instance, contact area, peak indentation load, and maximum and final depth of penetrations have a one-to-one relationship with all forms of work-of-indentation. A unified correlations diagram capable of depicting all possible correlations was developed for all the materials used in his study. Whether these relationships are applicable for multiphase cementitious materials is not known. Again, nanoindentation load-displacement curves may comprise a dwelling portion at peaks, which is normally desired to minimize the effect of non-elastic deformations, such as creep, on the measured mechanical properties. Nemecek [9] found that a strong size effect on elastic properties is

inevitable for cement paste subject to increasing loading cycles with no dwelling portion at peaks. A long dwelling portion is also essential when parameters that lead to the determination of viscoelastic properties, e.g. contact creep modulus, are required to be measured. Attaf did not consider the dwelling portion while defining the energy constants. Since a material deforms continuously during dwelling at constant peak indentation load, it increases the total work done. Omission of the total work done during dwelling may lead to erroneous energy constants, and thus, a modification in their definitions is warranted. In the last two chapters, we have shown that the energy constants may be used to determine the initial unloading stiffness and hardness of a material. It would be appropriate to examine how effective these procedures are in the determination of nanomechanical properties from the load-displacement data pertaining to cementitious materials. Therefore, this chapter focuses on three aspects of load-displacement data analysis: (1) definitions of energy constants; (2) empirical correlations between nanomechanical quantities; and (3) development of a model to measure the elastic modulus and hardness of cementitious materials.

6.2 Experimental program

At the nanoscale, the measurement of mechanical properties is conveniently done by performing nanoindentation experiments. This sophisticated experimental technique requires certain protocol to follow with respect to sample preparation. Sample preparation technique, equipment used and loading sequences are described as follows:

6.2.1 Materials

Cement paste samples were prepared out of type I Portland cement with water-to-cement ratios (w/c) equal to 0.3, 0.4, and 0.5. It should be noted that the w/c affects only the volume

fraction not the mechanical properties of the phases present in the cement paste composite. The purpose of employing different w/c's is to capture the mechanical properties of unhydrated phases with a very low degree of hydration that may not be present at a higher w/c. The ASTM standard C305 was followed during the mixing process of cement and water. The cement paste mixture was poured into a cylindrical rubber mould with internal diameter and height of 25 mm. Samples were demoulded after 24 hours and cured in water for 28 days at room temperature.

6.2.2 Sample surface preparation

One of the key requirements of the nanoindentation experiment is to have a smooth surface of the sample to be indented. A rough surface may yield spurious values of mechanical properties and damage the indenter tip permanently. After 28 days of curing, samples were remolded by immersing them in the mixture of epoxy resin and hardener in a slightly bigger mould with internal diameter and height of 30.50 mm and kept in the vacuum to remove the entrapped air from the mixture. This step in surface preparation is necessary as it protects the sample from damage during grinding and polishing. Samples were demoulded after 24 hours for the next process of grinding and polishing. Coarse to fine grinding was applied to epoxy encased samples using abrasive paper of different grit sizes of 80, 52, 35, 22 and 15 μm. The speed of the revolving disc on which the abrasive paper was attached was maintained at 100 revolutions per minute (rpm) for the first three grit sizes and then increased to 150 rpm for the rest of the sizes. Each paper was used for approximately 3 to 6 minutes (longer for smaller grit size paper). A continuous flow of water was allowed during the entire grinding process. All samples were examined with the help of an optical

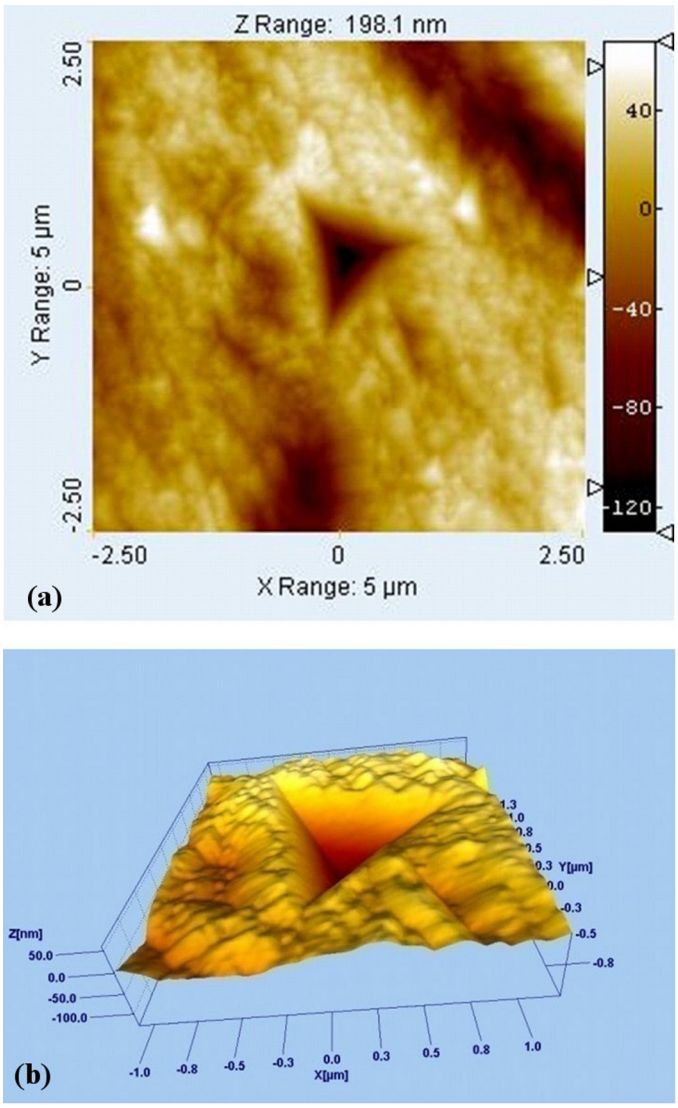

Figure 6.1: SPM images showing residual impression and surface roughness of polished samples: (a) top; and (b) three-dimensional views.

microscope at the end of each step of grinding to check its effectiveness. The sample surface was gently cleaned in running water after all the grinding steps were completed. Diamond suspension in water having a gradation of 7, 3, 1 and 0.1 µm on textmat cloth were successively used for polishing. Maintaining the speed of the disc at 150 rpm, polishing was done for about 5 minutes in each step. Finally, all the samples were again gently cleaned with

water for about 1 minute to remove the debris deposited during polishing and subsequently air dried. The technique described herein produces a very smooth surface, as shown in figure 6.1.

6.2.3 Nanoindentation equipment

The indentation experiment was performed using a Hysitron Triboindenter which is a fully automated nanomechanical testing system. The Triboindenter is equipped with the Scanning Probe Microscope (SPM) imaging capability which can capture images at a nanoscale resolution. A three-sided pyramidal Berkovich tip having a radius of 100 nm was used as the probe. The specimens were subjected to a trapezoidal load history with a varying magnitude of maximum load applied, but not exceeding 1250mN. The loading, dwelling and unloading period were kept equal to 10, 2 and 10 seconds, respectively.

6.2.4 Indentation modulus and hardness

Nanoindentation tests were performed on approximately 28-day-old samples of the cement paste having a smooth surface at random locations. The grid indentation technique over a representative area is preferred for nanoindentation in the case of heterogeneous materials like cement paste [27]. Since the objective is to analyze the individual nanoindentation curve corresponding to each phase of cement paste and not the determination of their volume fraction, performing the grid indentation over a large area is not required. As mentioned earlier, the phases of cement paste are not distinguishable optically; therefore, we followed the trend of characterizing different phases of cement paste based on their mechanical properties. Following Mondal et al. [28], phases were grouped into anhydrous particles and three forms of Calcium-Silicate-Hydrate (C-S-H), the main

hydration product, namely low stiffness (LS), medium stiffness (MS), and high stiffness (HS) C-S-H. These hydration products are sometimes respectively referred to as Low density (LD), high density (HD) and ultra high density (UHD) [2, 3, 29-30]. Representative values of the indentation modulus and hardness for all of these phases were determined based on the statistical analysis of the measured data. The average values of the indentation modulus and hardness along with their standard deviations are shown in Table 6.1, which agrees well with those reported in the literature [1-3,28]. It should be noted here that average mechanical properties, for all the phases, correspond to the peak indentation load of 1000 μN.

Table 6.1: Indentation modulus and Hardness (in GPa) of different phases of cement paste.

Phase	**Anhydrous**		**LS C-S-H**		**MS C-S-H**		**HS C-S-H**	
Properties	E	H	E	H	E	H	E	H
Mean	132.44	8.36	22.03	0.72	30.42	0.85	38.95	1.21
SD	28.45	2.42	2.32	0.22	1.78	0.27	2.46	0.35

Test were also performed at several locations to capture the load-displacement curves corresponding to each of these four phases of the cement paste sample with different peak indentation load of 250, 500, 750, 1000, and 1250 μN, respectively. Ideally, the combined load-displacement diagram with different peak indentation load is such that the loading curves have the same curvatures and all the unloading curves are parallel. Load-displacement diagrams corresponding to different peak indentation load are shown in figure 6.2 for all four phases considered here. As can be seen, the desired combined load-displacement diagrams

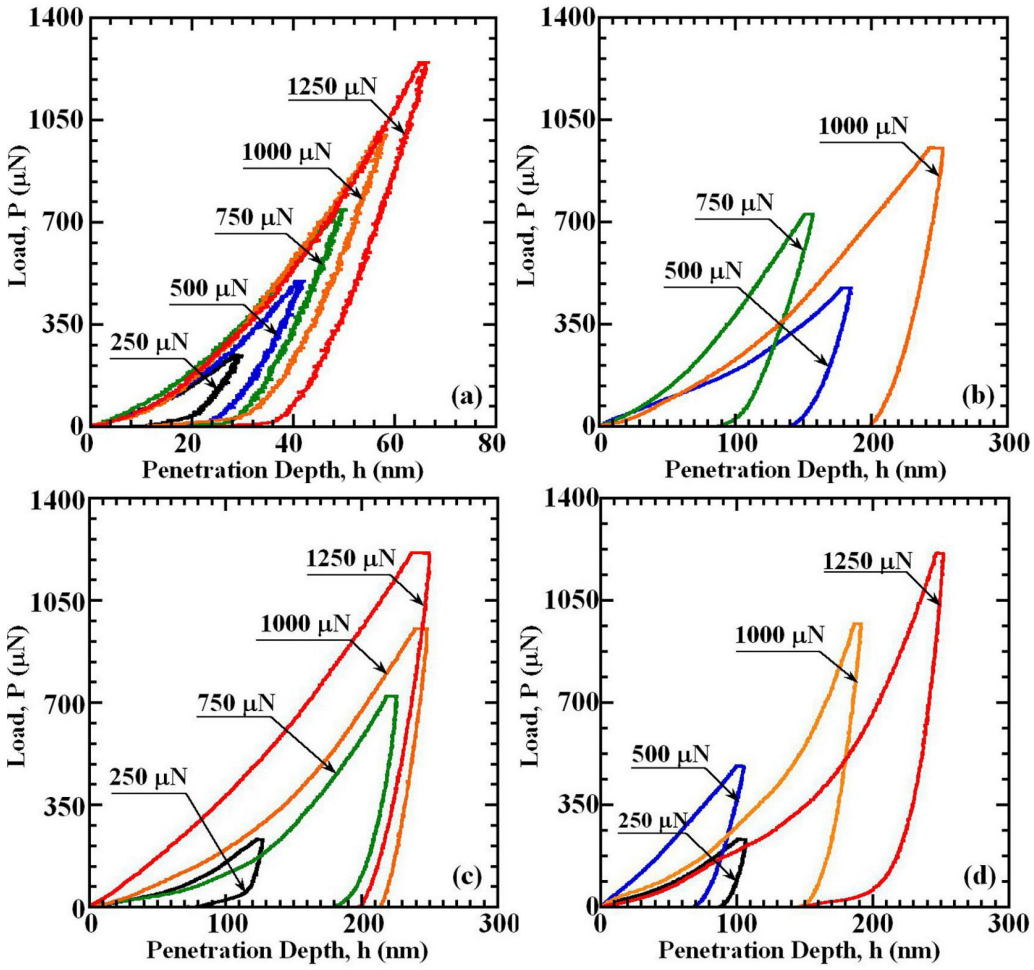

Figure 6.2: Experimental (nanoindentation) load-displacement curves for: (a) anhydrous phase; (b) LS C-S-H; (c) MS C-S-H; and (d) HS C-S-H.

may not be possible due to the residual stress effect [31]. However, the unloading curves are almost parallel in all cases, and therefore their modulus values match. Typical outputs of the nanoindentation experiment are given in Table 6.2 where unloading curve fitting parameters A_0 and m are also shown. Scrutiny of the output data reveals that the exponent of the power law can take any value beyond the range of 1.2 to 1.6, for cementitious materials. As shown in Table 6.2, the indentation modulus and hardness values increase with the increase in the peak indentation load, a trend normally observed in the reverse order due to

Table 6.2: Nanoindentation test data pertaining to different phases of cement paste.

Phase	P_{max} (μN)	h_{max} (nm)	h_c (nm)	h_f (nm)	A_c (nm^2)	A_0	m	S (μN/nm)	E_r (GPa)	H (GPa)
A**	244.36	29.91	23.65	15.06	30319.93	1.71	1.86	31.58	160.69	8.06
	498.03	42.23	32.72	21.32	50116.07	2.99	1.70	41.28	163.38	9.94
	742.05	50.46	38.03	26.00	63644.61	6.02	1.52	47.43	166.58	11.66
	995.66	58.51	44.31	26.90	81440.92	2.79	1.71	55.05	170.92	12.23
	1244.61	66.72	51.20	35.21	103213.53	6.20	1.54	61.65	170.02	12.06
LS**	472.04	185.37	168.43	130.24	824648.34	0.03	2.45	21.04	20.53	0.57
	724.16	157.36	127.68	93.20	498918.39	0.87	1.61	18.12	22.73	1.45
	951.35	253.03	231.05	187.86	1481032.89	0.10	2.20	31.83	23.17	0.64
MS**	231.17	127.54	120.87	83.74	452229.79	4.46E-6	4.69	24.52	32.31	0.51
	719.92	226.11	212.66	169.76	1268679.94	3.48E-3	3.03	38.20	30.05	0.57
	950.70	248.39	231.96	210.84	1491996.93	2.15	1.67	41.44	30.06	0.64
	1208.92	250.04	228.34	189.56	1448741.80	0.30	2.01	39.38	28.99	0.83
HS**	231.37	106.87	100.60	79.82	326588.33	0.01	3.11	26.32	40.81	0.71
	481.09	105.63	88.95	69.67	263306.06	1.49	1.61	21.48	37.08	1.83
	967.51	191.71	176.08	146.60	894678.14	0.26	2.16	46.32	43.39	1.08
	1207.74	252.28	235.58	180.22	1535901.54	1.46E-3	3.18	53.04	37.92	0.79

the so-called indentation size effect. This effect is more pronounced when indentation is carried out at the same location for different depths. Here, the load-displacement curves with different maximum loads are grouped based on the indentation modulus and hardness values, just to check the proportionality between different forms of energies.

6.3 Indentation energies

In the case of certain kinds of ceramics, all forms of energy dissipated during indentation bear specific relation among themselves and also with other parameter such as peak indentation load, penetration depths, and contact area. Since these materials have a single composition, all empirical relationships yield a very good value of correlation coefficient. In this section, we are going to examine whether those energy relationships are also relevant for the multi-phase cementitious materials. The absolute work is evaluated as defined in chapter 2. Similarly, the total (W_T), elastic (W_E) and plastic (W_P) works of indentation for all the phases are computed numerically using the nanoindentation results shown in figure 6.2. It should be noted here that the total work of indentation is evaluated during loading only; i.e., the work done during dwelling is ignored. The results are then displayed as absolute energy vs. total, elastic and plastic energies; total energy vs. elastic and plastic energies; and elastic energy vs. plastic energy plots for all four phases of the cement paste, as shown in figures 6.3 – 6.6. As can be seen, all forms of energy are proportional to each other in each case, albeit with a varying degree of goodness in the linear fit. For the anhydrous phase, the linear correlation is perfect because the loading curve follows the same path and all unloading curves are parallel. However, such a combination is not always possible owing to the heterogeneity present in the cementitious materials especially when the manual indentations

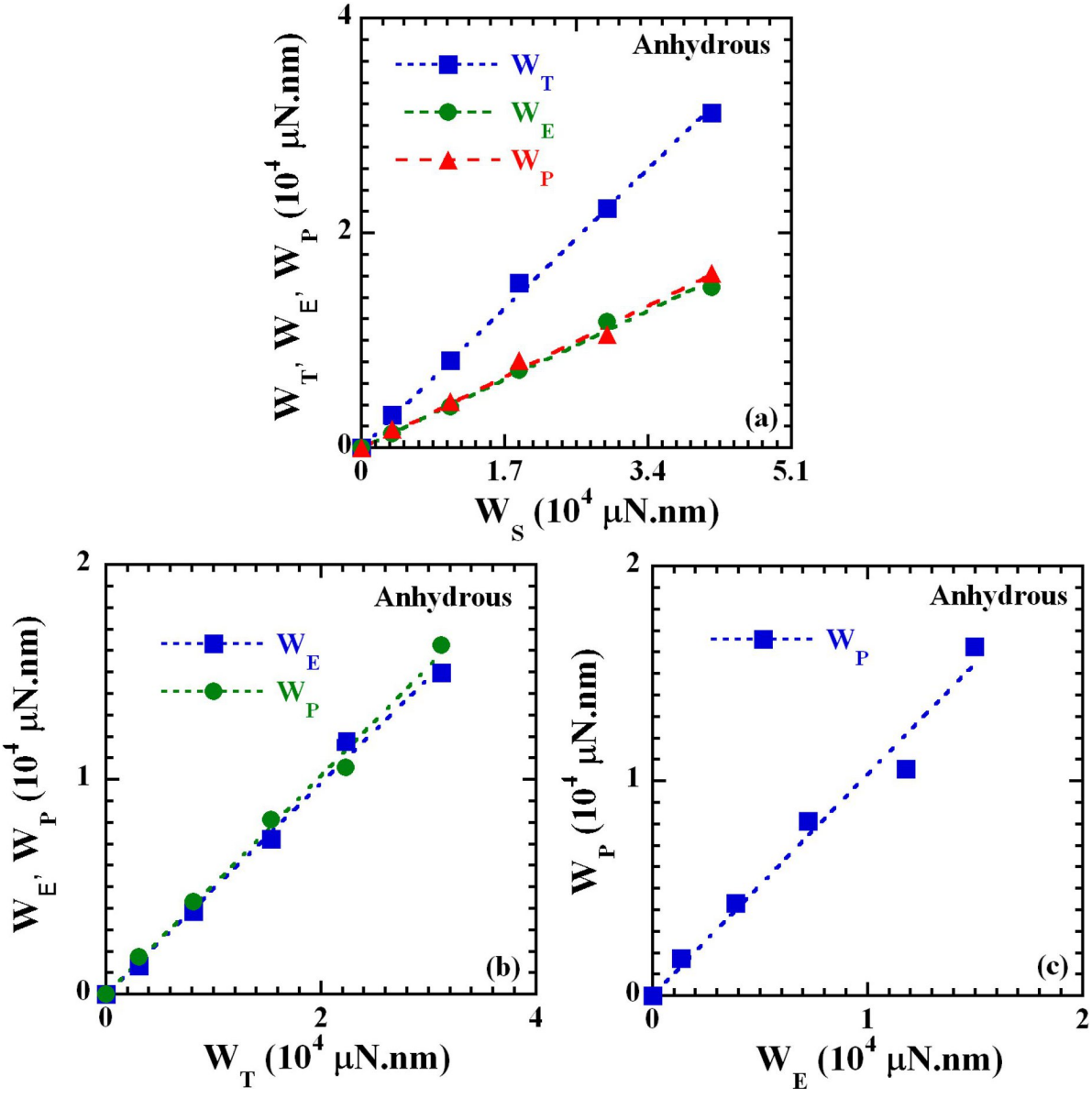

Figure 6.3: Correlation between different forms of dissipated energy: (a) W_S vs. W_T, W_E and W_P; (b)) W_T vs. W_E and W_P; and (c) W_E vs. W_P for anhydrous phase.

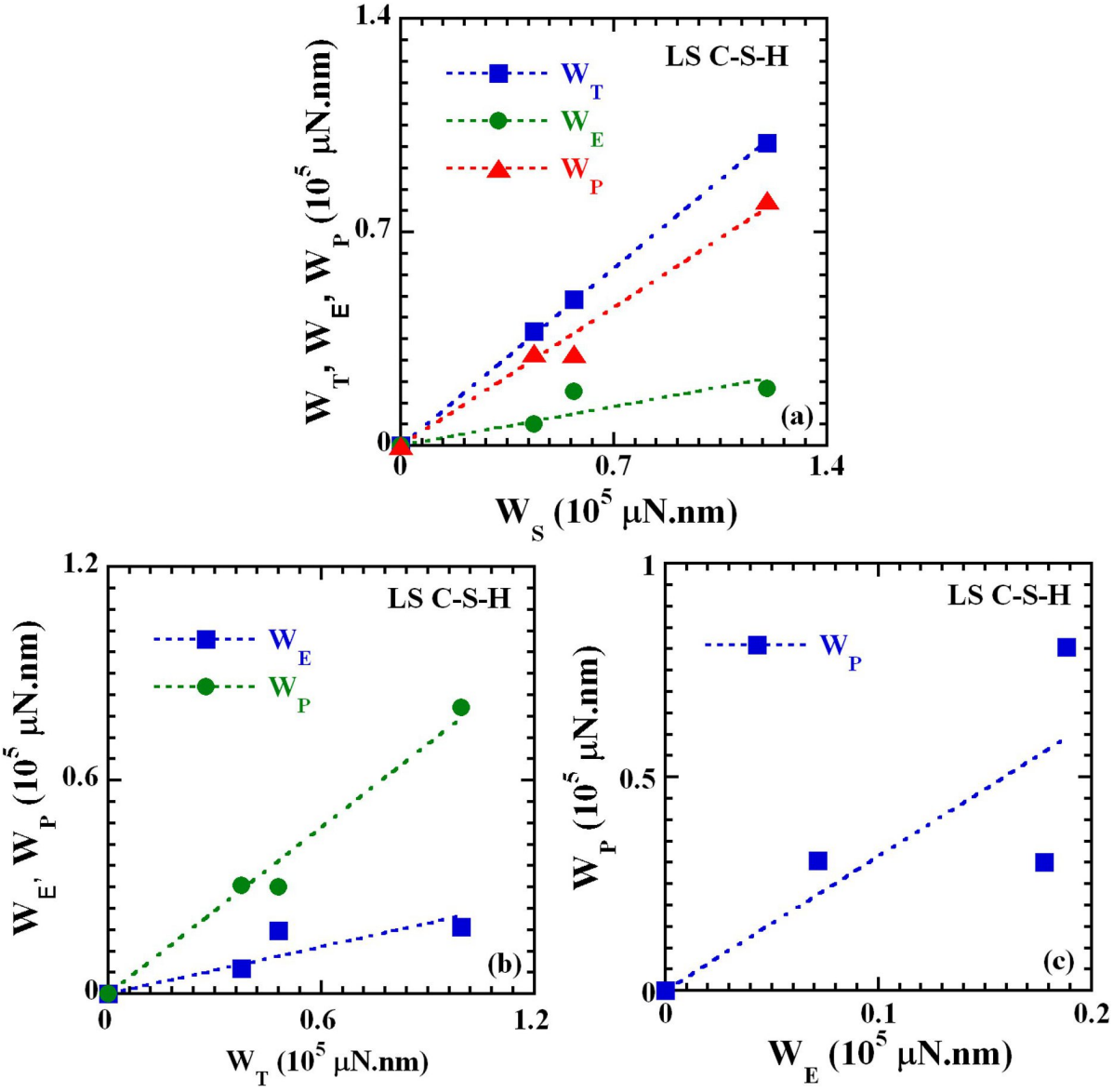

Figure 6.4: Correlation between different forms of dissipated energy: (a) W_S vs. W_T, W_E and W_P; (b) W_T vs. W_E and W_P; and (c) W_E vs. W_P LS C-S-H phase.

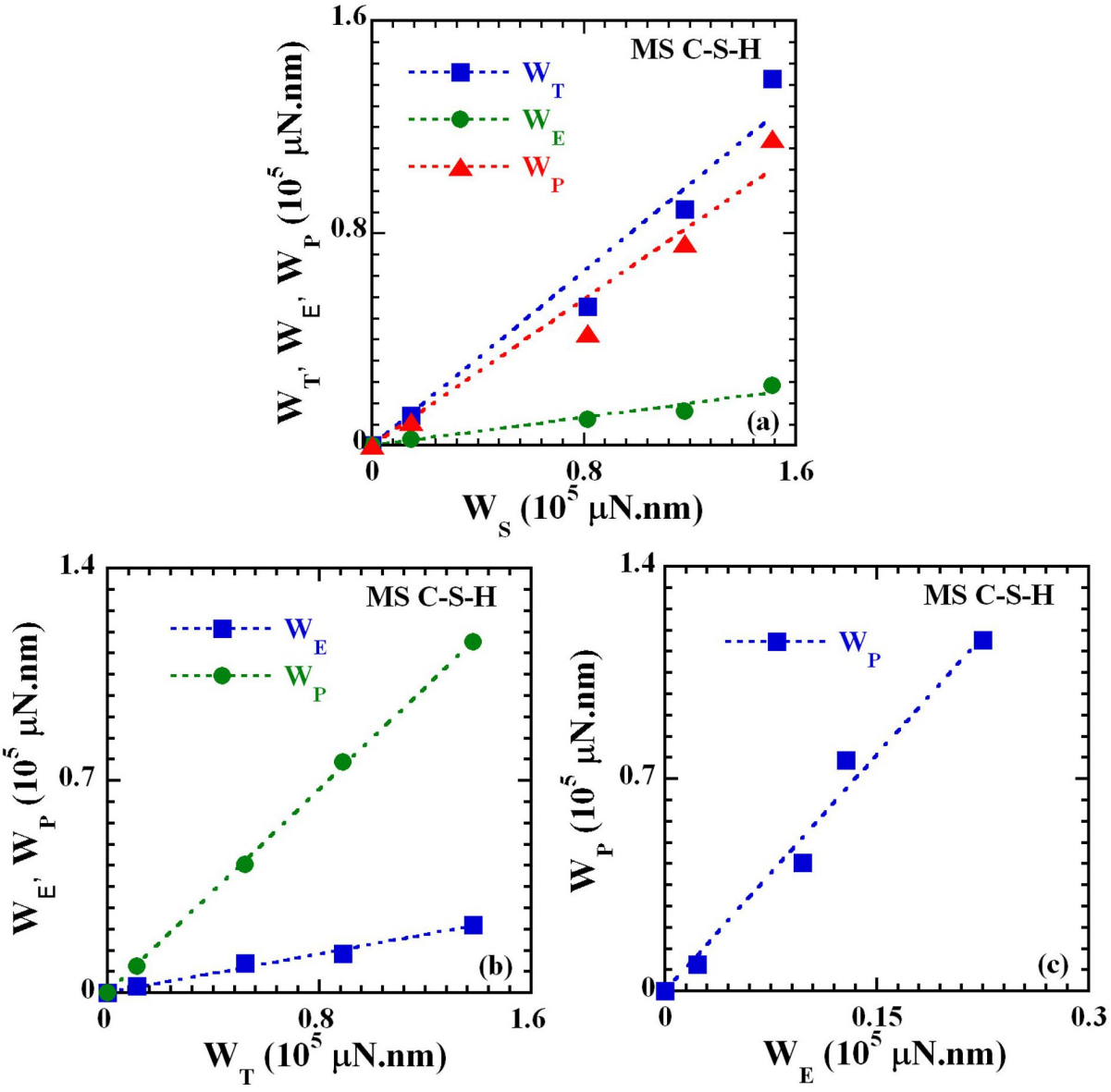

Figure 6.5: Correlation between different forms of dissipated energy: (a) W_S vs. W_T, W_E and W_P; (b) W_T vs. W_E and W_P; and (c) W_E vs. W_P MS C-S-H phase.

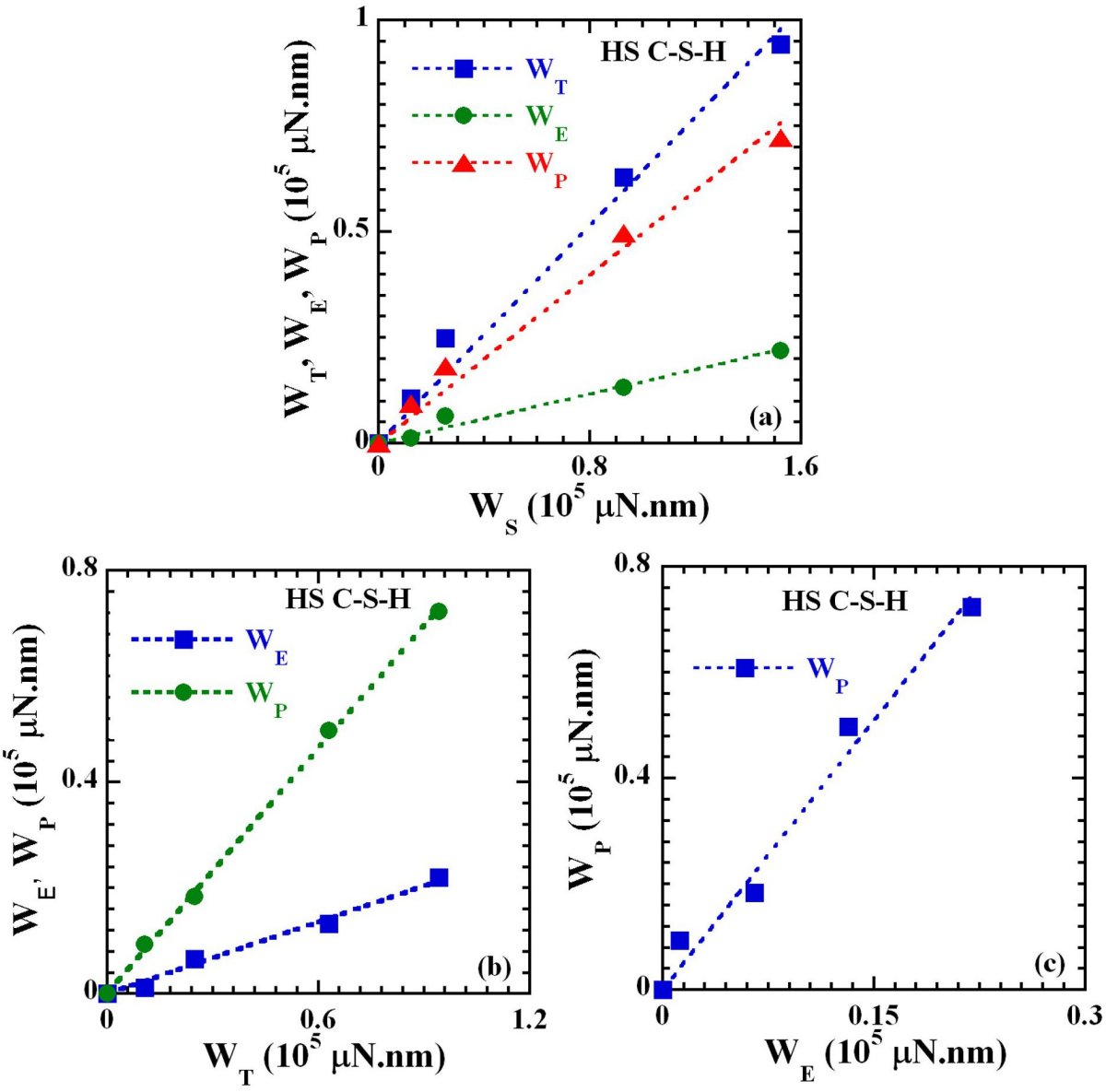

Figure 6.6: Correlation between different forms of dissipated energy: (a) W_S vs. W_T, W_E and W_P; (b) W_T vs. W_E and W_P; and (c) W_E vs. W_P HS C-S-H phase.

are carried out, as evident in figures 6.2b – 6.2d, which correspond to the C-S-H of different stiffnesses. Note that the curvature of the loading curve is affected by the indenter's tip bluntness and the residual stress that arises during indentation and material properties.

Table 6.3: Typical values for various energies for anhydrous phase.

P_{max} (mN)	h_{max} (nm)	W_S (μN.nm)	W_T (μN.nm)	W_E (μN.nm)	W_P (μN.nm)	v_T	v_E
0.00	0.00	0.00	0.00	0.00	0.00	-	-
244.40	29.911	0.3655	0.3078	0.1329	0.1749	1.187	2.750
498.00	42.229	1.0515	0.8155	0.3843	0.4312	1.289	2.736
742.00	50.460	1.8722	1.536	0.7233	0.8127	1.219	2.588
995.70	58.515	2.913	2.2336	1.1762	1.0574	1.304	2.477
1244.60	66.720	4.152	3.1209	1.4969	1.6241	1.330	2.774

Anhydrous phases are characterized by the degree of hydration (measured in percent) whose upper and lower bounds correspond to pure clinker and hydrated C-S-H, respectively. Thus, these phases can have different characteristic load-displacement diagrams with remarkably different values of mechanical properties, which in turn, depending upon the degree of hydration results in multiple values for energy ratios. Correlating energy ratios with a degree of hydration is a matter of extensive research that requires the combined application of cement chemistry and nanoindentation analysis, and thus, is beyond the scope of this study. On the other hand, the mechanical properties shown in Table 6.3 for C-S-H are the results of statistical analysis and would not be meaningful if the same process is used for the determination of energy ratios for a particular phase as well. In fact, each indentation

corresponds to a unique phase of the cement paste. Due to these reasons, it would be advantageous to use these energy ratios as the characteristic parameters of the individual load-displacement curve, rather than the intrinsic material properties.

6.4 Definition of energy ratios

As mentioned earlier, the total and elastic energy ratios defined by Attaf [] is no longer applicable when a dwelling portion (phase) is also present in the load-displacement curves. In the presence of the dwelling portion, the total and elastic energy ratios may be expressed as:

$$v_T = \frac{W_{SL}}{W_T}; \quad v_E = \frac{W_{SE}}{W_E} \tag{6.1}$$

In the above expressions, W_{SL} and W_{SE} represent the absolute works of indentation corresponding to the loading and unloading curves, respectively, as. Quantities W_T and W_E, as usual, denote the total work done and the energy recovered after the complete withdrawal of the indenter, respectively. Indentation works are usually determined by evaluating the area under the respective curves, as schematically shown in figures 6.7a and 6.7b.

The proposed definitions can be validated by modeling the experimental load-displacement curves obtained from cementitious materials. In the presence of the dwelling phase, the entire load-displacement curves may be modeled using following set of expressions:

$$P = \begin{cases} P_{\max}\left(\dfrac{h}{h_L}\right)^{2v_T-1} & \textit{Loading} \\ P_{\max} & \textit{Dwelling} \\ P_{\max}\left(\dfrac{h}{h_{\max}}\right)^{2v_E-1} & \textit{Unloading} \end{cases} \tag{6.2}$$

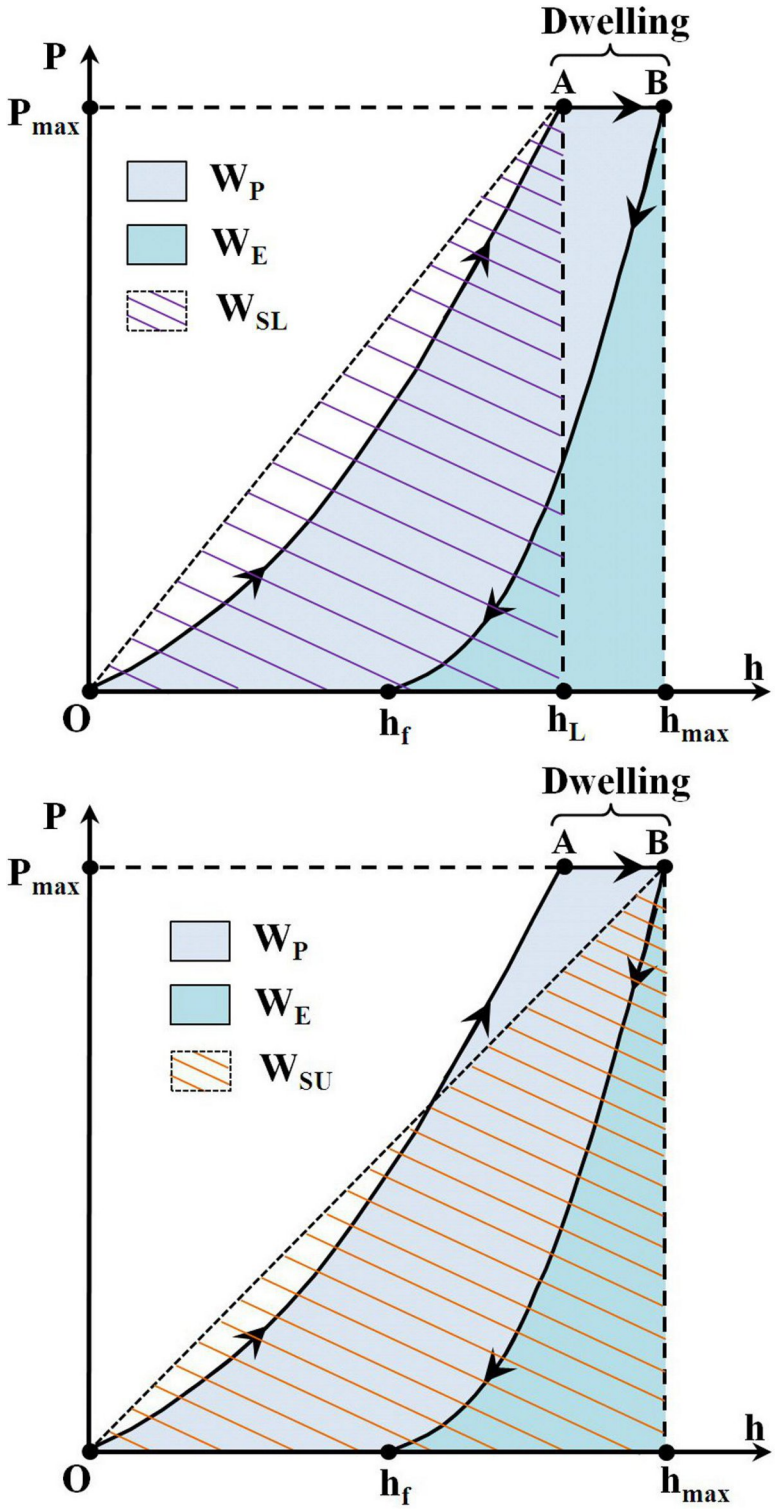

Figure 6.7: Schematic load-displacement curves with dwelling Phase and definition of absolute work.

where h_L is the penetration depth at which the loading is supposed to be ceased. The load-displacement curves modeled by Eq. (6.2) with total and elastic energy ratios defined by Eq. (6.1) are shown in figure 6.8 for the low stiffness C-S-H. As can be seen, there is an excellent agreement between the theoretical and experimental curves, and thus it validates the proposed definitions concerning energy ratios. The elastic energy ratio defined in this way is also used to determine the contact depth from:

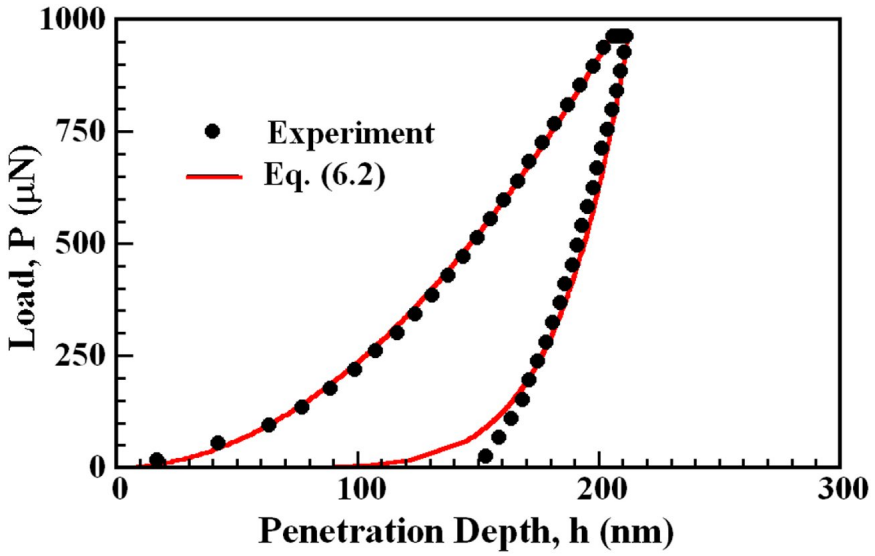

Figure 6.8: Modeling of load-displacement curves for LS C-S-H obtained with $P_{\max} \approx 1000\mu N$.

$$h_c = \frac{2(v_E - 1)}{(2v_E - 1)} h_{\max} \tag{6.3}$$

Figure 6.9 shows the comparison between the contact depths obtained by Eq. (6.3) with that obtained from experiment, where an excellent agreement between them is evident regardless of the phases present in the cementitious materials. Finally, the initial unloading stiffness is

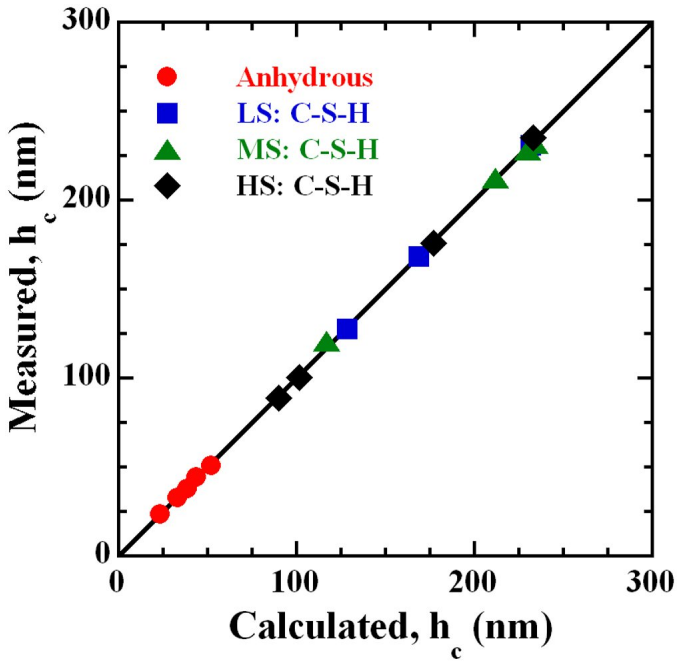

Figure 6.9: Plot showing the comparison of measured vs. calculated contact depths using Eq. (6.3) for all four phases of cement paste.

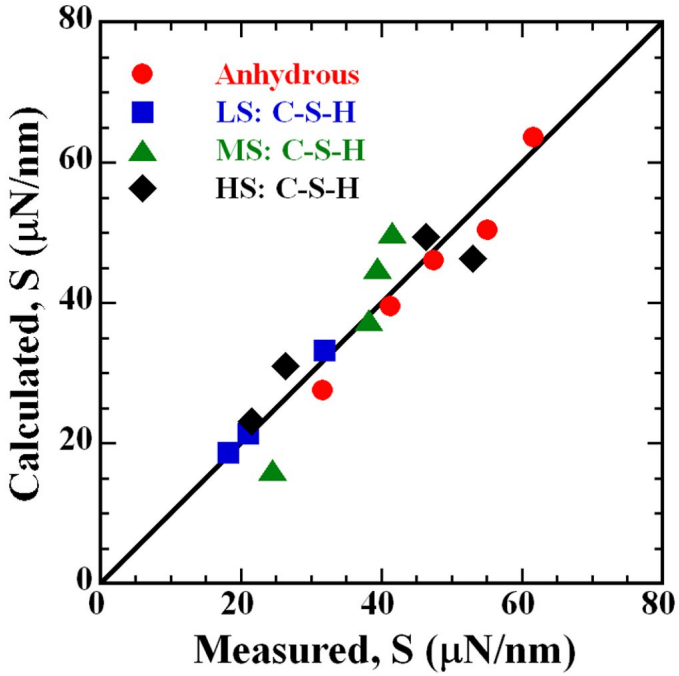

Figure 6.10: Comparison of measured and calculated initial unloading stiffnesses for all four phases of the cement paste.

calculated according to the procedure described in Chapter 4 and is compared with that obtained experimentally, as shown in figure 6.10. In all cases, accuracy better than 10% is obtained irrespective of the phases present.

6.5 Empirical relations

Empirical relations play an important role in the analysis of load-displacement data. As discussed in Chapter 2, nanomechanical quantities such as peak indentation load, penetration depths, indentation works and area of contact all are related to each other empirically. These relations provide insight on the nanomechanical behavior of a material and simplify the data analysis procedure significantly. This section focuses on some of these empirical relations that are relevant to cementitious materials.

6.5.1 Contact area and tip bluntness relationship

Contact area is one of the most important nanomechanical quantities and is determined from the known contact depth. For an ideally sharp indenter, it is given by: $A_c = C_1 h_c^2$; where C_1 is 24.56 for a Berkovich indenter. In reality, no indenter is ideally sharp as every tip has finite radius. To account for the finite tip radius, Oliver and Pharr developed a method that essentially establishes an area function using test materials (fused quartz) prior to indentation on actual materials. The area function has the following form:

$$A_{c1}\left(h_c\right) = \sum_{i=0}^{n} C_i \left(h_c\right)^{\frac{1}{2^i - 1}} \tag{6.4}$$

Coefficients C_i appearing in Eq. (6.4), except the leading term, take the indenter tip bluntness into account. These are determined iteratively as explained in Chapter 2. There is

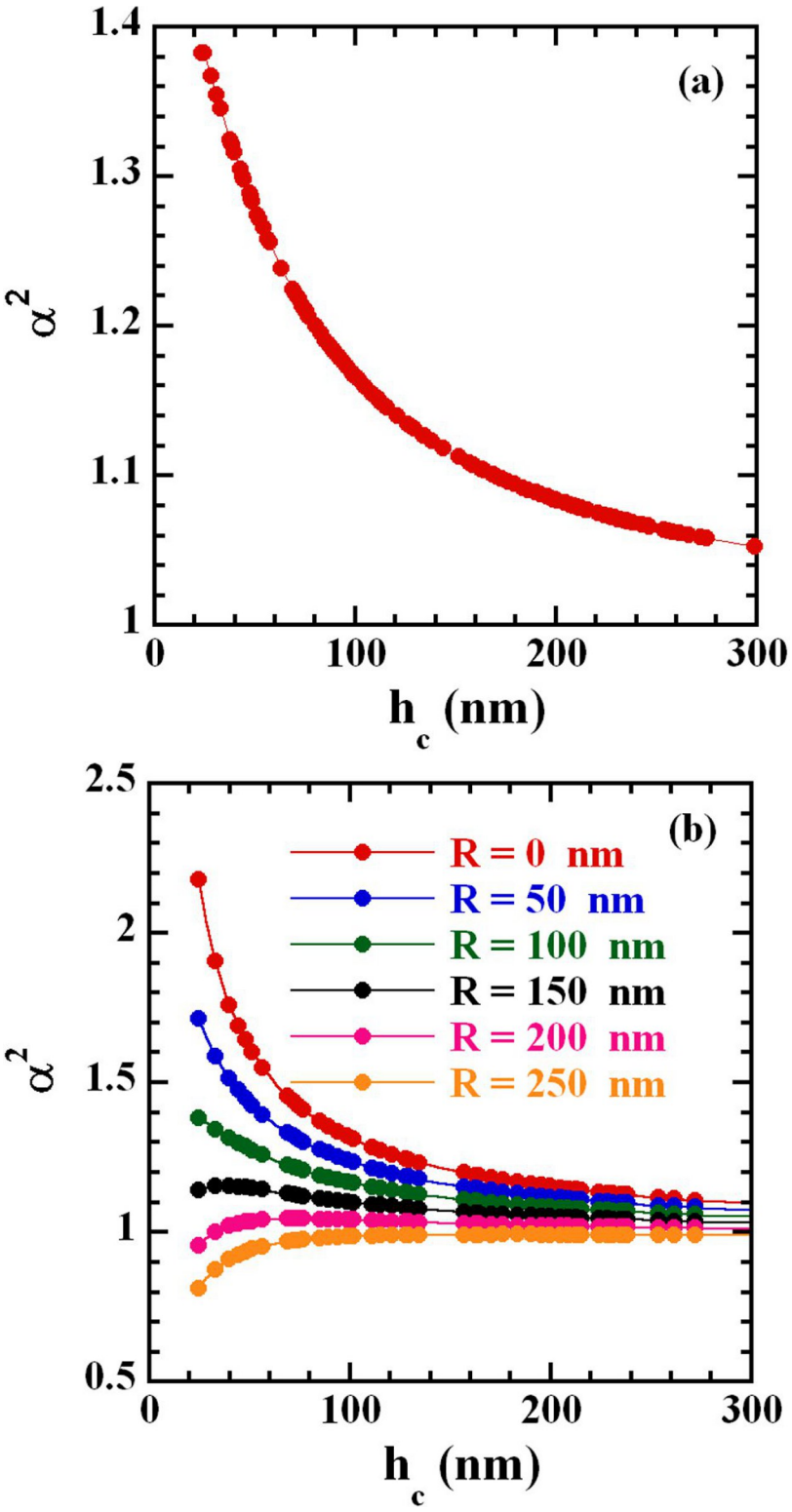

Figure 6.11: (a) Variation of area ratio with contact depth; and (b) effect of tip bluntness on the area ratio.

an alternative way to evaluate the contact area as well. Knowing the bluntness of the indenter tip, the contact area may also be evaluated using the following relation:

$$A_{c2}\left(h_c\right) = C_1\left(h_c + \xi\right)^2 \tag{6.5}$$

The term ξ represents the apex height (as shown in figure 2.10), a measure of the tip bluntness; it is equal to 6.22 nm for a new Berkovich indenter having the tip radius $R = 100\ nm$ used in this study. However, the contact area determined using these two area functions differs greatly, especially when the contact depth is smaller. The discrepancy between them can be quantitatively expressed by plotting their ratios $\left(\alpha^2 = A_{c1} / A_{c2}\right)$ with respect to the contact depth, as shown in figure 6.11a. It is clear from the figure that the ratio decreases, almost exponentially, with the increase in the contact depth and eventually becomes equal. To gain further insight qualitatively, the area function, A_{c2}, is calculated for several values of the indenter radius (0, 50, 100, 150, 200, 250 nm) and the ratios corresponding to each of these radii are again plotted against the contact depth, as shown in figure 6.11b. It is apparent from the figure that the discrepancy between these two area functions becomes significant when the contact depth is small. Note that apex height can be determined according to the procedure describe in Chapter 3.

6.5.2 Maximum, plastic, contact and residual depths

Using the data on ceramics, Attaf [25] has shown that each of these maximum, plastic contact and residual depths are linearly related to the other. In indentation measurement, plastic depth is defined as a point on the h-axis of the P-h diagram where a tangent to the unloading curves at the peak indentation load meets. While maximum, residual and contact

depths are obtained as experimental outputs, plastic depth is calculated using the following expression:

$$h_P = \frac{P_{\max}}{mA_0\left(h_{\max} - h_f\right)^{m-1}} \tag{6.6}$$

Figures 6.12a-6.12c show the variation of maximum depth of penetration with each of the contact, plastic and residual depths, respectively. As can be seen, linear relationships between them do exist even for the heterogeneous cementitious materials. However, the correlation is somewhat poor in the case of residual vs. maximum penetration depth (figure 6.12c) as compared to the other two, which may be attributed to the sensitivity of residual depth due to surface roughness. Based on linear fit, the variation of the maximum depth of penetration with contact, plastic and residual depths may be expressed respectively as:

$$h_{\max} = K_c h_c \tag{6.7}$$

$$h_{\max} = K_P h_P \tag{6.8}$$

$$h_{\max} = K_f h_f \tag{6.9}$$

The values for the proportionality constants appearing in the above equations are summarized in Table 6.4. Note that the accuracy of these linear expressions can be significantly improved with more experimental data, which would also allow us to develop such equations for different phases present in the cementitious composite. The advantage of using Eqs. (6.4) and (6.5) is that the contact area and initial unloading stiffness may be calculated in one of the simplest ways. We opined that these empirical correlations can be used as tools for sanity checks while carrying out more rigorous data analysis. Note that K_f can be expressed as a function of the elastic energy constant, as given in Eq. (6.3)

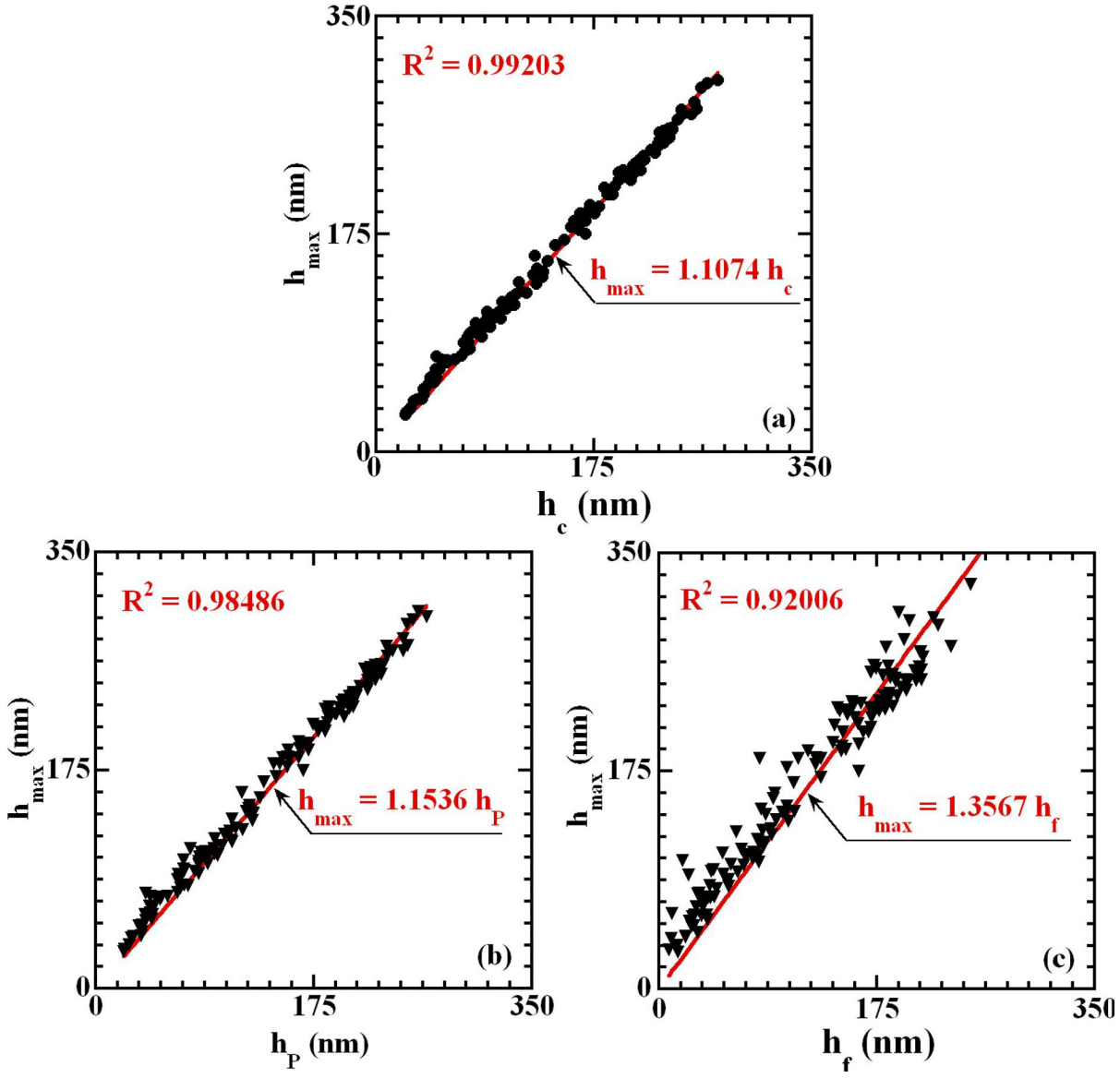

Figure 6.12: Relationship between various penetration depths: (a) h_c vs. h_{max}; (b) h_P vs. h_{max}; and (c) h_s vs. h_{max}.

6.5.3 Contact area and penetration depth relationships

In a similar fashion, a direct relationship between contact area and different penetration depths could be established. The general trend is such that the contact area is proportional to the square of each of the penetration depths. To develop equations capable of predicting the contact area from the known maximum and contact depths, the measured contact area vs. the square of each of these depths are plotted, as shown in figures 6.13a and 6.13b. Linear regression analysis shows that the proportionality between the contact area and square of the maximum depth of penetration is also valid in the case of cementitious materials with a high regression coefficient value. However, in the case of contact depth, the relationship is linear only when the contact depth is in excess of 125 nm. Below this value, the contact area varies with the square of the contact depth according to a form given by a second order polynomial apparently due to the bluntness in the tip of the indenter, which is more pronounced at shallow depths. With these trends, the expressions for the contact area as a function of the maximum depth of penetration and contact depth, for cementitious materials, may respectively be expressed as:

$$A_c = K^{A}_{\max} h^2_{\max} \tag{6.10}$$

and

$$\begin{aligned} A_c &= K^{AP}_{c1} h_c^2 + K^{AP}_{c2} \left(h_c^2\right)^2 \quad h_c \le 125\ nm \\ A_c &= K^{AL}_{c1} h_c^2 + K^{AL}_{c2} \quad h_c > 125\ nm \end{aligned} \tag{6.11}$$

Table 6.4 summarizes the values of constants appearing in the above equations. Again, with the large database, regression analysis would yield more accurate and refined equations pertaining to each phase of the cementitious materials. Variations of contact area with the

square of plastic and residual contact depths are more scattered and may produce erroneous results if used in the subsequent data analysis.

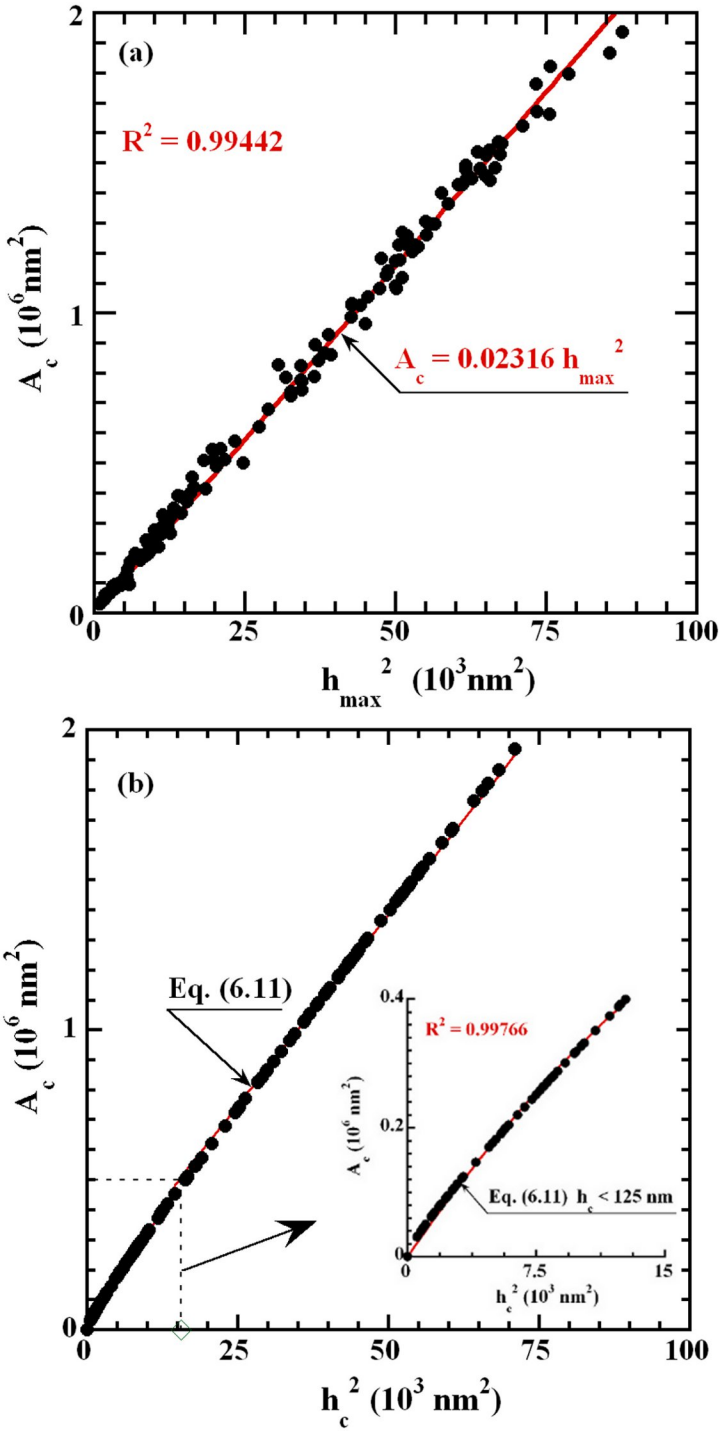

Figure 6.13: Relationship between: (a) contact area vs. maximum penetration depth; and (b) contact area vs. contact depth.

Table 6.4: Values of various constants found in this study for cement paste.

Constant	Value	Constant	Value
$K^{A}_{\max}$	0.02316	K^{AL}_{c1}	0.025384
K_c	1.1074	K^{AL}_{c2}	0.11591
K_p	1.1536	K^{AP}_{c1}	0.038377
K_f	1.3567	K^{AP}_{c2}	-5.71E-04

6.5.4 Validation and discussion

The validity of the empirical equations given in the previous subsections may be examined by evaluating the elastic modulus and hardness of all the phases of the cement paste. By substituting them in the Sneddon's solution one by one, the modulus and hardness may be evaluated, depending on the empirical equations used, by three different ways. Note that the initial unloading stiffness is evaluated as described in Jha et al. [].

Method 1: When the contact area is expressed in terms of $h_{\max}$

$$E_r = \frac{\sqrt{\pi}\,\varepsilon\left(2\nu_E - 1\right)}{2\sqrt{K^{A}_{\max}}}\frac{P_{\max}}{h^2_{\max}}$$
$$H = \frac{P_{\max}}{K^{A}_{\max} h^2_{\max}} \tag{6.12}$$

Method 2: When the contact area is given as a function of h_c

$$E_r = \frac{\sqrt{\pi}\,\varepsilon\left(2\nu_E - 1\right)P_{\max}}{2\sqrt{K^{A}_{c} h_c}}$$
$$H = \frac{P_{\max}}{K^{A}_{c} h^2_c} \tag{6.13}$$

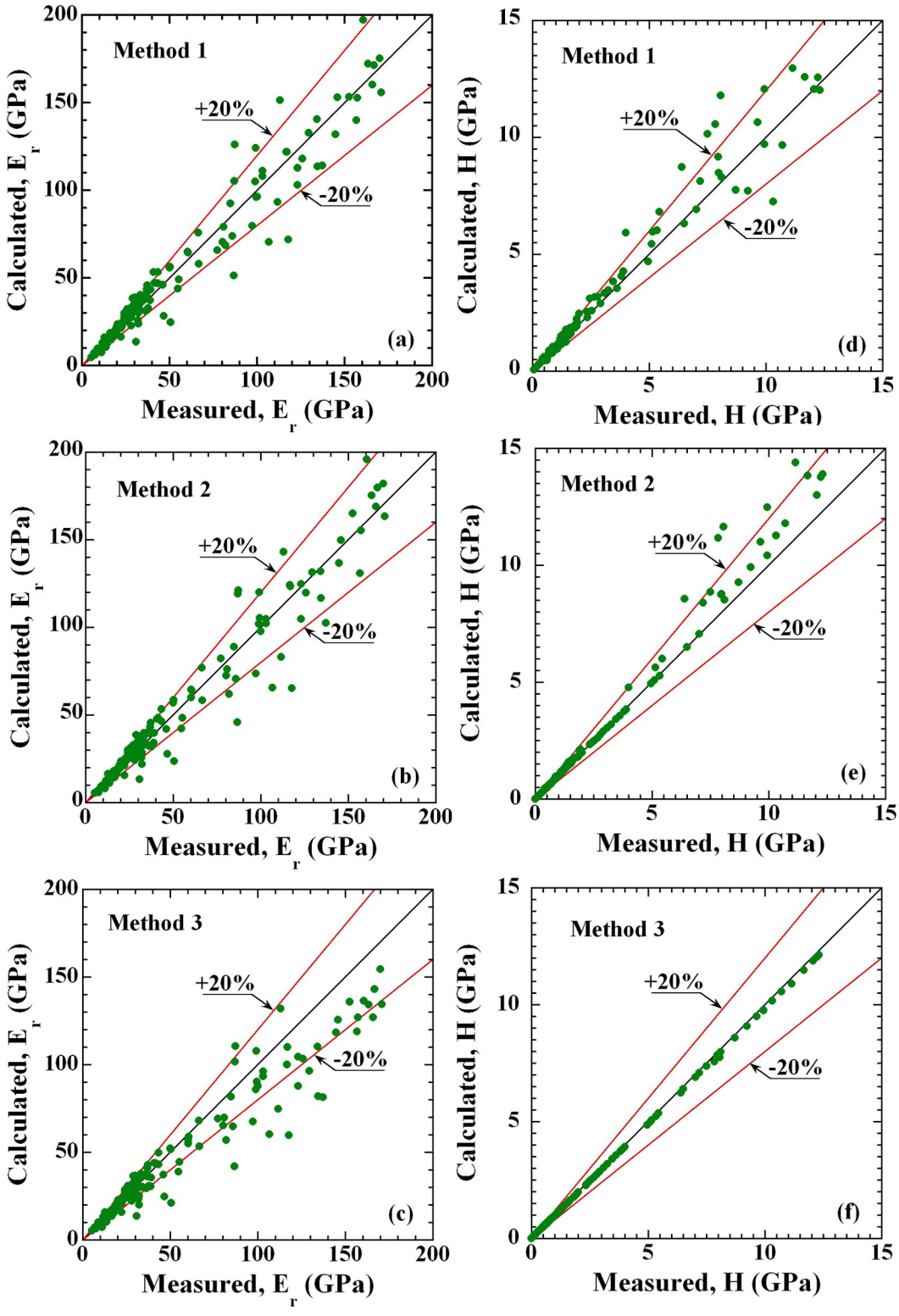

Figure 6.14: Comparison of Elastic Modulus and Hardness using the empirical relationships obtained in this study to those obtained from conventional Oliver and Pharr method.

If the contact depth is greater than 125 nm, then Eq. (6.13) will have the following form.

$$E_r = \frac{\sqrt{\pi}\,\varepsilon\left(2v_E - 1\right)P_{\max}}{2\sqrt{K_{c1}^{A}\,h_c^2 + K_{c2}^{A}\left(h_c^2\right)^2}}$$
$$H = \frac{P_{\max}}{K_{c1}^{A}\,h_c^2 + K_{c2}^{A}\left(h_c^2\right)^2} \tag{6.14}$$

Method 3: Similarly, the contact area is a function of ξ and h_c

$$E_r = \frac{\sqrt{\pi}\,\varepsilon\left(2v_E - 1\right)P_{\max}}{2\sqrt{C}\alpha\left(h_c + \xi\right)h_{\max}}$$
$$H = \frac{P_{\max}}{C\alpha^2\left(h_c + \xi\right)^2} \tag{6.15}$$

The elastic modulus and hardness values determined using above equations are compared with those obtained experimentally, as shown in figures 6.14a – 6.14c. The agreement is reasonable as the calculated values deviate by a maximum of ±20% for some indentations only. A better accuracy is obtained in the case of hardness than indentation modulus as the effect of deviation in the initial unloading stiffness does not affect the later. Note that, in Eq. (6.15), α^2 is determined by fitting α^2 vs. $h_{\max}$ curve shown in figure 6.11a using a higher degree polynomial. Hardness values obtained this way may be used to determine the elastic modulus of the cementitious material using loading curve.

6.6 Determination of mechanical properties: Energy based method

Based on the analysis presented thus far, one may conclude that the indentation energies may be employed in the Sneddon's solution for punch problem to determine the elastic

modulus and hardness of a material. The steps involved in the method developed in this study are summarized in the following.

1. Obtain the peak indentation load $\left(P_{\max}\right)$ and maximum depth of penetration $\left(h_{\max}\right)$ from the load-displacement curves.
2. Compute the total $\left(W_T\right)$ and elastic $\left(W_E\right)$ work done from the area under the loading and unloading curves, respectively and evaluate the total and elastic energy constants according to the relation:

$$v_{T0} = \frac{W_{SL}}{W_{TL}}; \quad v_E = \frac{W_{SE}}{W_E} \tag{6.16}$$

where is the total work done during loading only.

3. Determine the initial unloading stiffness using the elastic energy constant as:

$$S_E = \alpha_s \varepsilon \left(2v_E - 1\right) \frac{P_{\max}}{h_{\max}} \tag{6.17}$$

A value of 0.75 may be used for the geometric factor ε. The stiffness correction factor is given by:

$$\alpha_s = \begin{vmatrix} A_1 - B_1 \log\left(v_E\right) & v_E \le 8.50 \\ A_2 - B_2 \log\left(v_E\right) & v_E > 8.50 \end{vmatrix} \tag{6.18}$$

The initial unloading stiffness determined in this way for cementitious materials is compared with obtained by the OP method, as shown in figure 6.15a, where reasonable agreement between then could be observed.

4. Evaluate the nominal hardness of a material from the total work done during indentation from:

$$H_n = \frac{kP_{\max}^3}{9W_T^2} \tag{6.19}$$

5. Calculate the conventional (normal) hardness of a material from the nominal one using:

$$H_C = \left(\frac{K_N}{v_{T0}}\right) K_D H_n \tag{6.20}$$

where K_N is hardness conversion factor for the case involving an ideally sharp indenter. It may also be used in the case of a non-perfect indenter provided it is divided by the total energy constant. The dwelling portion was not considered while developing a relation between the conventional and nominal hardness values in Chapter 4. It is found that the work done during dwelling can be incorporated using the following factor:

$$K_D = 4.89 - 3.88\frac{h_L}{h_{\max}} \tag{6.21}$$

where h_L is the penetration depth at the end of the loading. Note that when h_L approaches $h_{\max}$, K_D becomes equal to 1 thereby corresponding to a case where no dwelling is present.

6. Finally, evaluate the indentation modulus (or reduced modulus) using the Sneddon's solution, which may be written in the following form:

$$E_r = S_E \frac{\pi}{2}\sqrt{\frac{P_{\max}}{H_c}} \tag{6.22}$$

Figure 6.15b shows the comparison between the hardness values determined by above procedure and the OP method. For reduced modulus, similar comparison is shown in figure 15c. In general, the computed results accord well with those obtained from the experiment in

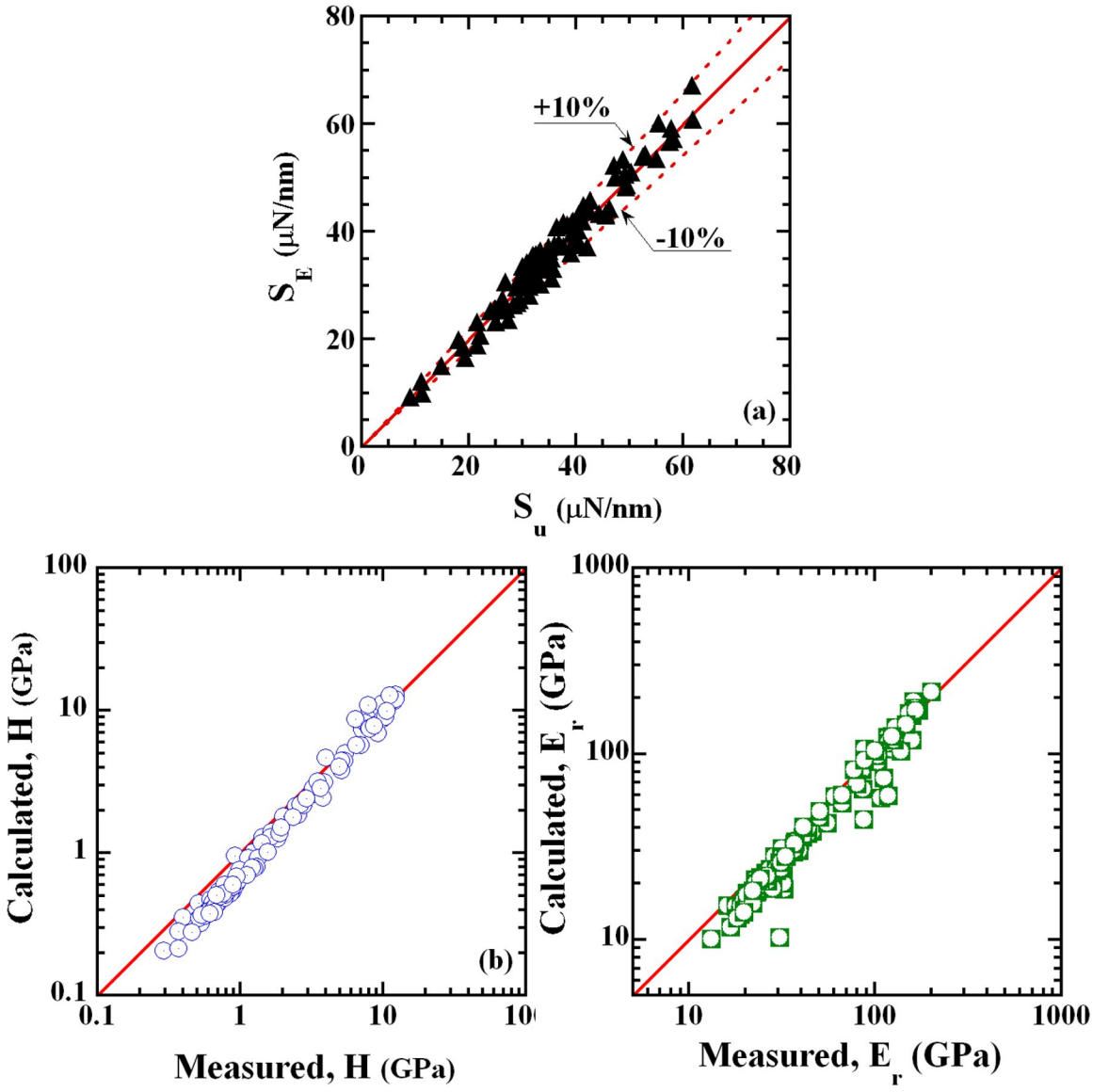

Figure 6.15: Plots showing the comparison of: (a) initial unloading stiffness; (b) conventional hardness; and (c) reduced modulus determined by the energy-based approach developed in this study and by the conventional Oliver and Pharr method.

either case. However, better accuracy can be achieved as we move from LS C-S-H to the anhydrous phase. The energy based approach developed in this study offers several advantages over the conventional method. It is computationally efficient; incorporates factors

such as the peak indentation load, dwelling period, and indenter's tip bluntness explicitly; and most importantly, it does not require the computation of the contact area at all.

6.7 References

[1] Velez, K., Maximilien, S., Demidot, D., Fantozzi, G., and Sorrentino, F. (2001). "Determination by nanoindentation of elastic modulus and hardness of pure constituents of Portland cement clinker." *Cement and Concrete Research*, 31, 555-561.

[2] Constantinides, G., Ulm, F.J., and Van Vliet, K.J. (2003). "On the use of nanoindentation for cementitious materials." *Materials and Structures*, 36, 191-196.

[3] Vandamme, M., Ulm, F.J., and Fonollosa, P. (2010). "Nanogranular packing of C-S-H at substochiometric conditions." *Cement and Concrete Research*, 40, 14-26.

[4] Constantinides, G., and Ulm, F.J. (2004). "The effect of two types of C-S-H on the elasticity of cement-based materials: Results from nanoindentation and micromechanical modeling." *Cement and Concrete Research*, 34, 67-80.

[5] Constantinides, G., and Ulm, F.J. (2007). "The nanogranular nature of C-S-H." *Journal of the Mechanics and Physics of Solids*, 55, 64-90.

[6] Hughes, J. J., and Trtik, P. (2004). "Micro-mechanical properties of cement paste measured by depth-sensing nanoindentation: A preliminary correlation of physical properties with phase type." *Materials Characterization*, 53, 223-231.

[7] Mondal, P., Shah, S.P., and Marks, L.D. (2008). "Nanoscale characterization of cementitious materials." *ACI Materials Journal*, 105, 174-179.

[8] Zhu, W., Hughes, J. J., Bicanic, N., and Pearce, C. J. (2007). "Nanoindentation mapping of the mechanical properties of cement paste and natural rocks." *Materials Characterization*, 58, 1189-1198.

[9] Nemecek, J. (2009). "Creep effects in nanoindentation of hydrated phases of cement pastes." *Material Characterization*, 60, 1028-1034.

[10] Vandamme, M., and Ulm, F.J. (2009). "Nanogranular origin of concrete creep." *Proceedings of the National Academy of Sciences*, 106, 10552-10557.

[11] Pichler, C., and Lackner, R. (2009). "Identification of logarithmic-type creep of calcium-silicate-hydrates by means of nanoindentation." *Strain*, 45, 17-25.

[12] Jones, C.A., and Grasley Z.C. (2011). "Short-term creep of cement paste during nanoindentation." *Cement and Concrete Composites*, 33, 12-18.

[13] Bernard, O., Ulm, F.J., and Lemarchand, E. (2003). "A multiscale micromechanics-hydration model for the early-age elastic properties of cement-based materials." *Cement and Concrete Research*, 33, 1293-1309.

[14] Pharr, G.M., and Bolshakov, A. (2002). "Understanding nanoindentation unloading curve." *Journal of Materials Research*, 17, 2660-2671.

[15] Oliver, W.C., and Pharr, G.M. (1992). "An improved technique for determining hardness and elastic modulus using load and displacement sensing indentation experiments." *Journal of Materials Research*, 7, 1564-1583.

[16] Oliver, W.C., and Pharr, G.M. (2004). "Measurement of hardness and elastic modulus by instrumented indentation: Advances in understanding and refinements of methodology." *Journal of Materials Research* 19, 3-20.

[17] Gong, J., Peng, Z., and Miao, H. (2005). "Analysis of the nanoindentation load-displacement curves measured on a high-purity fine grained alumina." *Journal of the European Ceramic Society*, 25, 649-654.

[18] Gong, J., Miao, H., and Peng, Z. (2004). "Analysis of the nanoindentation data measured with a Berkovich indenter for brittle materials: Effect of the residual contact stress." *Acta Materialia*, 52, 785-793.

[19] Jha, K.K., Suksawang, N., Lahiri, D., and Agarwal, A. (2012): "Energy-based analysis of nanoindentation curves for cementitious materials." *ACI Materials Journal,* 109, 81-90.

[20] Cheng, Y.T., and Cheng, C.M. (2004). "Scaling, dimensional analysis, and indentation measurements." *Materials Science and Engineering R*, 44, 91-149.

[21] Malzbender, J. (2005). "Comment on the determination of mechanical properties from the energy dissipated during indentation." *Journal of Materials Research,* 20, 1090-1092.

[22] Sakai, M. (1993). "Energy principle of the indentation-induced inelastic surface deformation and hardness of brittle materials." *Acta Metallurgica et Materialia*, 41, 1751-1758.

[23] Attaf, M.T. (2003). "New ceramics related investigation of the indentation energy concept." *Material Letters*, 57, 4684-4693.

[24] Attaf, M.T. (2004). "Step by step building of a model for the Berkovich indentation

cycle." *Material Letters*, 58, 507-512.

[25] Attaf, M.T. (2003). "A unified aspect of power-law correlations for Berkovich hardness testing of ceramics." *Material Letters*, 57, 4627-4638.

[26] Attaf, M.T. (2004). "New formulation of the nanomechanical quantities using the β-material concept and the indentation function." *Material Letters*, 58, 889-894.

[27] Ulm, F.J., Vandamme, M., Bobko, C., Ortega, J. A, Tai, K., and Ortiz, C. (2007). "Statistical indentation techniques for hydrated nanocomposites: Concrete, Bone and Shale." *Journal of the American Ceramic Society*, 90, 2677-2692.

[28] Mondal, P., Shah, S.P., and Marks, L.D. (2007). "A reliable technique to determine the local mechanical properties at the nanoscale for cementitious materials." *Cement and Concrete Research*, 37, 1440-1444.

[29] Jennings, H.M. (2000). "A model for the microstructure of calcium silicate hydrate in cement pastes." *Cement and Concrete Research*, 30, 101-116.

[30] Tennis, P.D., and Jennings, H.M. (2000). "A model for two types of calcium silicate hydrates in the microstructure of the cement pastes." *Cement and Concrete Research*, 30, 855-863.

[31] Suresh, S., and Giannakopoulos, A. (1998). "A new method for estimating residual stress by instrumented sharp indentation." *Acta Materialia*, 46, 5755-5767.

CHAPTER 7

CONCLUSIONS AND RECOMMENDATIONS

7.1 Summary of main findings

In this thesis, a novel method for the determination of the elastic modulus and hardness of a material is developed within the framework defined by contact mechanics. The proposed method is based on indentation energies, which can be evaluated from the load-displacement data measured in a nanoindentation experiment. The main strengths of the proposed energy-based approach are: (1) it incorporates the effect of peak indentation load, dwelling period and indenter tip bluntness explicitly; (2) it does not require the determination of the contact area between the indenter and the specimen; and (3) it computes the elastic modulus and the hardness of a material in one of the most efficient ways, as the required parameters can be readily obtained from the experimental curves. The main conclusions of this study are enumerated as follows:

1. The total and elastic energy constants are related to the curvature of the loading and unloading curves, respectively. While the former quantifies the bluntness in the tip of the indenter, the later measures the fraction of the deformations that are plastic.
2. For the Berkovich indenter, the total energy constant is a function of the indenter tip radius to the maximum penetration depth ratio alone if the indentation is elastic. For elasto-plastic indentations, it also depends on the material properties when this ratio exceeds a value of 2. It is independent of the radius-to-depth ratio, but is found to be unique, corresponding to a given elastic modulus to yield a strength ratio for a spherical indenter. On the other hand, the elastic energy depends on both material properties as

well as the radius-to-depth ratio. However, the rate at which it decreases with respect to the radius-to-depth ratio remains the same irrespective of the material properties.

3. The total energy constant varies in the range 1.0 - 1.50 and 1.0 – 1.25 for Berkovich and spherical indenters, respectively. In the case of the Berkovich indenter, it decreases with the increase in the radius-to-depth ratio. It remains constant with respect to the radius-to-depth ratio for a spherical indenter. However, in either case, it increases as a material becomes more elastic. As far as the elastic energy constant is concerned, it may fall in the range 1 - ∞ with the upper limit corresponds to a completely plastic material.
4. By the way of application, we have shown that the indenter tip radius and nominal hardness of a material may be evaluated using the total energy constant with great accuracy. We have also shown that the expression used for the determination of contact depth from the elastic energy constant for the Berkovich indenter is valid for the spherical indenter as well. The consequence of using an average value of this constant in the determination of contact depth is also discussed.
5. This study provides a superior alternative to the curve-fitting methods used for evaluating the initial unloading stiffness from the nanoindentation response. The energy-based power function may be employed to model the unloading response fairly accurately. Analytical differentiation of such a function, however, yields erroneous results. A comprehensive analysis of the indentation data pertaining to oxide-based ceramics, coating and metals revealed that the error associated with this quantity could be expressed as a function of the elastic energy constant. By introducing a stiffness correction factor, an expression for the determination of initial unloading stiffness is derived in this study. The use of the elastic energy constant is more appropriate, in

comparison to the conventional power-law parameters, as it characterizes the unloading response of a material to indentation. The proposed method is also validated using literature data from different materials acquired with a relatively large peak indentation load (in excess of 100mN). Excellent agreement between the calculated and measured initial unloading stiffness is obtained for all the materials considered herein irrespective of the magnitude of the peak indentation load used to acquire their responses.

6. This study shows that the existing work-of-indentation used in the determination of the nominal hardness of a material is modified in view of the bluntness at the tip of the indenter, thus allows us to calculate the same, even when the peak indentation load is small. A theoretical framework is developed to obtain a conventional hardness from a nominal for an ideally sharp conical and Berkovich indenter. Similar conversion can be carried out for the blunt indenter using the phenomenological correction factors developed in this study. These correction factors are found to be a function of percentage elastic recovery and energy constant. The modified approach is validated using the nanoindentation data pertaining to wide range of materials and peak indentation loads.
7. New definitions for the total and elastic energy constant are given in consideration of the dwelling period. When a dwelling portion is also included in the load-displacement response, the absolute works for the total and elastic energy constants should be evaluated from the initial and final depth of dwelling, respectively. Similarly, the total work done during loading should be ignored while determining the total energy constant. The energy constants obtained in this way can model the indentation load-displacement curves with dwelling period and provides initial unloading stiffness and hardness of cementitious materials very accurately.

8. Nanoindentation data obtained from hardened cement paste samples are analyzed to establish relationships between different nanomechanical quantities. Unlike metals and ceramics, limited numbers of equation with high regression coefficient are applicable to heterogeneous cementitious material. It has been found that the maximum depth of penetration is proportional to each of the plastic, residual and contact depths. Similarly, the contact area varies as the square of the maximum depth of penetration. However, in the case of contact depth, it varies linearly only when the former is in the excess of 125 nm. Below this value, contact area can be represented by a second degree polynomial. Again, contact area can also be expressed as a function of contact depth and bluntness of the tip of indenter. The discrepancy between the area measured by this relation with that obtained by the Oliver and Pharr method is about 15% when the contact depth is approximately greater than 125nm. These relationships provide reasonably values for the elastic modulus and hardness for cementitious materials when used in the Sneddon's solution.
9. A semi-analytical energy-based method is developed in this study, which employs the indentation energy to evaluate the initial unloading stiffness, hardness and elastic modulus. The proposed method is validated using the nanoindentation data from the cementitious materials which shows excellent agreement between the measured and computed mechanical properties.

7.2 Limitations and recommendations for future research

Although the proposed method evaluates the elastic modulus and hardness of a material with a reasonable level of accuracy, further studies are needed to enhance its efficiency and

accuracy, to extend its capability to evaluate other mechanical properties of interest, and to examine its efficacy in the multiscale material modeling and in the development of a more robust nanomechanical properties evaluation procedure. The correction factor employed to account for the effect of the indenter tip bluntness on the computed hardness values by the modified work-of-indentation approach appears to be a function of peak indentation load. Experimental studies can be pursued to establish a relation between the tip bluntness correction factor and the peak indentation load. Likewise, this study does not consider the correction factors due to the lack of axial symmetry of the indenter and due to improper boundary condition used in the Sneddon's solution. Incorporation of these correction factors would significantly enhance the accuracy of the proposed method. The energy-based approach presented herein is limited to the determination of the elastic modulus and hardness only. Its realm of application can be extended if the concept used is applied in the determination of yield strength, strain hardening exponent, fracture toughness, other time-dependent properties etc. A future study may be directed toward examining its effectiveness in the evaluation of macroscopic mechanical properties of concrete via the multiscale material modeling. Developing a loading curve based nanomechanical properties evaluation procedure based on the findings of this study would be an interesting topic for future research.

VITA

KAUSHAL KUMAR JHA

1991-1994	B.E., Civil Engineering Tribhuvan University Kathmandu, Nepal
1995-1998	Engineer, Government of Nepal
1998-2000	M.E., Civil Engineering (Geotechnical) Saitama University Saitama, Japan
2000-2001	Invited Researcher Saitama University Saitama, Japan
2001 -2003	M.E., Civil Engineering (Structural) Asian Institute of Technology Bangkok, Thailand
2003 -2003	Research Associate Asian Institute of Technology Bangkok, Thailand
2004 -2006	Lecturer Purvanchal University Kathmandu, Nepal
2006 -2007	Design Engineer BASF, The Chemical Company Bangkok, Thailand
2008 -2012	PhD Candidate Florida International University Miami, FL
	Teaching/Research Assistant Florida International University Miami, FL

PUBLICATIONS

1. Jha, K.K., and Suksawang, N. (2012). "*Modified Two-slope Method to Compute Nanomechanical Properties for Cementitious Materials."* 4th International Symposium on Nanotechnology in Construction, NICOM 4, Crete, Greece, May 20-22.

2. Jha, K.K., Suksawang, N., Lahiri, D., and Agarwal, A. (2012). "*Energy-Based Analysis of Nanoindentation Curves for Cementitious Materials."* ACI Materials Journal, 109 (1): 81-90.

3. Jha, K.K., Suksawang, N., and Agarwal, A. (2011). "*Analytical Approach for the Determination of Nanomechanical Properties for Metals*." MEMS and Nanotechnology, Vol. 4, Proceedings of the conference of the Society for Experimental Mechanics Series, Uncasville, CT, 65-71.

4. Jha, K.K., and Suksawang, N. (2011). "*Emerging Trend in the Measurement of Mechanical Properties of Cementitious Materials at Nanoscale and Computational Challenges*." fib symposium: Concrete Engineering for Excellence and Efficiency, Prague, Czech Republic, pp. 791-794.

5. Jha, K.K., Suksawang, N., and Agarwal, A. (2011). "*The Sensitivity of β-Material Parameter and its Determination based on Optimization of Error in the Mechanical Properties."* Computational Materials Science, 50: 2891-2897.

6. Jha, K.K., Suksawang, N., and Agarwal, A. (2010). "*Analytical Method for the Determination of Indenter Constants used in the Analysis of Nanoindentation Loading Curves."* Scripta Materialia, 63: 281-284.